NON-LINEAR PARAMETER ESTIMATION USING WAVELET TRANSFORMS

by

RAJKUMAR PORWAL

DEPARTMENT OF MECHANICAL ENGINEERING

INDIAN INSTITUTE OF TECHNOLOGY KANPUR

DECEMBER 2010

NON-LINEAR PARAMETER ESTIMATION USING WAVELET TRANSFORMS

A Thesis Submitted

in Partial Fulfillment of the Requirements

for the Degree of

DOCTOR OF PHILOSOPHY

by

RAJKUMAR PORWAL

to the

DEPARTMENT OF MECHANICAL ENGINEERING

INDIAN INSTITUTE OF TECHNOLOGY KANPUR

DECEMBER 2010

CERTIFICATE

It is certified that the work contained in the thesis titled "*NON-LINEAR PARAMETER ESTIMATION USING WAVELET TRANSFORMS*" by *Rajkumar Porwal* (Roll No. : Y4105084) has been carried out under my supervision and that this work has not been submitted elsewhere for the award of a degree.

Dr. Nalinaksh S. Vyas 29·12·10

Professor & Head

Department of Mechanical Engineering

Indian Institute of Technology, Kanpur

SYNOPSIS

Name of the student : Rajkumar Porwal   **Roll Number** : Y4105084

Degree for which Submitted : Ph.D.   **Department** : Mechanical Engineering

Thesis Title: Nonlinear Parameter Estimation using Wavelet Transforms

Name of the thesis Supervisor : Dr. Nalinaksh S. Vyas

Month and Year of Submission : December 2010

Nonlinear system identification and parameter estimation are relevant research areas and different techniques have been adopted for such determination in mechanical systems. Nonlinear systems exhibit varied characteristic behavior under different excitations. Identification methods should be mathematically sound to adequately capture these characteristics and establish proper input-output relationships to subsequently estimate system parameters.

The present study makes an attempt to utilize properties of Wavelet Transforms for system identification and parameter estimation, in the context of mechanical systems. Transient response of weakly nonlinear systems can be modeled through signals whose amplitude envelope and instantaneous frequency change with time. Instantaneous frequency depends on the amplitude of vibration and the form of stiffness, while the amplitude envelope of the response depends on the form of damping. Analytical solutions obtained from Krylov-Bogoliubov technique establish the relationships for instantaneous frequency and amplitude envelope for weakly nonlinear systems (Nayfeh, 1973). Instantaneous frequency and amplitude envelope of the given signal can also be determined numerically using the Wavelet Transforms (Mallat, 1998). The numerical results obtained from Wavelet Transforms are used in conjunction with analytical solutions from Krylov-Bogoliubov technique to determine the system parameters.

Presence of many forms of the nonlinearities in the restoring force and dissipative forces makes identification and parameter estimation in nonlinear systems quite involved.

Parameter estimation procedures generally assume that sufficient apriori information about the mathematical structure of the system is available. Subsequently system parameters are estimated using input-output data for the assumed form of nonlinearities. For complex engineering systems, it is difficult to recognize the actual form of nonlinearity. Wavelet Transform based nonlinear system identification and parameter estimation procedures mostly consider a Duffing system or systems with symmetric polynomial forms of stiffness terms. However, for engineering applications, it is also important to identify the types of nonlinearities actually governing the system response. A systematic procedure, based on Wavelet Transforms, is proposed to classify polynomial form of stiffness nonlinearity governing the system.

A nonlinear system having third degree polynomial form of stiffness is considered in the present study. In general, Krylov-Bogoliubov method is unable to incorporate the effect of quadratic nonlinearity in the response of the system (Mickens, 1995). Due to the asymmetric behavior of the quadratic stiffness term, Krylov-Bogoliubov method is applied separately to positive half and negative half cycle of the response. It is shown that the law governing the instantaneous frequency is different during the two half cycles. A mixed parity nonlinear oscillator is numerically simulated to validate the findings. The concepts are used for further classification of nonlinearity. Wavelet Transforms of the response signal using standard Morlet wavelet and complete Morlet wavelet are used. Presence of symmetric and asymmetric forms of nonlinearity is explored. Asymmetric forms of nonlinearity are further classified into quadratic and mixed parity nonlinear oscillators. The sign of the nonlinear parameter is also determined.

Researchers have earlier estimated parameters for linear and nonlinear system and reported the estimation errors. In this thesis, reasons of estimation error are addressed and dependence of the errors on the magnitude of nonlinear parameters themselves is investigated. The error in parameter estimation of single degree of freedom (SDOF) system is considered and the limitation of the procedure is discussed. Two systems are taken for numerical illustration. The first example pertains to the Duffing oscillator,

which contains cubic stiffness nonlinearity and the second example is that of a self excited system of van der Pol type. The two systems are simulated numerically for a wide range of system parameters and errors in estimation are attributed to the magnitude of system parameters itself. The dependence of estimation error on system parameters is shown as an error surface.

In the case of nonlinear multi degree of freedom (MDOF) systems, researchers have attempted identification using Wavelet Transforms, by separating individual modes in the time-frequency plane. The problem of close modes was also addressed by optimizing wavelet parameters for specific applications. In the present study a strategy based on response preprocessing, using Fourier-Bessel expansion is proposed to analyze MDOF systems. The coefficients of Fourier-Bessel expansion, obtained from the system response, are used to separate the modal components. Individual modal components are then analyzed by employing the procedure developed for SDOF systems. The procedure is numerically illustrated on a 2-dof system.

Resonance phenomenon of rotor-bearing system under acceleration, has been studied by few researchers earlier. Capability of Wavelet Transforms to decompose the response signal into its component in time frequency plane is used in the present study, to analyze the rotor response as it accelerates through a critical speed. Experiments are performed on a rotor-bearing test rig in the laboratory. Acceleration response recorded at the bearings caps are decomposed using Morlet wavelet. The Wavelet Transforms exhibit distinct ridges arising due to continuously increasing rotational speed and that due to the natural frequency of the system. The nonlinearity present in the system stiffness is clearly visible as the frequency of vibration shows amplitude dependence.

To summarize, Wavelet Transform based procedures for nonlinear system identification are proposed. SDOF system is rigorously classified for polynomial type of stiffness nonlinearity. Classification is carried further to explore the presence of symmetric and asymmetric forms of nonlinearity. Asymmetric forms of nonlinearity are then classified

between quadratic and mixed parity nonlinear oscillators. The sign of the nonlinear parameter is also determined. Error issues in parameter estimation of SDOF system are addressed and limitations of the procedure are discussed. For MDOF systems Fourier-Bessel expansion procedure is proposed for separation of the response in individual components, which are then separately analyzed for estimation of nonlinear parameters. Experimental investigations have been carried out on a rotor-bearing test rig and acceleration signals, while passing through critical speed are recorded and processed through Wavelet Transforms, for illustration of the suggested procedures.

ACKNOWLEDGEMENTS

December 2010   Rajkumar Porwal

Contents

List of Figures

List of Tables

Nomenclatures

a	Scale parameter
a_r	Scale corresponding to the ridge
b	Translational parameter
c	Damping coefficients
e	Unbalance eccentricity
$f(t), x(t), ...$etc	Small letters are used for functions in time domain
$g(t)$	Wavelet function
$h(t)$	Window function
j	Imaginary number $\sqrt{-1}$
k_1	Linear stiffness coefficient
k_2	Quadratic nonlinear stiffness coefficient
k_3	Cubic nonlinear stiffness coefficient
$\bar{t}$	Time centre of mother wavelet function
$\bar{t}_{b,a}$	Time centre of daughter wavelet function
$x(t),\ y(t)$	Response signal
$F(\omega), X(\omega)...$etc	Capital letters are used for corresponding functions in frequency domain
$G(\omega)$	Fourier Transform of wavelet function
$H(\omega)$	Fourier Transform of the window function
$\bar{H}, \bar{G}...$etc	Bar over the symbol is for corresponding complex conjugate quantity
α	Angular acceleration
$W(a,b)$	Wavelet Transform
ϵ_2	Nondimensional quadratic nonlinear stiffness parameter
ϵ_3	Nondimensional cubic nonlinear stiffness parameter
ω_0	Central frequency of the wavelet function
ω_n	Natural frequency of the system
$\bar{\omega}$	Frequency centre of mother wavelet function
$\bar{\omega}_{b,a}$	Frequency centre of daughter wavelet function

$\phi(t)$ Phase of the signal

σ_t Standard deviation of mother wavelet function in time domain

σ_ω Standard deviation of mother wavelet function in frequency domain

$\sigma_{t_{b,a}}$ Standard deviation of daughter wavelet function in time domain

$\sigma_{\omega_{b,a}}$ Standard deviation of daughter wavelet function in frequency domain

τ Nondimensional time

ζ Damping factor

$<>$ Inner product operator

Chapter 1

Introduction

Determination of the mathematical model and estimation of the various parameters therein, is crucial in nonlinear analysis. Response behaviour of nonlinear systems under specific excitation conditions can be predicted accurately only when the system structure and the parameters are appropriately known. While extensive research has been carried out in identification and parameter estimation of linear systems, research on nonlinear system identification has been relatively less. In the context of mechanical systems, while linearly behaving models need information about the mass, damping coefficient and stiffness parameters and techniques like experimental modal analysis are well established, nonlinear systems pose a more complex problem, due to the possibility of existence of various forms of the restoring and dissipative forces. Nonlinearity in these forces can be of a polynomial or non-polynomial form. The Duffing oscillator is a typical example of a system with polynomial form of restoring force nonlinearity, whereas quadratic damping, hysteretic damping and fractional power stiffness in rolling element bearings are some examples of non-polynomial forms of nonlinearity. Nonlinearity can be a symmetric function of displacement, as in Duffing oscillator or asymmetric as in the case of a bilinear oscillator. System definition problem of a nonlinear system, therefore, consists of (i) identification of the form of nonlinearity and representation through an appropriate

mathematical model and (ii) subsequent estimation of the various parameters in the mathematical model. Relatively less work has been done on the identification of the form of nonlinearity. Most of the reported works suggest parameter estimation procedures based on some assumed nonlinearity model.

Surveys of Kerschen et al. (2006) and Peng and Chu (2004) reveal that there is considerable interest in employing Wavelet Transforms based technique for linear and nonlinear system identification. In the present work, techniques based on Wavelet Transforms are investigated for nonlinear system identification and parameter estimation. The suggested procedures involve use of free vibration response of the system for its identification. The transient free vibration response of a weakly nonlinear system has been modeled as a signal whose amplitude envelope and instantaneous frequency change with time. Instantaneous frequency of response depends on amplitude of vibration and the type of stiffness present in the system while amplitude envelope of the response depends on the type of damping. Closed form analytical solutions are obtained from Krylov-Bogoliubov technique to establish the relationships for instantaneous frequency and amplitude envelope for a weakly nonlinear system (Nayfeh, 1973). Instantaneous frequency and amplitude envelope of the given signal have also been determined numerically, using the Wavelet Transforms (Mallat, 1998). The numerical results obtained from Wavelet Transforms and analytical solutions from Krylov-Bogoliubov technique are used in conjunction, to determine the system parameters.

A detailed literature review pertaining to Wavelet Transforms and their application in system identification is presented in Chapter 2.

In Chapter 3, a procedure developed to obtain free vibration response of damped quadratic and mixed parity oscillators using Krylove-Bogoibove method has been described. An approximate analytical solution for the nonlinear system has been provided. The Krylove-Bogoliubov method is applied separately to the positive and negative half-cycles of the free vibration response to account for asymmetric behavior of the nonlinear system. The solution is in the form of an asymptotic response signal, which establishes the relation-

ship for amplitude envelope and instantaneous frequency of response signal. Results developed in this chapter form the basis for the classification of stiffness nonlinearities, which is the subject matter of the next chapter. The approximations involved are also discussed in this Chapter.

Nonlinearity classification based on the form of the restoring force has been discussed in Chapter 4. Wavelet Transforms based procedures have been suggested to distinguish between various polynomial forms of stiffness nonlinearities. Initially, Wavelet Transforms and their properties are discussed briefly. Asymmetric nonlinearity in the form of quadratic oscillator and mixed parity oscillator is considered. Standard Morlet Wavelet and Complete Morlet Wavelet are used together to distinguish between the nonlinearities.

Parameter estimation procedure for Single Degree of Freedom (SDOF) nonlinear systems is described in Chapter 5. Emphasis is given on the accuracy of estimation. Analysis of the errors and approximations has been carried out and factors influencing accuracy of estimates are discussed. Duffing and van der Pol oscillators are considered for numerical illustration.

Multi degree of freedom (MDOF) system parameter estimation is considered in Chapter 6. Various modes of the system can be separated in time frequency plane using Wavelet Transforms, if the natural frequencies are well separated and analysis may be carried out in a manner similar to that employed for SDOF systems. However, for closely separated modes such an approach may give erroneous results. This problem is addressed by using Fourier-Bessel expansion as a preprocessor for modal separation. Cubic stiffness nonlinear terms with coupling are considered and the procedures are numerically illustrated. Damping is taken as linear.

Experimental investigations on a rotor-bearing system have been carried out to illustrate the proposed Wavelet Transforms based procedures. These are described in Chapter 7. Transient vibrations of the rotor, as it passes through critical speed, are acquired and processed for detection and identification of nonlinearity. Numerical simulation of the

response is carried out parallely for providing comparison with experimental response. The laboratory rig and instrumentation are discussed. While quantitative estimation of parameters of the rotor is not attempted, distinctive presence of stiffness nonlinearity has been demonstrated through the use of Wavelet Transforms.

Conclusions are presented in Chapter 8 along with scope for future work.

Chapter 2

Literature Review

Nonlinear system identification has been attempted by researchers in various branches of science and engineering. A detailed survey on nonlinear system identification may be found in a review paper by Kerschen et al. (2006). They have made a comparative study of the various prevalent procedures. Research in this area is ongoing as no generic technique can possibly accommodate all types of nonlinearity. Areas of investigations can be classified according to the method of analysis viz. Method of Linearization, Time Domain Methods, Frequency Domain Methods, Modal Methods, Time-Frequency Methods, Black-Box approach, Structural Modal Updating etc. Detailed description of some of these methods can be found in Worden and Tomlinson (2001). The presented work is primarily concerned with usage of Wavelet Transforms for nonlinear system identification. Wavelet Transforms are time- frequency representations of signals. Other time-frequency representations of signals include Short Time Fourier Transform (STFT), Wigner-Ville Distribution and Cohen Class distribution etc. A comprehensive description and comparison of various time-frequency methods can be found in Hammond and White (1996). Research pertaining to Wavelet Transforms usage is discussed in more detail in the following sections.

2.1   Historical Development of Wavelet Transforms

While the origin of wavelet functions can be traced back to Haar, (1910), active research in the area began only in the year 1984, through the works of Jean Morlet. Grossman gave a mathematical foundation to the ideas of Morlet and they published their work in 1985. They were the first to use the word 'Wavelet' (Hubbard, 1996). After the publication of the above mentioned paper, Yves Meyer (1986) was among the first to point out the earlier existence of wavelets in the field of mathematics. He provided concepts of orthogonal wavelets. This made wavelet functions, easier to work with. In 1986, Stephane Mallat, a former student of Meyer's linked the theory of Wavelet Transforms to the previously existing research in the field of image processing on subband coding and quadrature mirror filters. That too made the application of Wavelet transforms much easier (Mallat, 1998). Ingrid Daubechies proposed a new class of Wavelets in 1987. These were orthogonal and based on concepts of digital filtering. Daubechies' Wavelets are known as db1, db2...db10 after her name. (Daubechies, 1992). Most text books (Chui, 1992; Daubechies, 1992) dealing with the mathematical aspects of Wavelet Transforms came out in the early 1990's. Books related to engineering applications of Wavelet Transforms appeared in late 90's (Carmona and Torresani, 1998; Mallat, 1998).

Systematic application of Wavelet transforms in mechanical engineering problems, specifically for vibrations and acoustics, are relatively recent. The text book by Newland (1993) was among the first to deal the application of Wavelet Transforms to problems in the field of mechanical vibrations. He explained the theory of Daubechies Wavelet and applied it to analyze the vibration of a multi-storied building close to an underground railway. He also proposed new wavelets which came to be known as Harmonic Wavelets. In a series of papers Newland (1994a,b, 1999) applied the Wavelet Transforms to the problems related to acoustics.

Applications of Wavelet Transforms in mechanical vibration analysis, can be broadly classified into two categories: (i) Condition monitoring and (ii) System identification.

Review paper by Peng and Chu (2004) discussed efforts of various researchers in condition monitoring using Wavelet Transforms.

The present thesis is related to nonlinear system identification. The following section describes the ongoing work in this area in more detail.

2.2   Wavelet Transforms in System Identification

The response of a system to an impulse excitation is non-stationary. Time-frequency methods are an appropriate choice to analyze such non-stationary signals. Such time-frequency analysis normally provides significant insight into the system properties and provides help in estimating the parameters of the system. Surveys of Kerschen et al. (2006) and Peng and Chu (2004) reveal that there has been considerable interest in employing wavelet techniques for nonlinear system identification during the past decade. The techniques use free vibration response of the system for its identification. System identification using Wavelet Transforms can be classified in the following categories: (i) Linear System Identification and (ii) Nonlinear System Identification - both for systems with one degree of freedom or more than one degrees of freedom.

2.2.1   Linear System Identification

Wavelet techniques were initially used for linear system identification. For a linear Single Degree of Freedom (SDOF) System , identification involves estimation of damping and natural frequency of the system while for Multi Degree of Freedom (MDOF) linear systems, it involves estimation of modal parameters viz modal damping ratios, natural frequencies and mode shapes.

Ruzzene et al. (1997) and Staszewski (1997) were among the first to apply Wavelet Transforms for estimation of parameters of linear SDOF and MDOF systems. Staszewaski pro-

vided a rigorous background and explored various aspects of Wavelet transformed data. Ruzzene et al. (1997) analyzed the free response of the system using Morlet wavelet. After transforming the free response in time scale domain through Wavelet Transforms they extracted the envelope and phase of the transform along a particular scale. Using these data they were able to estimate the damping ratio and natural frequency. They extended the same idea to MDOF system. They showed the modes are decoupled in the time- frequency domain and hence each mode can be analyzed by the method developed for the SDOF system. The theory was justified by numerical simulation and application to real data of Queensborough Bridge in Canada. They also conducted the comparative study between Wavelet Transforms based methods and Hilbert Transform based methods and showed the superiority of Wavelet Transforms based methods over the Hilbert Transform based method. The two limitations of the procedure as highlighted by the authors were that close modes could not be decoupled and mode shapes could not be estimated.

Staszewski (1997) analyzed the data of Wavelet Transforms in the three different ways namely Wavelet Transforms cross section, impulse response recovery using wavelet reconstruction formula and ridges and skeletons of the Wavelet Transforms. Above three methods were applied to the simulated data of SDOF and 2-DOF systems, and study shows that the method based on wavelet ridges and skeletons gives the best accuracy in presence of noise in the data.

There were issues related to the accuracy in parameter estimation and separation of close modes. Improvement in accuracy of parameter estimation was achieved by addressing the presence of edge effect in Wavelet Transforms of the response signal. Separation of close modes was improved by optimizing the parameters of Morlet wavelet. Errors occur at the beginning and end time indexes while calculating Wavelet Transforms of the response signal. This phenomenon, known as edge effect or end effect, was analyzed by Kijewski and Kareem (2002) who considered the Morlet wavelet function and quantified the length of the data affected by the edge effect. They proposed a padding scheme

to reduce the edge effect. A signal mirroring scheme was suggested by Simonovski and Boltezar (2003) to minimize the edge effect. They considered the examples of Gabor, Morlet and General harmonic wavelet functions. Boltezar and Slavic (2004) studied the edge effect problem in detail and suggested three methods for its remedy, namely, (i) reflected-window method, (ii) equal-window area method and (iii) adaptive wavelet function method.

Lin and Qu (2000) modified the classical Morlet wavelet in an optimal way, using the criterion of minimum wavelet coefficient entropy. The criterion modifies the Morlet wavelet function such that the total number of Wavelet Transforms coefficients of the signal is lowest. He used the modified Morlet wavelet function in a feature extraction problem for mechanical fault diagnosis. Later this concept was introduced for linear and nonlinear system parameter estimation. The optimized Morlet wavelet is useful in separation of modes of a MDOF system in time-frequency plane.

Later, investigators have taken into account the edge effects and employed modified Morlet wavelet for system identification. A theoretical and experimental study for damping identification was carried out by Slavic et al. (2003) taking edge effect into account. Lardies and Gouttebroze (2002) modified the Morlet wavelet and determined modal parameters such as natural frequency, damping ratio and mode shapes of a tower excited by the wind. Le and Argoul (2004) considered three complex wavelets, namely Morlet, Cauhy and Harmonic wavelets and compared their suitability to determine the modal parameters of the system.

2.2.2   Nonlinear System Identification

The capability of Wavelet Transforms to capture instantaneous frequency and amplitude envelope makes it suitable for the identification of nonlinear systems also. Developments in nonlinear system identification techniques took place contemporarily with the linear

system identification. Procedures use free vibration response of the system for its iden-
tification. The transient free vibration response of a weakly nonlinear system can be
modeled as a signal whose amplitude envelope and instantaneous frequency change with
time. The closed form solutions obtained from Krylov-Bogoliubov technique establish
the relationships for amplitude envelope and instantaneous frequency for a weakly non-
linear system (Nayfeh, 1973). Instantaneous frequency and amplitude envelope of the
given signal can also be determined numerically using the Wavelet Transforms (Mallat,
1998). The numerical results obtained from Wavelet Transforms and closed form solu-
tions from Krylov-Bogoliubov technique are used in conjunction to determine the system
parameters.

Staszewski (1998) employed the Morlet wavelet function and applied the methodology
based on ridges and skeleton of Wavelet Transforms to estimate nonlinear parameters.
He numerically simulated two nonlinear systems; one had coulomb damping with cubic
stiffness non-linearity and the other was an MDOF system with cubic stiffness nonlin-
earity in one of the modes. The error in estimation of nonlinear parameter was of the
order of 3 % in absence of noise.

Argoul and Le (2003) employed continuous Cauchy wavelet for the analysis of accelero-
metric response of a structure. They proposed four instantaneous indicators to charac-
terize nonlinear mechanical structure from their transient response.

Lardies and Ta (2005) considered a system containing the nonlinear damping. The
modified Morlet wavelet function was used. The edge effect was taken into account. The
two methods for analysis, (i) wavelet cross section method and (ii) ridges and skeleton
method, were used. They concluded that the method based on ridge and skeleton is
better in presence of noise in the data. The error in parameter estimation was of the
order of 5 % in presence of noise.

Ta and Lardies (2006) addressed systems having polynomial type of nonlinearity on
damping and stiffness. They demonstrated the application of the procedure on the

systems with symmetric polynomial type of stiffness nonlinearities. They took three examples for numerical simulation to validate the procedure: the first example pertains to cubic stiffness nonlinearity, the second involves composite nonlinearities on damping and stiffness and the third example contains cubic stiffness nonlinearity in MDOF system. The range of parameter estimation errors was 0.4-5.2 % for different nonlinear parameters and for different noise levels in the response.

2.3   Remarks

The literature review revels that the Wavelet Transforms have been used to estimate the linear and nonlinear system parameters. In case of nonlinear system, symmetric stiffness nonlinearities like the Duffing oscillators are generally assumed and subsequently system parameters are estimated. Hence, the nonlinear parameter estimation is limited to the assumptions of symmetric nonlinearities. Moreover, the researchers have used specific nonlinear systems for simulations and validation of Wavelet Transform based parameter estimation procedures. The mathematical models were not nondimensionalised and therefore the results obtained can not be generalized. Accuracy of parameter estimation is improved by addressing the problem of edge effect in Wavelet Transforms. Separation of close modes in case of MDOF system is achieved using modified Morlet wavelets. It is observed that the close modes give rise to inaccuracy in parameter estimation due to presence of cross terms in scalogram representation of Wavelet Transforms.

In this thesis, we propose an improved way of estimation of nonlinear parameters of SDOF and MDOF system by adopting a different approach as discussed below. We have used nondimensional mathematical models for the nonlinear systems and therefore the results can be applied to a class of systems represented by the same nondimensional mathematical models. The refining algorithm is used to estimate the ridge location accurately in time frequency plane. This results in smooth backbone curve which leads

to better estimation of nonlinear parameter. Two famous nonlinear oscillators namely the Duffing oscillator and the van der Pol oscillator are simulated over a wide range of parameters and estimation errors are analyzed. The algorithm is checked for robustness against noise and its sensitivity for the sampling frequency. These findings help in design of experiments for the parameter estimations of nonlinear systems

The presented work emphasizes on the classification of stiffness nonlinearities using Wavelet Transforms before we estimate the system parameters. This classification helps in the development of better mathematical model of a system. Krylov-Bogoliubov method is adopted to obtain the response of quadratic and mixed-parity type of asymmetric nonlinear oscillators. Analytical solution so obtained is used in conjunction with the Wavelet Transforms of the response for the classification of nonlinearities.

In case of MDOF nonlinear system, response is considered as multi-component signal which is separated in its individual components using Fourier-Bessel expansion. Separation of individual components in this way avoids the difficulties arising due to cross terms in the scalogram. Subsequently each separated component is analyzed by the method developed for SDOF system.

Finally, study of a accelerated rotor passing through critical speed is carried out. The vibration signals at resonance are separated in its components, in time frequency plane using Wavelet Transforms. Wavelet Transform ridges for the individual components are used to identify nonlinearities. Simulated results of linear and nonlinear rotors along with the experimentally obtained results of a rotor are suggested for the quantification of nonlinear parameters.

Chapter 3

Response of Damped Quadratic and Mixed-Parity Nonlinear Oscillator

In this chapter, response of undamped quadratic and mixed parity nonlinear oscillators obtained by various researchers is initially discussed. Thereafter approximate analytic solutions of linearly damped quadratic and mixed parity nonlinear oscillators are obtained using Krylov-Bogoliubov method.

Krylove - Bogoliubov method provides the approximate analytical solution to a nonlinear system in the form of asymptotic response signal, which establishes the relationship for amplitude envelope and instantaneous frequency of response signal. The method is applied separately to positive and negative half cycles of the oscillations to account for asymmetric characteristic of system. The solution so obtained is validated using numerical simulations.

The results obtained here forms the basis for the classification of stiffness nonlinearity which is the subject matter of next chapter.

3.1   Introduction

Undamped oscillators having quadratic and mixed parity type of nonlinearity in stiffness have been investigated by many researchers (Nayfeh, 1979, 1981; Mickens, 1995; Hu, 2006, 2007). Structures showing different stiffness in tension and compression and those constructed in asymmetric form can be modeled by these nonlinearities. For example the eardrum is best modeled by quadratic nonlinear oscillator while the nonlinear free vibrations of thin laminated plates are best modeled by mixed parity nonlinear oscillators (Mickens, 1995).

Quadratic nonlinear oscillator

Mickens (1995) represented the undamped quadratic nonlinear oscillator in nondimensional form as

$$\ddot{y}(\tau) + y(\tau) + \epsilon y^2(\tau) = 0, \qquad y(0) = A, \qquad \dot{y}(0) = 0 \tag{3.1}$$

where dot ($\dot{\ }$) represents differentiation with respect to nondimensional time parameter τ. He analyzed the system with weak quadratic nonlinearity using different methods like Lindstedt-Poincare perturbation method, Krylov-Bogoliubov method and the Krylov-Bogoliubov-Mitropolsky method. A brief description of the solutions obtained by these methods is given below. The first order approximation by any of these methods is unable to incorporate the effect of quadratic nonlinearity on the oscillation frequency. The second order approximation by Lindstedt-Poincare perturbation method gives the following result

$$
\begin{aligned}
y(\theta, \epsilon) &= y_0(\theta) + \epsilon y_1(\theta) + \epsilon^2 y_2(\theta) + ... \tag{3.2} \\
&= A\cos\theta + \epsilon\left(\frac{A^2}{6}\right)(-3 + 2\cos\theta + \cos 2\theta)... \\
&\quad + \epsilon^2\left(\frac{A^3}{3}\right)\left[-1 + \left(\frac{29}{48}\right)\cos\theta + \left(\frac{1}{3}\right)\cos 2\theta + \left(\frac{1}{16}\right)\cos 3\theta\right] + O\left(\epsilon^3\right) \tag{3.3}
\end{aligned}
$$

where $\theta = \omega(\epsilon)\tau$, and

$$\omega(\epsilon) = 1 + \epsilon\omega_1 + \epsilon^2\omega_2 + ... \tag{3.4}$$

$$= 1 - \epsilon^2\left(\frac{5A^2}{12}\right) + O\left(\epsilon^3\right) \tag{3.5}$$

The Krylov-Bogoliubov method which is a first order averaging technique is unable to incorporate effects of small quadratic nonlinearity in the analytic expression governing the response of the system (Mickens, 1995).

Krylov-Bogoliubov-Mitropolsky method is used for second order approximation and the response of the system is as follows

$$y = A_0\cos\left[\left(1 - \frac{5\epsilon^2 A_0^2}{12}\right)\tau + \theta_0\right] + \epsilon\left(\frac{A_0^2}{6}\right)\left\{\cos\left[2\left(1 - \frac{5\epsilon^2 A_0^2}{12}\right)\tau + 2\theta_0\right] - 3\right\} \tag{3.6}$$

where A_0 and θ_0 are constants. These results show that the effect of quadratic nonlinearity on fundamental frequency of oscillation appears in the second order approximation. Similar finding was also reported by Nayfeh (1981).

Hu (2006) studied the solution by the Lindstedt-Poincare perturbation method and presented an improved solution using Harmonic Balance methods. He analyzed the positive and negative displacement parts of oscillatory motion separately for better accuracy. He showed that the first order approximate solution by Harmonic Balance method is more accurate than the second order approximate solution obtained by Lindstedt-Poincare perturbation method. The solution is as given below

$$y = A\cos\left(\sqrt{1 + \frac{8\epsilon A}{3\pi}}\right)\tau \qquad \text{for} \quad y > 0 \tag{3.7}$$

$$y = B\cos\left(\sqrt{1 - \frac{8\epsilon A}{3\pi}}\right)\tau \qquad \text{for} \quad y < 0 \tag{3.8}$$

$$B = \frac{1}{4\epsilon}\left[3 + 2\epsilon A - 3\sqrt{1 - \frac{4}{3}\epsilon A(1 + \epsilon A)}\right] \tag{3.9}$$

The amplitude of oscillation, B in the negative direction was obtained by integrating the conservative system equation (3.1) and then solving the resulting cubic algebraic equation.

Mixed parity nonlinear oscillator

Mickens (1995) represented the undamped mixed parity nonlinear oscillator in its nondimensional form as

$$\ddot{y} + y + \epsilon_2 y^2 + \epsilon_3 y^3 = 0, \qquad y(0) = A, \qquad \dot{y}(0) = 0 \tag{3.10}$$

He analyzed the oscillator using Lindstedt-Poincare perturbation method with proper scaling. The solution obtained was

$$
\begin{aligned}
y(\theta, A) &= A\cos\theta + \left(\frac{\epsilon_2 A^2}{6}\right)[-3 + 2\cos\theta + \cos 2\theta] \\
&+ \left(\frac{A^3}{3}\right)\left[-\epsilon_2^2 + \left(\frac{174\epsilon_2^2 - 27\epsilon_3}{288}\right)\cos\theta + \left(\frac{\epsilon_2^2}{3}\right)\cos 2\theta + \left(\frac{2\epsilon_2^2 + 3\epsilon_3}{32}\right)\cos 3\theta\right] \\
&+ O(A^3)
\end{aligned}
\tag{3.11}
$$

where $\theta = \omega\tau$, and

$$\omega(A) = 1 + A^2\left(\frac{9\epsilon_3 - 10\epsilon_2^2}{24}\right) + O(A^3) \qquad \text{where} \quad 0 < A << 1 \tag{3.12}$$

Hu (2007) studied the above solution and presented improved solution using Harmonic Balance methods. He nondimensionalized the equation in the following form

$$\ddot{y} + y + \epsilon y^2 + y^3 = 0, \qquad y(0) = A > 0, \qquad \dot{y}(0) = 0 \tag{3.13}$$

He analyzed the positive and negative displacement parts of the oscillatory motion separately, for better accuracy. He showed that for large amplitude of oscillations, the first order approximate solution by Harmonic Balance method is more accurate than the

second order approximate solution by Lindstedt-Poincare perturbation method. The solution is as given below

$$y \;=\; A\cos\left(\sqrt{1+\frac{8\epsilon A}{3\pi}+\frac{3A^2}{4}}\,\right)\tau \qquad\qquad \text{for}\quad y>0 \qquad\qquad (3.14)$$

$$y \;=\; B\cos\left(\sqrt{1-\frac{8\epsilon B}{3\pi}+\frac{3B^2}{4}}\,\right)\tau \qquad\qquad \text{for}\quad y<0 \qquad\qquad (3.15)$$

The amplitude B in the negative direction was obtained in terms of A by integrating the conservative equation (3.13) and then solving the resulting fourth order algebraic equation.

The study of relevant literature shows that most of the previous works were related to the study of periodic solutions of undamped oscillators having quadratic and mixed parity type of nonlinearity in the stiffness of the system. In the present work linearly damped oscillators having quadratic and mixed parity type of nonlinearity in stiffness of the system are considered. The transient solution of the damped oscillator is obtained using the Krylov-Bogoliubov method. The positive and negative displacement parts of the oscillatory motion are considered separately, by considering two equivalent auxiliary equations of the system. The amplitude of oscillations during the positive motion and negative motion are obtained using the Principle of Energy Balance. The analytic solution and the solution obtained through numerical simulation using fourth order Runge-Kutta method are compared.

3.2 Response of Damped Quadratic and Mixed-Parity Nonlinear Oscillator

Krylov-Bogoliubov method is discussed in brief and then response of the damped quadratic and mixed parity nonlinear oscillator is obtained.

Krylov-Bogoliubov Technique

This method is based on averaging technique. For a weakly nonlinear system represented by

$$\ddot{x} + \omega_n^2 x = \epsilon f(x, \dot{x}),$$

(3.16)

the response, when $\epsilon = 0$, is given by

$$x = A\cos(\omega_n t + \theta)$$

(3.17)

where A and θ are constant and depend on the initial conditions. To determine an approximate solution to equation (3.16) for small ϵ but different from zero, Krylov and Bogoliubov assumed that the solution is still given by expression (3.17) but with time varying A and θ, and subjected to the following conditions (Nayfeh, 1973).

$$
\begin{aligned}
x & = A(t)\cos[\omega_n t + \theta(t)] \\
& = A(t)\cos\phi && \text{where} \quad \phi = [\omega_n t + \theta(t)] && (3.18) \\
\dot{x} & = -A(t)\omega_n \sin[\omega_n t + \theta(t)] \\
& = -A(t)\omega_n \sin\phi && && (3.19)
\end{aligned}
$$

$A(t)$ is known as the amplitude envelope of the response signal. The instantaneous frequency of the response signal is time derivative of the phase i.e. $[\omega_n + \dot{\theta}(t)]$.

Further simplification results in expressions for $\dot{A}(t)$ and $\dot{\theta}(t)$ as follows.

$$
\begin{aligned}
\dot{A}(t) & = -\frac{\epsilon}{\omega_n}\sin\phi f(A\cos\phi, -A\omega_n\sin\phi) && (3.20) \\
\dot{\theta}(t) & = -\frac{\epsilon}{A\omega_n}\cos\phi f(A\cos\phi, -A\omega_n\sin\phi) && (3.21)
\end{aligned}
$$

Hence the original second order differential equation (3.16) is converted into two first order differential equations given by equation (3.20) and (3.21). In other words we can say that the original second order differential equation is exactly equivalent to the two

first order differential equations. No approximation has been made till this stage and it is merely equivalent to coordinate transformation from rectangular to polar.

Following argument is made to solve it approximately. The right hand side of these two equation are periodic function with respect to variable ϕ. Hence $\dot{A} = O(\epsilon)$ and also $\dot{\theta} = O(\epsilon)$. Thus A and θ are slowly varying function of time because ϵ is small, hence they change very little during the time $T = \frac{2\pi}{\omega_n}$ (the period of the terms on the right hand side of these equations). Averaging these two equation over the interval $[t, t+T]$, during which A and θ can be taken to be constant on the right hand side of these equations, we obtain the following expressions.

$$
\begin{aligned}
\dot{A}(t) &= -\frac{\epsilon}{2\omega_n} f_1(A) & \text{(3.22)} \\
\dot{\theta}(t) &= -\frac{\epsilon}{2A\omega_n} g_1(A) & \text{(3.23)}
\end{aligned}
$$

where

$$
\begin{aligned}
f_1(A) &= \frac{1}{\pi} \int_0^{2\pi} \sin\phi f(A\cos\phi, -A\omega_n \sin\phi) \mathrm{d}\phi & \text{(3.24)} \\
g_1(A) &= \frac{1}{\pi} \int_0^{2\pi} \cos\phi f(A\cos\phi, -A\omega_n \sin\phi) \mathrm{d}\phi & \text{(3.25)}
\end{aligned}
$$

Here $f_1(A)$ and $g_1(A)$ are simply two coefficients of Fourier series expansion of $f(x, \dot{x})$ or $f(A\cos\phi, -A\omega_n \sin\phi)$.

Response of damped mixed parity nonlinear oscillator

The linearly damped mixed parity nonlinear oscillator is analyzed here. The damped quadratic nonlinear oscillator is considered as the special case of the mixed parity nonlinear oscillator in which cubic stiffness term is absent. Free vibrations of the oscillator, initiated by imparting some initial velocity, can be modeled as

$$
mx'' + cx' + k_1 x + k_2 x^2 + k_3 x^3 = 0, \qquad x(0) = 0, \qquad \dot{x}(0) = B \tag{3.26}
$$

where ($'$) represents the differentiation with respect to time t. The above equation is converted to nondimensional form by defining the following parameters.

$$\frac{k_1}{m} = \omega_n^2 \qquad \frac{c}{2m\omega_n} = \zeta \qquad \tau = \omega_n t \qquad x = \frac{B}{\omega_n} y$$

$$\dot{x} = \frac{\mathrm{d}x}{\mathrm{d}\tau} \qquad \epsilon_2 = \frac{k_2}{k_1}\frac{B}{\omega_n} \qquad \epsilon_3 = \frac{k_3}{k_1}\left(\frac{B}{\omega_n}\right)^2$$

Using the above parameters, equation (3.26) can be represented in the following nondimensional form

$$\ddot{y} + 2\zeta\dot{y} + y + \epsilon_2 y^2 + \epsilon_3 y^3 \;=\; 0, \qquad y(0) = 0 \qquad \dot{y}(0) = 1 \tag{3.27}$$

In absence of quadratic term, the response of the system is given by Mickens (1995)

$$y(\tau) \;=\; A_0 e^{-\zeta\tau} \cos\left[\tau + \int_0^\tau \frac{3}{8}\epsilon_3 A^2(\tau)\mathrm{d}\tau + \theta_0\right] \tag{3.28}$$

where amplitude envelope $A(\tau)$ and instantaneous frequency $\omega(\tau)$ are given by the following expressions

$$A(\tau) \;=\; A_0 e^{-\zeta\tau} \tag{3.29}$$

$$\omega(\tau) \;=\; 1 + \dot{\theta}(\tau)$$

$$\;=\; 1 + \frac{3}{8}\epsilon_3 A^2(\tau) \tag{3.30}$$

Presence of quadratic term makes the problem little involved. The stiffness characteristic of the system is different during positive and negative displacement due to the presence of $\epsilon_2 y^2$ term in the system equation. To analyze the motion in positive and negative direction separately by Krylov-Bogoliubov technique, following two equivalent auxiliary equations are considered

$$\ddot{y} + 2\zeta\dot{y} + y + \epsilon_2 y\,|y| + \epsilon_3 y^3 = 0 \qquad \text{when} \quad y > 0 \tag{3.31}$$

$$\ddot{y} + 2\zeta\dot{y} + y - \epsilon_2 y\,|y| + \epsilon_3 y^3 = 0 \qquad \text{when} \quad y < 0 \tag{3.32}$$

The positive displacement motion is governed by the equation (3.31). Analyzing the equation for its instantaneous amplitude $A(\tau)$ and $\dot{\theta}(\tau)$ using Krylov-Bogoliubov method we get (refer Appendix A)

$$A(\tau) = A_{pi}e^{-\zeta\tau} \tag{3.33}$$
$$\dot{\theta}(\tau) = \frac{4\epsilon_2 A(\tau)}{3\pi} + \frac{3\epsilon_3 A^2(\tau)}{8} \tag{3.34}$$

Therefore the instantaneous frequency is given by

$$\omega_{ipi}(t) = \left(1 + \frac{4\epsilon_2 A(\tau)}{3\pi} + \frac{3\epsilon_3 A^2(\tau)}{8}\right) \tag{3.35}$$

For small damping the average frequency (ω_{pi}) during the positive half motion can be approximated by

$$\omega_{pi} = \left(1 + \frac{4\epsilon_2 Y_{pi}}{3\pi} + \frac{3\epsilon_3 Y_{pi}^2}{8}\right) \tag{3.36}$$

where Y_{pi} is amplitude of oscillation during i^{th} positive motion. Therefore the response can be represented by

$$y_{pi}(\tau) = A_{pi}e^{-\zeta\tau}\cos\left[\omega_{pi}\tau + \theta_{pi}\right] \tag{3.37}$$

where A_{pi} and θ_{pi} are constants and depend on the conditions at the beginning of the motion.

The negative displacement motion is governed by the equation (3.32). The analysis in the similar way as performed for positive displacement motion provides the average frequency during j^{th} negative displacement as

$$\omega_{nj} = \left(1 - \frac{4\epsilon_2 Y_{nj}}{3\pi} + \frac{3\epsilon_3 Y_{nj}^2}{8}\right) \tag{3.38}$$

where Y_{nj} is amplitude of oscillation during j^{th} negative motion. Therefore the response can be represented by

$$y_{nj}(\tau) = A_{nj}e^{-\zeta\tau}\cos\left[\omega_{nj}\tau + \theta_{nj}\right] \qquad (3.39)$$

where A_{nj} and θ_{nj} are constants and depend on the conditions at the beginning of the motion.

A representative response of damped mixed parity nonlinear oscillator is shown in Figure 3.1. Further analysis of oscillatory motion is described with reference to this figure. We have assumed that the free vibrations are initiated by imparting initial velocity to the system.
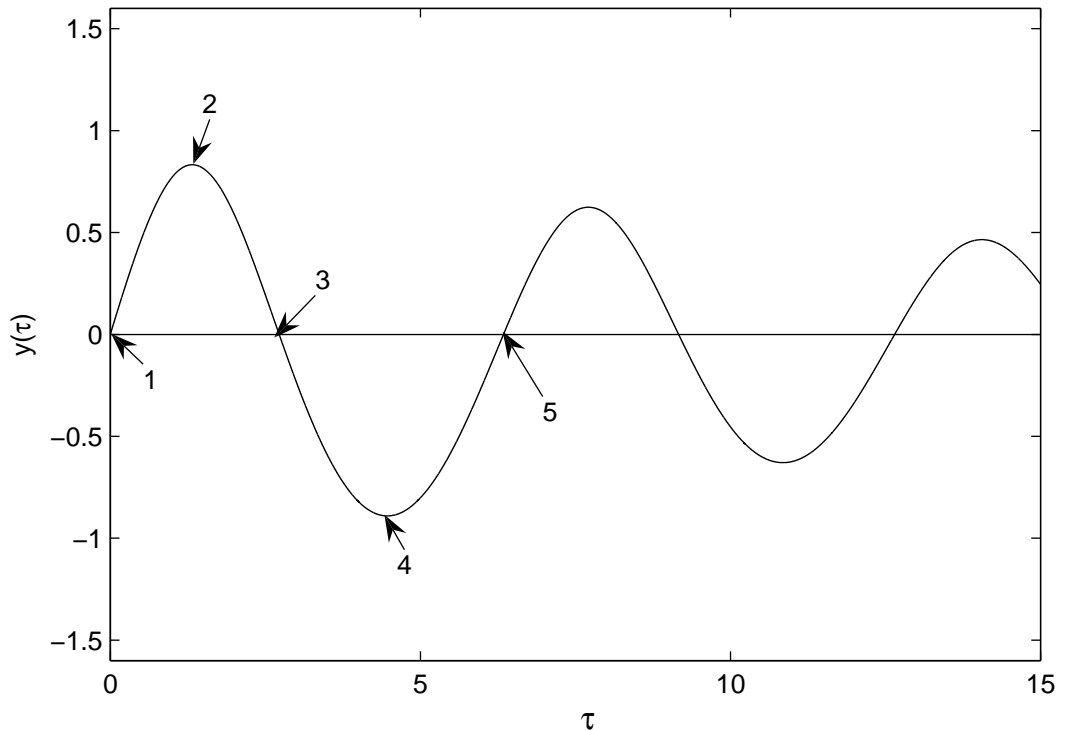
Figure 3.1: Response of a linearly damped mixed parity nonlinear oscillator

3.2.1   Response During Positive Half Cycle

Let the motion between points 1-2-3 in Figure 3.1 as 1st positive half displacement of the oscillation, therefore the response (3.37) can be written as

$$y_{p1}(\tau) \;=\; A_{p1}e^{-\zeta\tau}\cos\left[\omega_{p1}\tau + \theta_{p1}\right] \qquad\qquad \tau_1 \le \tau \le \tau_3 \qquad\qquad (3.40)$$

where τ_i represent the time at i^{th} instance during the motion. Here $\tau_1 = 0$. The nondimensionalized model of the system has the following initial conditions.

$$y_{p1}(\tau_1) \;=\; 0 \qquad\qquad\qquad\qquad (3.41)$$

$$\dot{y}_{p1}(\tau_1) \;=\; v_1 \qquad\qquad \text{where} \quad v_1 = 1 \qquad\qquad (3.42)$$

Solving the above two equations for the unknown constants A_{p1} and θ_{p1}, the response of the system is

$$y_{p1}(\tau) \;=\; \frac{v_1}{\omega_{p1}}e^{-\zeta(\tau-\tau_1)}\sin\left[\omega_{p1}(\tau - \tau_1)\right] \qquad\qquad \tau_1 \le \tau \le \tau_3 \qquad\qquad (3.43)$$

The velocity during the motion is obtained by differentiating the above equation

$$\dot{y}_{p1}(\tau) = v_1 e^{-\zeta(\tau-\tau_1)}\cos\left[\omega_{p1}(\tau - \tau_1)\right] - \zeta\frac{v_1}{\omega_{p1}}e^{-\zeta(\tau-\tau_1)}\sin\left[\omega_{p1}(\tau - \tau_1)\right] \qquad (3.44)$$

At instance 3, the time τ_3 is $[\tau_1 + (\pi/\omega_{p1})]$. Therefore the velocity at instance 3 is

$$\dot{y}_{p1}(\tau_3) = -v_1 e^{-\zeta\pi/\omega_{p1}} \qquad\qquad (3.45)$$

The response during the positive half of the oscillation is represented by the equation (3.43) in which ω_{p1} depends on the amplitude of oscillation Y_{p1}, which is unknown at present. The amplitude of oscillation Y_{p1} and the frequency ω_{p1} is calculated by applying

energy balance between instance 1 and instance 2 of the motion. The energy balance equation can be written as

$$E2 - E1 + EL12 = 0 \tag{3.46}$$

where $E1$ and $E2$ are the total energy of the system at instances 1 and 2 respectively while $EL12$ is energy loss due to viscous friction during the motion 1-2. The total energy at instance 1 is kinetic energy and is given by $(v_1^2/2)$ while the total energy at instance 2 is potential energy and is given by $\left(\frac{Y_{p1}^2}{2} + \epsilon_2 \frac{Y_{p1}^3}{3} + \epsilon_3 \frac{Y_{p1}^4}{4} \right)$.
Therefore,

$$\frac{Y_{p1}^2}{2} + \epsilon_2 \frac{Y_{p1}^3}{3} + \epsilon_3 \frac{Y_{p1}^4}{4} - \frac{v_1^2}{2} + EL12 = 0 \tag{3.47}$$

$$\omega_{p1} = 1 + \frac{4\epsilon_2 Y_{p1}}{3\pi} + \frac{3\epsilon_3 Y_{p1}^2}{8} \tag{3.48}$$

$$\tau_2 = \tau_1 + \frac{1}{\omega_{p1}} \tan^{-1} \left(\frac{\omega_{p1}}{\zeta} \right) \tag{3.49}$$

$$EL12 = \int_{\tau_1}^{\tau_2} 2\zeta \left[\dot{y}_{p1}(\tau) \right]^2 \mathrm{d}\tau \tag{3.50}$$

where τ_2 is the time when velocity is zero and amplitude attains the maximum value. The set of above four equations (3.47) – (3.50) are solved for unknown quantities ω_{p1} and Y_{p1} through standard numerical methods. Equation (3.47) is first solved numerically for Y_{p1} using some approximate guess value for $EL12$. Then ω_{p1}, τ_2 and $EL12$ are calculated using the equations (3.48), (3.49) and (3.50) respectively. Using the value of $EL12$ obtained, equations (3.47) – (3.50) are solved iteratively till the desired accuracy is obtained. The iterative procedure is stopped when two consecutive values of Y_{p1} are having difference less then 0.001.

3.2.2   Response During Negative Half Cycle

For the motion between points 3-4-5 in Figure 3.1 (1st negative half displacement of oscillation), the response (3.39) is written as

$$y_{n1}(\tau) \quad = \quad A_{n1}e^{-\zeta\tau}\cos\left[\omega_{n1}\tau + \theta_{n1}\right] \qquad\qquad \tau_3 \leq \tau \leq \tau_5 \qquad\qquad (3.51)$$

Initially, at time τ_3, the displacement is zero and the velocity is given by the equation (3.45); hence the initial conditions for the motion are

$$y_{n1}(\tau_3) \quad = \quad 0 \qquad\qquad (3.52)$$

$$\dot{y}_{n1}(\tau_3) \quad = \quad v_3 \qquad\qquad (3.53)$$

Solving the above two equations for the unknown constants A_{n1} and θ_{n1}, we get the response of the system as

$$y_{n1}(\tau) \quad = \quad \frac{v_3}{\omega_{n1}}e^{-\zeta(\tau-\tau_3)}\sin\left[\omega_{n1}(\tau-\tau_3)\right] \qquad\qquad \tau_3 \leq \tau \leq \tau_5 \qquad\qquad (3.54)$$

The velocity during the motion is obtained by differentiating the above equation

$$\dot{y}_{n1}(\tau) = v_3 e^{-\zeta(\tau-\tau_3)}\cos\left[\omega_{n1}(\tau-t_3)\right] - \zeta\frac{v_3}{\omega_{n1}}e^{-\zeta(\tau-\tau_3)}\sin\left[\omega_{n1}(\tau-\tau_3)\right] \qquad\qquad (3.55)$$

At instance 5, the time τ_5 is $[\tau_3 + (\pi/\omega_{n1})]$. Therefore the velocity at instance 5 is

$$\dot{y}_{n1}(\tau_5) = -v_3 e^{-\zeta\pi/\omega_{n1}} \qquad\qquad (3.56)$$

The response during the negative half of the oscillation is represented by the equation (3.54) where ω_{n1} depends on the amplitude of oscillation Y_{n1}, which is unknown at present. The amplitude of oscillation Y_{n1} and the frequency ω_{n1} are calculated by applying energy balance between instance 3 and instance 4 of the motion. The energy balance equation can be written as

$$E4 - E3 + EL34 = 0 \qquad\qquad (3.57)$$

where $E3$ and $E4$ are the total energy of the system at instances 3 and 4 respectively while $EL34$ is energy loss due to viscous friction during the motion 3-4. The total energy at instance 3 is kinetic energy and is given by $(v_3^2/2)$ while the total energy at instance 4 is potential energy and is given by $\left(\frac{Y_{n1}^2}{2} - \epsilon_2 \frac{Y_{n1}^3}{3} + \epsilon_3 \frac{Y_{n1}^4}{4}\right)$. Therefore,

$$\frac{Y_{n1}^2}{2} - \epsilon_2 \frac{Y_{n1}^3}{3} + \epsilon_3 \frac{Y_{n1}^4}{4} - \frac{v_3^2}{2} + EL34 = 0 \tag{3.58}$$

$$\omega_{n1} = 1 - \frac{4\epsilon_2 Y_{nj}}{3\pi} + \frac{3\epsilon_3 Y_{nj}^2}{8} \tag{3.59}$$

$$\tau_4 = \tau_3 + \frac{1}{\omega_{n1}} \tan^{-1}\left(\frac{\omega_{n1}}{\zeta}\right) \tag{3.60}$$

$$EL34 = \int_{\tau_3}^{\tau_4} 2\zeta \left[\dot{y}_{n1}(\tau)\right]^2 d\tau \tag{3.61}$$

where τ_4 is the time when the displacement is maximum. Unknown parameters ω_{n1} and Y_{n1} are obtained by solving the set of above four equations, (3.58) – (3.61) iteratively through standard numerical methods. First iteration starts with the assumption of a reasonable value of $EL34$ in equation (3.58) and it continues till the desired accuracy is achieved. The iterative procedure is stopped when two consecutive values of Y_{n1} are having difference less then 0.001.

The analytical solution for the complete oscillatory motion can be obtained by applying the above procedure for positive and negative displacement repeatedly.

3.2.3 Illustration

The system response obtained through numerical simulation and analytical method are compared. Two response parameters are considered for this purpose, the amplitude of oscillation and the average frequency of oscillation during the positive and negative half cycles. Comparison is shown in Figures 3.2 and 3.3 and Table 3.1-3.4. The amplitude Y_{p1} and equivalent frequency ω_{p1} for the positive half cycle and amplitude Y_{n1} and equivalent frequency ω_{n1} for negative half cycle are obtained analytically as described in section 3.2. The corresponding quantities Y_{p1_s}, ω_{p1_s}, Y_{n1_s} and ω_{n1_s} are obtained through numerical

simulation. The percentage error is denoted by e, e.g. $e_{y_{p1}}$.

Damped quadratic nonlinear oscillator

The damped quadratic nonlinear oscillator is considered as a special case of mixed parity nonlinear oscillator in which the cubic stiffness nonlinearity is absent. Therefore equation (3.27) is simulated numerically through fourth order Runge-Kutta method for four different values of ϵ_2, with $\epsilon_3 = 0$. The four chosen values of ϵ_2 are $0.05, 0.1, 0.2$ and 0.4. A damping factor, $\zeta = 0.05$ is assumed in all simulation. The analytical response and that obtained numerically are shown in Figure 3.2 and the results are compared in Tables 3.1 and 3.2. It is observed from Figure 3.2 that analytical solutions are in good agreement with numerical results up to a low value of $\epsilon_2 = 0.2$. The deviation between the two responses is visible at the higher value of $\epsilon_2 = 0.4$. The tabulated results show that the deviation of the analytical solution from the numerical result increases with increase in nonlinear parameter ϵ_2. The maximum error in average frequency is 0.455% while the maximum error in amplitude is 1.648% for $\epsilon_2 = 0.2$. The corresponding maximum error increases to a value of 1.932% and 3.358% for $\epsilon_2 = 0.4$.

Damped mixed parity nonlinear oscillator

The analysis of damped mixed parity nonlinear oscillator is carried out in a way similar to the damped quadratic nonlinear oscillator. A constant value of $\epsilon_3 = 0.1$ is assumed in all the cases. The response obtained through numerical simulation and analytical method are shown in Figure 3.3 and in Tables 3.3 and 3.4. It is observed from Figure 3.3 that the analytical solutions are in good agreement with the numerical solution up to a low value of $\epsilon_2 = 0.2$. The deviation between the two responses is visible at higher value of $\epsilon_2 = 0.4$. The deviation of the analytical solution from the numerical solution increases with increase in nonlinear parameter ϵ_2. The maximum error in average frequency is 0.575% while the maximum error in amplitude is 2.521% for $\epsilon_2 = 0.2$. The corresponding maximum error increases to 1.239% and 3.515% respectively for $\epsilon_2 = 0.4$.
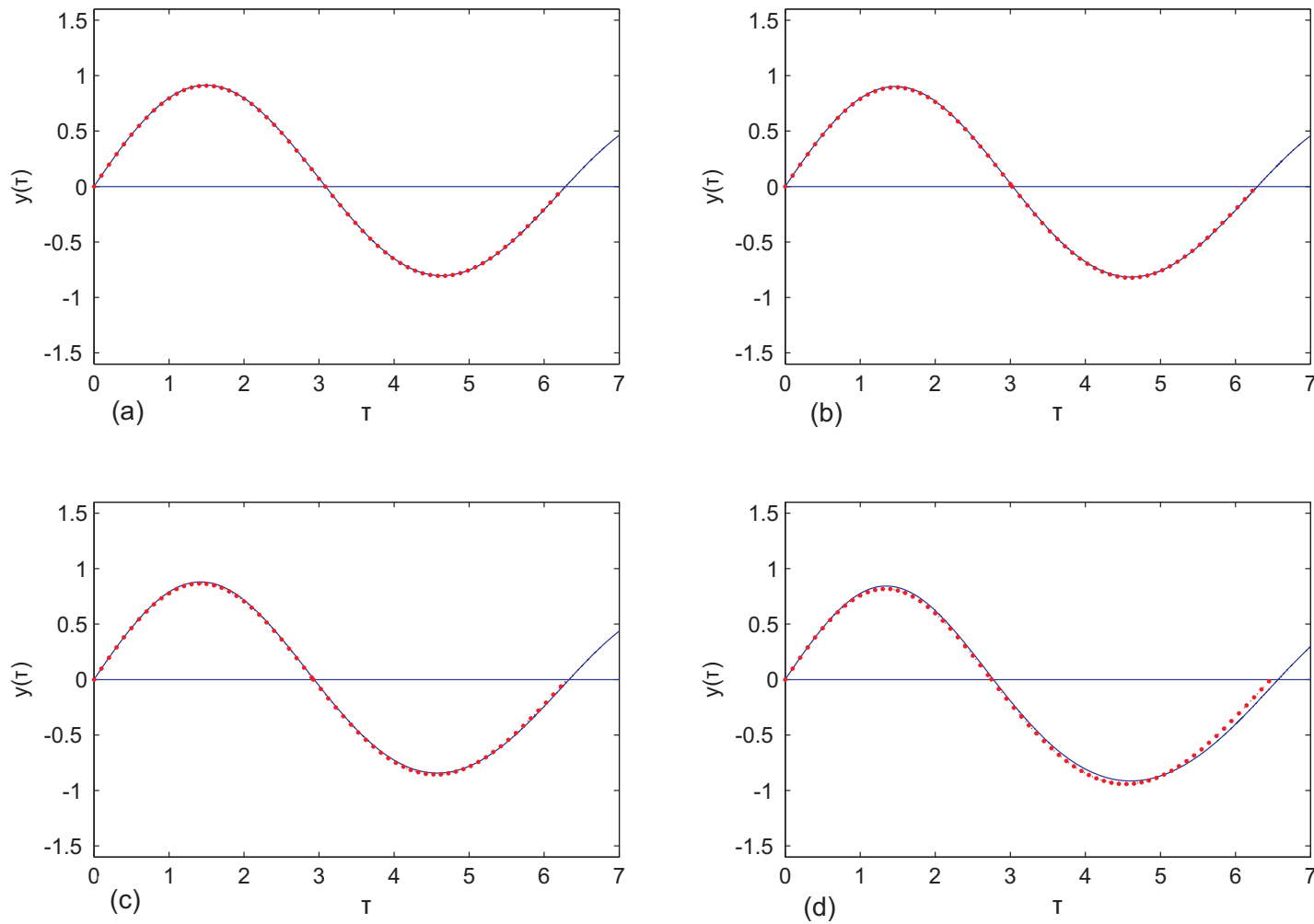
Figure 3.2: Response of the linearly damped quadratic nonlinear system for $\zeta = 0.05$, numerical simulation (solid line), analytic solution (dotted line) (a) $\epsilon_2 = 0.05$ (b) $\epsilon_2 = 0.1$ (c) $\epsilon_2 = 0.2$ (d) $\epsilon_2 = 0.4$

Table 3.1: Comparison between analytical and simulated response for quadratic oscillator: positive half of the oscillation $\zeta = 0.05$

ϵ_2	Y_{p1_s}	Y_{p1}	$e_{y_{p1}}$	ω_{p1_s}	ω_{p1}	$e_{\omega_{p1}}$
0.05	0.9137	0.9093	0.548	1.0180	1.0194	-0.138
0.10	0.9017	0.8940	0.944	1.0365	1.0383	-0.174
0.20	0.8797	0.8658	1.648	1.0711	1.0748	-0.345
0.40	0.8427	0.8173	2.779	1.1325	1.1435	-0.971

Table 3.2: Comparison between analytical and simulated response for quadratic oscillator: negative half of the oscillation $\zeta = 0.05$

ϵ_2	Y_{n1_s}	Y_{n1}	$e_{y_{n1}}$	ω_{n1_s}	ω_{n1}	$e_{\omega_{n1}}$
0.05	-0.8035	-0.8061	-0.285	0.9817	0.9829	-0.122
0.10	-0.8159	-0.8220	-0.676	0.9634	0.9653	-0.197
0.20	-0.8432	-0.8565	-1.512	0.9240	0.9282	-0.455
0.40	-0.9140	-0.9423	-3.358	0.8283	0.8443	-1.932

3.3   Remarks

The above comparison between numerical simulation and analytical solution by Krylov-Bogoliubov method along with energy balance approach shows that the analytical solution represents the system response with fairly good accuracy for lower values of nonlinear parameters, say for $\epsilon_2 \leq 0.2$ and for $\epsilon_3 \leq 0.1$. Modeling the positive half and negative half cycle separately is a better way to represent the mixed parity nonlinear oscillators.
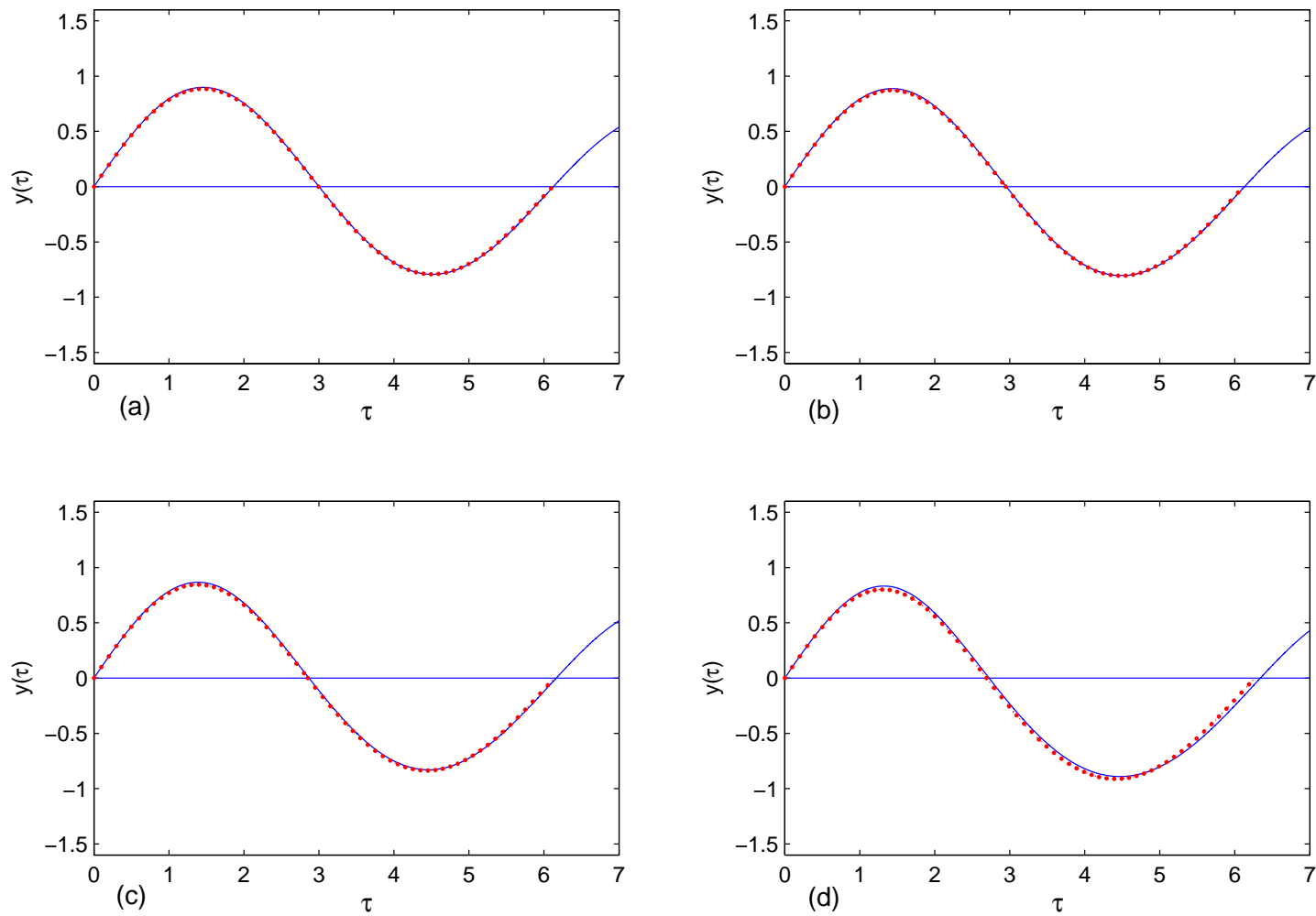
Figure 3.3: Response of the linearly damped mixed parity nonlinear system for $\zeta = 0.05$ and $\epsilon_3 = 0.1$, numerical simulation (solid line) analytic solution (dotted line) (a) $\epsilon_2 = 0.05$ (b) $\epsilon_2 = 0.1$ (c) $\epsilon_2 = 0.2$ (d) $\epsilon_2 = 0.4$

Table 3.3: Comparison between analytical and simulated response for mixed parity oscillator: positive half of the oscillation $\epsilon_3 = 0.1$, $\zeta = 0.05$

ϵ_2	Y_{p1_s}	Y_{p1}	$e_{y_{p1}}$	ω_{p1_s}	ω_{p1}	$e_{\omega_{p1}}$
0.05	0.8976	0.8852	1.563	1.0468	1.0494	-0.248
0.10	0.8867	0.8714	1.902	1.0639	1.0673	-0.320
0.20	0.8668	0.8459	2.521	1.0958	1.1021	-0.575
0.40	0.8325	0.8012	3.515	1.1537	1.1680	-1.239

Table 3.4: Comparison between analytical and simulated response for mixed parity oscillator: negative half of the oscillation $\epsilon_3 = 0.1$, $\zeta = 0.05$

ϵ_2	Y_{n1_s}	Y_{n1}	$e_{y_{n1}}$	ω_{n1_s}	ω_{n1}	$e_{\omega_{n1}}$
0.05	-0.7932	-0.7919	0.145	1.0056	1.0069	-0.129
0.10	-0.8045	-0.8063	-0.203	0.9889	0.9902	-0.131
0.20	-0.8291	-0.8372	-0.934	0.9529	0.9553	-0.252
0.40	-0.8904	-0.9119	-2.583	0.8683	0.8780	-1.117

In this way the Krylov-Bogoliubov method which is first order averaging method is able to incorporate the effect of quadratic nonlinearity on the response of the system. It also helps in defining the average frequency of oscillation during positive half and negative half cycle separately through equations (3.36) and (3.38) respectively.

Chapter 4

Classification of Stiffness Nonlinearity

Presence of many forms of the nonlinearities in the restoring force and dissipative forces makes identification and parameter estimation of nonlinear systems quite involved. System parameter estimation procedures generally assume that sufficient apriori information about the mathematical structure of the system is available. Subsequently system parameters are estimated using input-output data for the assumed form of nonlinearities. For complex engineering systems, it is difficult to recognize the actual form of nonlinearities. Wavelet Transforms based nonlinear system identification and parameter estimation procedures mostly consider Duffing system or systems with symmetric polynomial forms of stiffness nonlinearities.. However, for engineering applications, it is also important to identify the types of nonlinearities actually governing the system response.

Oscillators with third degree polynomial form of stiffness (quadratic and mixed parity oscillators) are considered in the present study. A methodology based on Wavelet Transforms using standard Morlet wavelet and complete Morlet wavelet is suggested to distinguish between the symmetric and asymmetric polynomial forms of stiffness nonlinearity.

Symmetric and asymmetric forms are further sub-classified depending on the signs of the

nonlinearities. Free vibration response of the system is Wavelet transformed. Ridges of the Wavelet transforms are estimated. Characteristics of ridges in conjunction with analytical solutions from Krylov-Bogoliubov method are used to classify the nonlinearities. The procedure is illustrated through numerical simulations.

Initially, Wavelet Transforms are described here, in brief and it is subsequently used to classify the stiffness nonlinearities.

4.1   Wavelet Transforms

Fourier transforms are widely used. They provide a decomposition of a time history in the frequency domain and vise-versa for a stationary process. Fourier Transforms, however suffer from the drawback that time information is completely lost during transformation to frequency domain. It is not possible to locate an event in time, while looking at the Fourier Transforms. It is therefore suitable only for a stationary process. In order to overcome the shortcoming, regarding non stationary processes, Gabor devised the Short Time Fourier Transform (STFT), whereby the Fourier Transform is applied on a time-windowed signal. The STFT, thus, contains the information about time and frequency both, but with limited precision. The precision, dependent on the fixed-size time-window, is given by Heisenberg uncertainty principle (Mallat, 1998).

Wavelet Transforms overcome the limitations of STFT and forms a logical sequence in this direction. The time-window in Wavelet Transforms is variable in size. The window is long (more time duration) when low frequency information is required with good frequency resolution and the window is short when high frequency information is required with good time resolution. This renders the Wavelet Transforms suitable for the study of non stationary processes.

The Continuous Wavelet Transform (CWT) for a finite energy signal $y(t)$, using admis-

sible wavelet function $g(t)$ is defined by the integral (Chui, 1992)

$$W_y(a,b) = \langle y, g(t,a,b) \rangle = \frac{1}{\sqrt{|a|}} \int_{-\infty}^{\infty} y(t) \overline{g}\left(\frac{t-b}{a}\right) \mathrm{d}t \tag{4.1}$$

$\overline{g}\left(\frac{t-b}{a}\right)$ is complex conjugate of $g\left(\frac{t-b}{a}\right)$. A wavelet $g(t)$ is a small wave satisfying certain mathematical properties to be a valid candidate for Wavelet Transforms. The wavelet $g(t)$ is called mother wavelet. Its scaled and translated version is called daughter wavelet / son wavelet and it is represented as

$$g(t,a,b) = \frac{1}{\sqrt{a}} g\left(\frac{t-b}{a}\right) \qquad\qquad a > 0,\, b \in \mathcal{R}$$

where a is scale parameter and b is translational parameter. The factor $(1\sqrt{|a|})$ is introduced in the above formula to maintain the same energy in the mother and daughter wavelets. Maintaining the same energy in mother and daughter wavelet means we are using L^2 normalization which can be put mathematically as

$$\|g(t)\|^2 = \|g(t,a,b)\|^2 \qquad\qquad \text{where } \|g(t)\|^2 = \int_{-\infty}^{\infty} |g(t)|^2 \,\mathrm{d}t \tag{4.2}$$

The conditions on mother wavelet $g(t)$ under which the above representation is valid are summarized as follows.

1. A wavelet function $g(t)$ must satisfy the admissibility condition which is stated as follows

$$c = \int_{-\infty}^{\infty} \frac{|G(\omega)|^2}{\omega} d\omega < \infty \tag{4.3}$$

   $G(0)$ should be zero for the above integral to be finite. Therfore, in other words we can say that for well-behaved functions it needs to be ensured that the mother wavelet has zero mean

$$\int_{-\infty}^{\infty} g(t)\mathrm{d}t = 0 \tag{4.4}$$

   This ensures that mother wavelet must oscillate in some manner

2. It should have finite energy

$$\int_{-\infty}^{\infty} |g(t)|^2 \,\mathrm{d}t < \infty \tag{4.5}$$

   i.e. it should decay toward $\pm\infty$

3. A secondary condition, which is generally imposed on the wavelet function is about normalization that gives rise to the mathematical condition that norm of the function $g(t)$ is equal to 1

$$\|g(t)\|^2 = \int_{-\infty}^{\infty} |g(t)|^2 \, \mathrm{d}t = 1 \qquad (4.6)$$

The above definition of Wavelet Transforms i.e. equation (4.1), which is in time domain can be converted in the frequency domain using Parseval identity (Chui, 1992)

$$W(a,b) = \frac{\sqrt{a}}{2\pi} \int_{-\infty}^{\infty} F(\omega)\overline{G}(a\omega)\mathrm{e}^{j\omega b}\mathrm{d}\omega \qquad (4.7)$$

Here $F(\omega)$ is the Fourier Transform of $f(t)$ and $G(\omega)$ is the Fourier Transform of $g(t)$. This result can be interpreted as an inverse Fourier Transform of the function $\sqrt{a}F(\omega)\overline{G}(a\omega)$. The equation (4.7) is most commonly used for computational work as the equation can use the available efficient Fast Fourier Transform (FFT) algorithms.

4.1.1 Time and Frequency Centre of Wavelet

The CWT of a function localizes a signal within a time frequency window around the time and frequency centre of the wavelet function. Time centre is defined as the mean of the mother wavelet function (Simonovski and Boltezar, 2003).

$$\bar{t} = \frac{1}{\|g(t)\|^2} \int_{-\infty}^{\infty} t \, |g(t)|^2 \, \mathrm{d}t \qquad (4.8)$$

Hence time centre of the translated and scaled wavelet (daughter wavelet) function is

$$\bar{t}_{b,a} = \frac{1}{\|g(t,a,b)\|^2} \int_{-\infty}^{\infty} t \, |g(t,a,b)|^2 \, \mathrm{d}t \qquad (4.9)$$

$$= a\bar{t} + b \qquad (4.10)$$

Let $G(\omega)$ be the Fourier Transform of the wavelet function $g(t)$; then the frequency centre of the mother wavelet function is defined as

$$\bar{\omega} = \frac{1}{\|G(\omega)\|^2} \int_{-\infty}^{\infty} \omega \, |G(\omega)|^2 \, \mathrm{d}\omega \qquad (4.11)$$

Hence frequency centre of the translated and scaled wavelet (daughter wavelet) function is

$$\bar{\omega}_{b,a} = \frac{1}{2\pi \left\| g(t,a,b) \right\|^2} \int_{-\infty}^{\infty} \omega \left| G(\omega,a,b) \right|^2 \mathrm{d}\omega \tag{4.12}$$

$$= \frac{1}{a} \bar{\omega} \tag{4.13}$$

4.1.2   Time and Frequency Spread of Wavelet

The square root of variance (also known as standard deviation) is a measure of the spread of a function. Time spread gives an effective duration in the time domain. It is defined as (Simonovski and Boltezar, 2003)

$$\sigma_t^2 = \frac{1}{\left\| g(t) \right\|^2} \int_{-\infty}^{\infty} (t - \bar{t})^2 \left| g(t) \right|^2 \mathrm{d}t \tag{4.14}$$

Hence the variance of translated and scaled wavelet function (daughter wavelet) in the time domain is

$$\sigma_{t_{b,a}}^2 = \frac{1}{\left\| g(t,a,b) \right\|^2} \int_{-\infty}^{\infty} (t - \bar{t}_{b,a})^2 \left| g(t,a,b) \right|^2 \mathrm{d}t \tag{4.15}$$

$$= a^2 \sigma_t^2 \tag{4.16}$$

$$\sigma_{t_{b,a}} = a \sigma_t \tag{4.17}$$

By this definition the spread of function in time around the time centre $\bar{t}_{b,a}$ is from $(\bar{t}_{b,a} - \sigma_{t_{b,a}})$ to $(\bar{t}_{b,a} + \sigma_{t_{b,a}})$. In other words, the spread of a function is one standard deviation on either side of the time centre of the function.

Variance of wavelet function in frequency domain is defined as

$$\sigma_\omega^2 = \frac{1}{\left\| G(\omega) \right\|^2} \int_{-\infty}^{\infty} (\omega - \bar{\omega})^2 \left| G(\omega) \right|^2 \mathrm{d}\omega \tag{4.18}$$

$$\sigma_\omega^2 = \frac{1}{2\pi \left\| g(t) \right\|^2} \int_{-\infty}^{\infty} (\omega - \bar{\omega})^2 \left| G(\omega) \right|^2 \mathrm{d}\omega \tag{4.19}$$

Hence the variance of translated and scaled wavelet function (daughter wavelet) in the frequency domain is

$$\sigma^2_{\omega_{b,a}} \quad = \quad \frac{1}{2\pi \left\| g(t, a, b) \right\|^2} \int_{-\infty}^{\infty} (\omega - \bar{\omega}_{b,a})^2 \left| G_{a,b}(\omega) \right|^2 \mathrm{d}\omega \qquad (4.20)$$

$$= \quad \frac{1}{a^2} \sigma^2_{\omega} \qquad (4.21)$$

$$\sigma_{\omega_{b,a}} \quad = \quad \frac{1}{a} \sigma_w \qquad (4.22)$$

By this definition the spread of function in frequency around the frequency centre $\bar{\omega}_{b,a}$ is from $(\bar{\omega}_{b,a} - \sigma_{\omega_{b,a}})$ to $(\bar{\omega}_{b,a} + \sigma_{\omega_{b,a}})$. In other words the spread of function in frequency is one standard deviation on either side of the frequency centre.

Hence, The CWT of a function $f \in L^2(\mathcal{R})$ localizes the signal with a time-frequency window w defined with the following cartesian product.

$$w = [\ \bar{t}_{b,a} \pm \sigma_{t_{b,a}}] \times [\bar{\omega}_{b,a} \pm \sigma_{\omega_{b,a}}] \qquad (4.23)$$

Please refer Figure 4.1, here $\bar{t}_{b,a}$ and $\bar{\omega}_{b,a}$ are the time and frequency centres of the daughter wavelet respectively which in turn are related to the time and frequency centre of the mother wavelet. $\sigma_{t_{b,a}}$ and $\sigma_{\omega_{b,a}}$ are the variance of the daughter wavelet in time and frequency domain respectively which in turn are related to the variance of the mother wavelet in time and frequency domain.
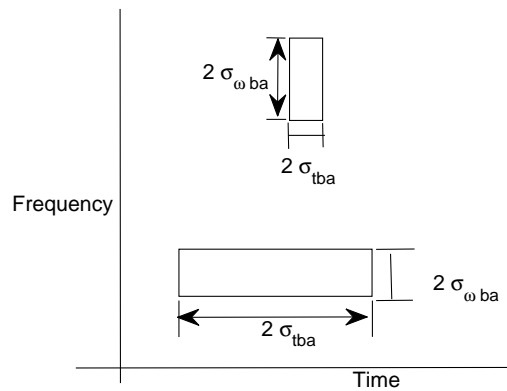
Figure 4.1: Time-Frequency Plane

Complex analytic wavelets can separate amplitude and phase components of the signal and thus help us in studying the time evolution of frequency transients. This property helps us in comparison of the numerical results from Wavelet Transforms and closed form solution of nonlinear system which finally leads to parameter estimation of a system. Fourier Transform of analytic wavelet is 0 when $\omega < 0$. Many of the analytic wavelet functions found in the continuous wavelet literature are of the following form

$$g(t) = h(t)e^{j\omega_0 t} \tag{4.24}$$

largely because they are most easily related to the concepts of frequency. Here $h(t)$ is a real and symmetric window and the wavelet $g(t)$ is constructed with a frequency modulation of $h(t)$. Hence Fourier Transform of $g(t)$ is

$$
\begin{aligned}
\mathcal{F}[g(t)] &= G(\omega) & (4.25)\\
&= \mathcal{F}\left[h(t)e^{j\omega_0 t}\right] & (4.26)\\
&= H(\omega - \omega_0) & (4.27)
\end{aligned}
$$

If $h(t)$ is such that $H(\omega) \approx 0$ for $|\omega| \geq \omega_0$ then $G(\omega) \approx 0$ for $\omega < 0$; hence $G(\omega)$ is assumed to be approximately analytic. This has been represented pictorially in Figure 4.2.

4.1.3   Choice of Wavelet Function

There are a few complex analytical wavelets like Gabor, Morlet, Cauchy, Harmonic wavelet etc. Gabor wavelet is obtained with frequency modulation of a Gaussian window. In general, Gabor and Morlet wavelet functions are preferred in Wavelet Transforms. The reason is that they employ a Gaussian window, which has optimal resolution in time and frequency domain. The resolution is same in both time and frequency domains and the spread of window in time and frequency domain is such that the requirement of Heisenberg's uncertainty principle is met at the lower bound of $1/2$.
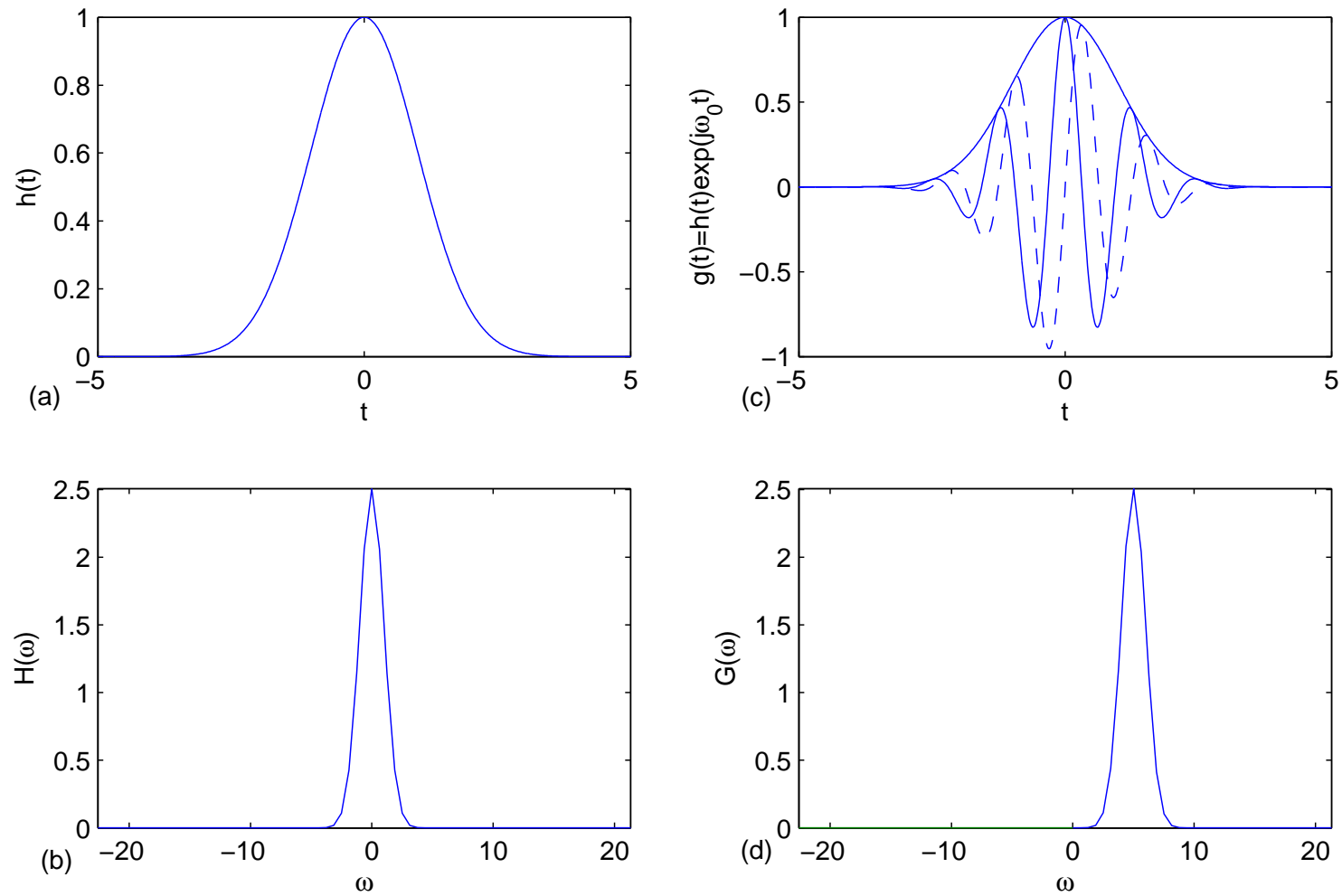
Figure 4.2: Morlet Wavelet (a) Window function h(t) (b) Fourier Transform of the window function $H(\omega)$ (c) wavelet function g(t) (d) Fourier Transform of Morlet wavelet function $G(\omega)$

For Gaussian windows $\sigma_\omega \sigma_t = \frac{1}{2}$, and secondly, the transforms can be correlated with instantaneous frequency with relative ease (Mallat, 1998; Chui, 1992).

The Gabor wavelet function is given by

$$g(t) = \frac{1}{(\sigma^2 \pi)^{1/4}} e^{-t^2/2\sigma^2} e^{j\omega_0 t} \tag{4.28}$$

Its Fourier Transform is

$$G(\omega) = \left(4\pi\sigma^2\right)^{1/4} e^{-\sigma^2(\omega-\omega_0)^2/2} \tag{4.29}$$

$\sigma = 1$ and $\omega_0 = 5$ are used to meet the admissibility criterion (Carmona and Torresani, 1998). Morlet wavelet is obtained with frequency modulation of a window $h(t)$ where

$$h(t) = e^{-\frac{t^2}{2}} \tag{4.30}$$

The Fourier Transform of $h(t)$ is

$$H(\omega) = \sqrt{2\pi} e^{-\omega^2/2} \tag{4.31}$$

and hence the wavelet function is

$$g(t) = e^{j\omega_0 t} e^{-0.5t^2} \tag{4.32}$$

Its Fourier Transform is given by

$$G(\omega) = \sqrt{2\pi} e^{-0.5(\omega-\omega_0)^2} \tag{4.33}$$

Morlet wavelet has some other mathematical forms also. The *Complete Morlet Wavelet* is defined as follows

$$g(t) = \frac{1}{\sqrt[4]{\pi}} \left(e^{j\omega_0 t} - e^{\frac{-\omega_0^2}{2}}\right) e^{-0.5t^2} \tag{4.34}$$

where ω_0 stands for the central frequency of the mother wavelet. The second term in the bracket is known as the correction term, as it corrects for the non-zero mean of the complex sinusoid of the first term. In practice it becomes negligibly small for $\omega_0 \geq 5$.

Hence the *Truncated Morlet Wavelet*

$$g(t) = \frac{1}{\sqrt[4]{\pi}} e^{j\omega_0 t} e^{-0.5t^2} \tag{4.35}$$

is often used in the literature and is often called Morlet wavelet. The factor $\frac{1}{\sqrt[4]{\pi}}$ makes the norm of the wavelet equal to unity. Comparison with the Gabor wavelet shows that the Morlet wavelet is the Gabor wavelet with parameter $\sigma = 1$.

Table 4.1: Properties of translated and scaled Morlet wavelet functions

Time center	Frequency center	Time spread	Frequency spread
$\bar{t}_{b,a}$	$\bar{\omega}_{b,a}$	$\sigma_{t_{b,a}}$	$\sigma_{\omega_{b,a}}$
b	$\frac{\omega_o}{a}$	$\frac{a}{\sqrt{2}}$	$\frac{1}{a}\frac{1}{\sqrt{2}}$

4.1.4 Approximation of Wavelet Transform of an Asymptotic Signal

A signal of the form

$$x(t) = A(t)\cos[\phi(t)] \qquad \text{where} \quad \dot{\phi}(t) = \omega(t) \tag{4.36}$$

is an asymptotic signal if oscillation due to the phase term $\phi(t)$ is more than that contributed by the amplitude term $A(t)$ (Carmona and Torresani, 1998; Abbate et al., 2002). An asymptotic signal can be approximated by the real part of the analytic signal

$$x(t) = \text{Re}[x_a(t)] \qquad \text{where} \quad x_a(t) = A(t)e^{j\phi(t)} \tag{4.37}$$

The CWT of an analytic signal $x_a(t)$ is twice the CWT of its real part $x(t)$ or mathematically (Mallat, 1998)

$$W_x(a,b) = \frac{1}{2}W_{x_a}(a,b) \tag{4.38}$$

Hence the Wavelet Transform of $x(t)$ can be written as

$$W_x(a,b) = \int_{-\infty}^{\infty} x(t)\overline{g}(t,a,b)\mathrm{d}t \qquad \text{where} \quad g(t,a,b) = \frac{1}{\sqrt{a}}g\left(\frac{t-b}{a}\right) \quad (4.39)$$

$$= \frac{1}{2}\int_{-\infty}^{\infty} x_a(t)\frac{1}{\sqrt{a}}\overline{g}\left(\frac{t-b}{a}\right)\mathrm{d}t \qquad (4.40)$$

$$= \frac{1}{2}\int_{-\infty}^{\infty} A(t)\mathrm{e}^{j\phi(t)}\frac{1}{\sqrt{a}}\overline{g}\left(\frac{t-b}{a}\right)\mathrm{d}t \qquad (4.41)$$

Substituting, $t = t + b$ and using Taylor Series expansion around b, we can write

$$A(t+b) = A(b) + t\dot{A}(b) + ... \qquad (4.42)$$

$$\phi(t+b) = \phi(b) + t\dot{\phi}(b) + ... \qquad (4.43)$$

Considering only zeroth order approximation for A and first order approximation for ϕ, we get

$$A(t+b) \approx A(b) \qquad (4.44)$$

$$\phi(t+b) \approx \phi(b) + t\dot{\phi}(b) \qquad (4.45)$$

Substituting equations (4.44) and (4.45) in equation (4.41), we get

$$W_x(a,b) \approx \frac{1}{2}\int_{-\infty}^{\infty} A(b)\mathrm{e}^{j(\phi(b)+t\dot{\phi}(b))}\frac{1}{\sqrt{a}}\overline{g}\left(\frac{t}{a}\right)\mathrm{d}t \qquad (4.46)$$

$$\approx \frac{\sqrt{a}}{2}A(b)\mathrm{e}^{j\phi(b)}\overline{G}(a\dot{\phi}(b)) \qquad (4.47)$$

$$\approx \frac{\sqrt{a}}{2}A(b)\mathrm{e}^{j\phi(b)}\overline{H}(a\dot{\phi}(b) - \omega_0) \qquad \text{if} \quad g(t) = h(t)\mathrm{e}^{j\omega_0 t} \qquad (4.48)$$

$$\approx \frac{\sqrt{a}}{2}A(b)\mathrm{e}^{j\phi(b)}H(a\dot{\phi}(b) - \omega_0) \qquad (4.49)$$

if $h(t)$ is symmetrical or even function then $\overline{H} = H$. Since the above analysis is based on the zeroth order approximation of $A(t)$ and first order approximation of $\phi(t)$, the above equation is applicable only when the variations of $A(t)$ and $\dot{\phi}(t)$ are negligible over the spread of wavelet function.

It can be said that the error in the above analysis is of the order of $\dot{A}(t)$ or $\ddot{\phi}(t)$, whichever is bigger. Mathematically,

$$W_x(a, b) = \frac{\sqrt{a}}{2} A(b) e^{j\phi(b)} G(a\dot{\phi}(b)) + O\left\|\dot{A}, \ddot{\phi}\right\| \tag{4.50}$$

$$W_x(a, b) = \frac{\sqrt{a}}{2} A(b) e^{j\phi(b)} H(a\dot{\phi}(b) - \omega_0) + O\left\|\dot{A}, \ddot{\phi}\right\| \tag{4.51}$$

With Gabor wavelet, a reasonable approximation of Wavelet Transform of an asymptotic signal (4.36) turns out to be (Mallat, 1998)

$$W_x(a, b) = \frac{\sqrt{a}}{2} A(b) e^{j\omega b} (4\pi\sigma^2)^{1/4} e^{-\sigma^2(a\omega - \omega_0)^2/2} \tag{4.52}$$

4.1.5   Scalogram

In general, Analytic Wavelet Transform (AWT) of a function is complex in nature. Squared modulus of AWT is known as scalogram. Thus,

$$\text{Scalogram} = |W(a, b)|^2 \tag{4.53}$$

The results of Wavelet transforms are generally presented in the form of the plot of scalogram in which intensity of scalogram is plotted as a function of (a, b), the scale and translational parameter of $W(a, b)$. Scalogram is spread over the time-scale plane around the time and frequency centers of the wavelet functions. The time and frequency centers of the wavelet functions are defined as the mean of wavelet functions in the time and frequency domains respectively. The spread of modulus of AWT is measured by corresponding standard deviations of the wavelet function in the time and frequency domains respectively. It is to be noted that Wavelet Transform is linear but scalogram representation is not linear. Let there be two signals $f1$ and $f2$ and their Wavelet transforms be given by $W_{f1}(a, b)$ and $W_{f2}(a, b)$ respectively; then Wavelet Transform of a composite signal $(f1 + f2)$ is given by $W_{f1}(a, b) + W_{f2}(a, b)$, but scalogram which is

square of the modulus is

$$\|W_{f1+f2}(a,b)\|^2 \quad = \quad \|W_{f1}(a,b) + W_{f2}(a,b)\|^2 \tag{4.54}$$

$$= \quad \|W_{f1}(a,b)\|^2 + \|W_{f2}(a,b)\|^2 + \underbrace{2\,\mathrm{Re}\left\{W_{f1}(a,b)(\overline{W_{f2}}(a,b)\right\}}_{Cross-Term}$$

$$\tag{4.55}$$

It is evident from the above equation that a scalogram representation contains cross terms.

4.1.6 Ridge and Skeleton

The critical feature of the AWT of an asymptotic signal is that it is concentrated along the curves, in the time-frequency domain, called 'ridges'. Rigdes can provide useful information about the asymptotic signal. Ridges are directly related to the instantaneous frequency of the signal while skeleton provides information about the envelope of the signal. A ridge is defined as the locus, in time-frequency plane, along which normalized scalogram attains a maxima; mathematically

$$\frac{\partial}{\partial a}\left(\frac{\left(|W_x(a,b)|^2\right)}{a}\right) = 0 \tag{4.56}$$

Substituting the transform (4.52) into (4.56), the locus of the ridge is found as

$$a_r(b) \quad = \quad \frac{\omega_0}{\omega(b)}\,, \tag{4.57}$$

where $a_r(b)$ is scale along the ridge. In order to determine the scale corresponding to ridge $a_r(b)$ the maxima of modulus of AWT is noted for each time location b in the time-frequency representation calculated by equation (4.7) and corresponding scale is obtained. Subsequently, the instantaneous frequency $\omega(b)$ at a particular time can be obtained by the equation (4.57).

The value of Wavelet Transform restricted to its ridge is known as the skeleton of the Wavelet Transform. The skeleton contains the maximal information and it is very close to the component of the signal itself. The skeleton of the asymptotic signal is given by

$$W_x(a_r(b), b) = \frac{1}{2}A(b)e^{j\omega b}(4\pi\sigma^2)^{1/4} \tag{4.58}$$

$$= C(b)A(b)e^{j\omega b} \tag{4.59}$$

where $C(b) = \frac{1}{2}(4\pi\sigma^2)^{1/4}$.

The modulus of the skeleton is given by

$$|W_x(a_r(b), b)| = C(b)A(b) \tag{4.60}$$

Once the Wavelet Transform of the signal is known along the ridge, the analytic signal can be obtained whose real part is the original signal and modulus is the envelope of the signal. The factor $C(b)$ is called the correction factor and it is completely determined by wavelet function. Hence the envelope of the signal $A(b)$ can be determined by equation (4.60).

4.1.7   Edge Effect

When calculating the AWT, errors occur at the start and end-time indexes. This is called the Edge effect or Cone of Influence and is caused by the fact that the AWT is calculated from a signal of finite length.

Although the wavelet is focused at a given time around the time centre and therefore Wavelet Transform of the signal represents the signal content in that vicinity, the wavelet window extends equally into the past and future. The span of this analysis window is dependent on both the parent wavelet and scale being analyzed. Near the ends of the signal, the wavelet's analysis window may extend significantly beyond the length of the data. Thus the resulting wavelet coefficients in these regions are based on incomplete

information and have questionable accuracy. Since the width of the wavelet function depends on the scale a, the width of the edge effect also depends on this scale. The edge effect width can be estimated using the time spread $\sigma_{t_{b,a}}$ of the daughter wavelet function.

A radius of trust R, can be defined as, a multiple k, of the time spread of wavelet function as

$$R \;=\; k\sigma_{t_{b,a}} \qquad\qquad k \geq 1 \qquad\qquad\qquad (4.61)$$

$$\;=\; ka\sigma_t \qquad\qquad\qquad\qquad\qquad\qquad\quad (4.62)$$

The value of k depends on the accuracy required in the CWT data. Generally it ranges from 3 to 5.

There are different ways to remove the edge effects in the wavelet transformed data

1. Discard the Wavelet Transform data which has been affected by the edge effect.

2. Increase the length of the signal by adding data suitably at both the ends.
   The influence of the edge effect can be reduced if the length of the signal is increased by mirroring the signal around the start- and end -time indexes. Now the edge effect influences the AWT values at the start- and end -time indexes of the lengthened signal. However these values can be disregarded because one is only interested in the AWT values corresponding to the time indexes of the original (shorter) signal.

When the sufficient number of data points are available then first option is easier to use. In case the number of available data points are less the second option is appropriate to use. For Gabor wavelet, time spread is given by

$$\sigma_{t_{b,a}} \;=\; a\frac{\sigma}{\sqrt{2}} \qquad\qquad\qquad\qquad\qquad\qquad (4.63)$$

$$\;=\; \frac{\omega_0}{\omega}\frac{\sigma}{\sqrt{2}} \qquad\qquad\qquad\qquad\qquad\quad (4.64)$$

By this definition, the Gabor wavelet is assumed to effectively span $2\sigma_{t_{b,a}}$ in the time domain or one standard deviation of the Gaussian Window. However there is a considerable portion of the window beyond one standard deviation of the mean value, therefore, depending on the desired level of accuracy, an integer multiple β of the standard deviation in the Wavelet Transform can be discarded at the ends. Thus the usable region t_j within a set of Wavelet-transformed data T can be written as

$$\beta\sigma_{t_{b,a}} \leq t_j \leq T - \beta\sigma_{t_{b,a}} \qquad\qquad \beta \geq 1 \qquad\qquad (4.65)$$

4.2 Wavelet Transform of the Response of Damped Quadratic and Mixed-Parity Nonlinear Oscillator

Consider the damped quadratic and mixed parity nonlinear oscillator, given by equation

$$\ddot{y} + 2\zeta\dot{y} + y + \epsilon_2 y^2 + \epsilon_3 y^3 \;\; = \;\; 0, \qquad y(0) = 0 \qquad \dot{y}(0) = 1 \qquad (4.66)$$

Under the assumption of low damping ($\zeta \approx 0.01$), the response signal given by equations (3.28), (3.37) and (3.39) can be assumed to be an asymptotic signal.

4.2.1 Wavelet Transform using Standard Morlet Wavelet

Wavelet Transform of the response signal is obtained through standard Morlet wavelet using the method described in section 4.1.4, as

$$W_x(a,b) = \frac{\sqrt{a}}{2} A(b) e^{j\omega b} (4\pi\sigma^2)^{1/4} e^{-\sigma^2(a\omega-\omega_0)^2/2} \qquad (4.67)$$

The instantaneous frequency is calculated using the ridge of the Wavelet Transform. From Section 4.1.6, we know that

$$a_r(b) \;\; = \;\; \frac{\omega_0}{\omega(b)}, \qquad\qquad (4.68)$$

where $a_r(b)$ is the scale along the ridge. In order to determine the scale corresponding to ridge $a_r(b)$, the maxima of normalized scalogram is noted for each time location b in the time-frequency representation and the corresponding scale is obtained. Subsequently, the instantaneous frequencies $\omega(b)$ at a particular time are determined.

4.2.2   Wavelet Transform using Complete Morlet Wavelet

Time resolution of Standard Morlet wavelet depends on ω_0 (Table 4.1). Its value is kept at least 5, for the mean of wavelet function to approach zero, a condition necessary to fulfill admissibility requirement. It is therefore, unable to capture any phenomenon, which is more temporal in nature.

In order to increase time resolution and capture the temporal phenomenon, use of Complete Morlet wavelet has been suggested. This allows usage of a lower value of central frequency ω_0. Since the central frequency is lower than the standard Morlet wavelet, it is also known as low-oscillation Morlet wavelet. $\omega_0 = 1$ is used in the present work to have better time resolution . Initially complete Morlet wavelet was used as a pattern matching tool to detect and classify P waves in ECG signal by Michaelis et al. (1993). Later Addison et al. (2002) explained the underlying mathematics and applied it to sonic echo NDT signal used for the analysis of structure elements. They also discussed briefly- the interrogation of arrhythmic ECG signal and the characterization of coherent structures in turbulent flow fields.

The *Complete Morlet Wavelet* is defined by equation (4.34). Its Fourier Transform is

$$G(\omega) = (4\pi)^{1/4} e^{-\left(\omega^2 + \omega_0^2\right)/2} \left(e^{\omega\omega_0} - 1\right). \tag{4.69}$$

With Complete Morlet wavelet, the Wavelet Transform of an asymptotic signal (4.36) can be written approximately as (Mallat, 1998)

$$W_y(a,b) = \frac{\sqrt{a}}{2} A(b) e^{j\phi(b)} (4\pi)^{1/4} e^{-\left(a\omega^2 + \omega_0^2\right)/2} \left(e^{a\omega\omega_0} - 1\right). \tag{4.70}$$

The wavelet ridge is obtained by employing the expression (4.56), thus

$$a_r = \frac{1}{\omega_0 \omega} \log \left(\frac{a_r \omega}{a_r \omega - \omega_0} \right). \tag{4.71}$$

Equation (4.71) is solved numerically for instantaneous frequency (ω) after determining locus of ridge (a_r) from the maxima of normalized scalogram at each time instant.

4.2.3   Illustration

Study of the nonlinear system is divided in the following three cases, with reference to equation (4.66)

1. $\epsilon_2 = 0$ and   (i) $\epsilon_3 = 0$ or   (ii) $\epsilon_3 = +ve$ or   (iii) $\epsilon_3 = -ve$,

2. $\epsilon_2 = +ve$ and   (i) $\epsilon_3 = 0$ or   (ii) $\epsilon_3 = +ve$ or   (iii) $\epsilon_3 = -ve$,

3. $\epsilon_2 = -ve$ and   (i) $\epsilon_3 = 0$ or   (ii) $\epsilon_3 = +ve$ or   (iii) $\epsilon_3 = -ve$.

The above three cases are classified according to the presence of ϵ_2 and its sign. All the three cases are further classified in three subclasses depending on the presence of ϵ_3 and its sign. Case (1) belongs to the symmetric polynomial form while cases (2) and (3) belong to asymmetric polynomial forms of stiffness nonlinearities, which consist of quadratic and mixed parity nonlinear oscillators.

The steps involved in classifying the system using ridges of Wavelet Transform are shown schematically in Figure 4.3 for a mixed parity nonlinear oscillator in which both ϵ_2 and ϵ_3 are positive. Figure 4.3(a) is a simulated response of the system obtained through Runge-Kutta method. Results in Figures 4.3 (b)- (d) are obtained using standard Morlet wavelet while the results in Figures 4.3 (e) - (g) are obtained using complete Morlet wavelet. Wavelet Transform of the response is shown in Figure 4.3(b). Ridge obtained over the relevant scale is shown in Figure 4.3(c). The data influenced by edge effect is discarded here. The length of end effect is considered as six times the standard deviation of the

wavelet function. Locus of ridge is converted to variation of instantaneous frequency with time in Figure 4.3(d). The trend of the graph shows that the frequency decreases continuously as the amplitude of oscillation decreases. The corresponding results in Figures 4.3 (e) - (g) indicate that the low oscillation Morlet wavelet is able to capture the change in instantaneous frequency from half cycle to half cycle. The instantaneous frequency shows oscillating behavior due to the different governing laws, during positive and negative motion and this fact is also evident from the equations (3.36) and (3.38).

The results obtained for the three different cases and its subclasses are shown in Figures 4.4-4.6 respectively. Damping factor $\zeta = 0.01$ is assumed in all the simulations. Figure 4.4 belongs to case (1). Figure 4.4(a) shows the response of the system for both ϵ_2 and ϵ_3 being zero. In fact, it is the case of a linear system and included here to provide reference signatures. Instantaneous frequencies obtained using standard Morlet wavelet and complete Morlet wavelet are shown in Figure 4.4(b) and Figure 4.4(c) respectively. Results obtained are same for both wavelets since in case of linear system, the frequency of oscillation is constant. Figures 4.4(d) - (f) shows the corresponding results with $\epsilon_3 = 0.1$ and Figures 4.4 (g) - (i) shows the corresponding results with $\epsilon_3 = -0.1$. Here also both the wavelets give similar results since the instantaneous frequency changes smoothly with the amplitude of oscillation as given by equation (3.30). Locus of frequency depends on the sign of ϵ_3. For positive ϵ_3, the instantaneous frequency decreases with reduction in amplitude of oscillation. It is more than unity and approaches unity as the amplitude decays. For negative ϵ_3, the instantaneous frequency increases with reduction in amplitude of oscillation. It is less than unity and approaches unity as the amplitude decays.

Figure 4.5 belongs to case (2). Here the two wavelets yield different loci for the instantaneous frequency. The standard Morlet wavelet gives a non-oscillatory curve for frequency with amplitude while the complete Morlet wavelet yields an oscillatory frequency plot. Characteristics of the oscillatory frequency plot depend on the sign of ϵ_2. For positive ϵ_2, the frequency locus maxima occur during the positive motion. This can be understood from the fact that the frequency of oscillation during positive motion is higher than that
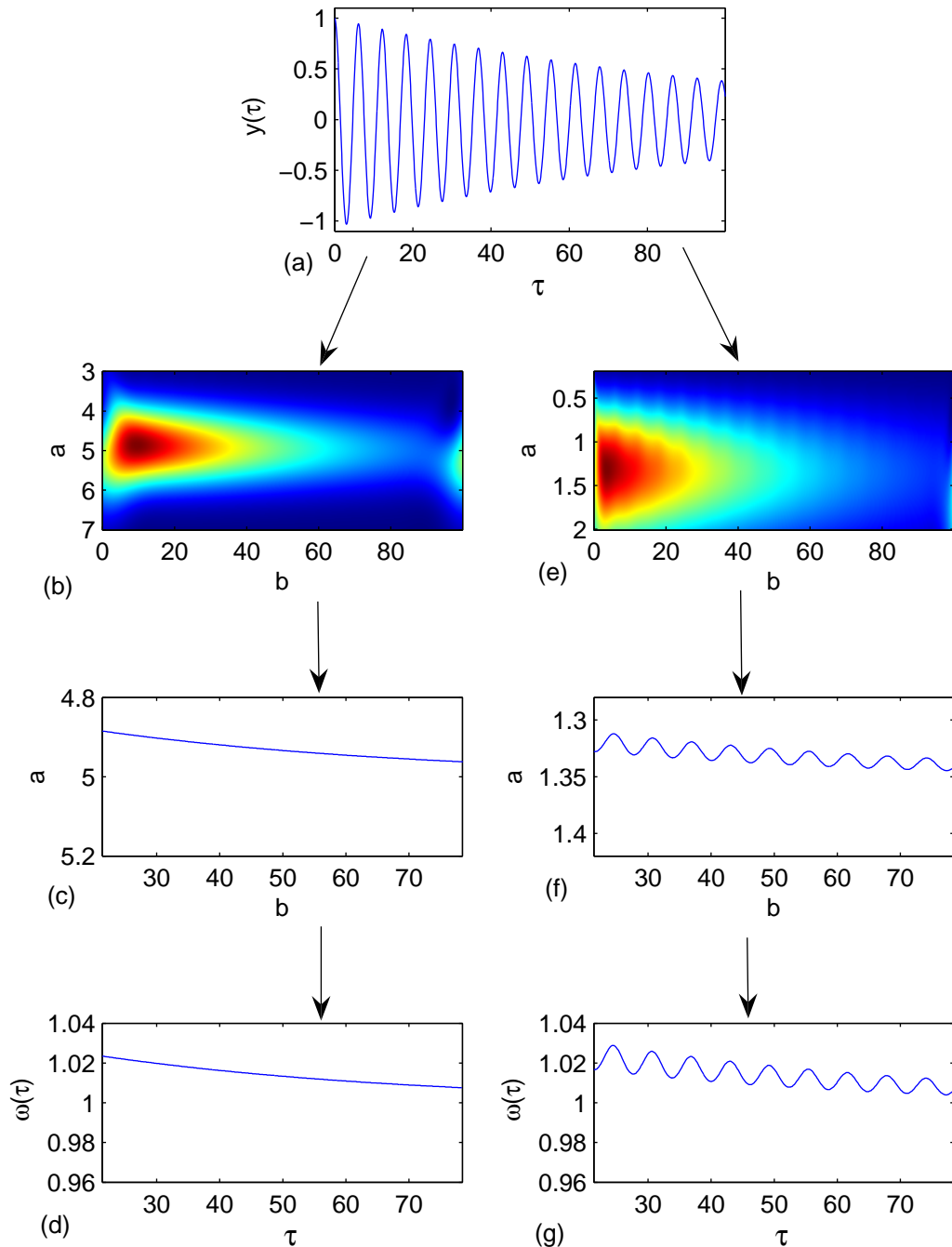
Figure 4.3: (a) Response of a mixed-parity nonlinear oscillator, $\epsilon_2 = 0.1$ and $\epsilon_3 = 0.1$ (b) Wavelet Transform of the response using standard Morlet wavelet (c) Ridge of the Wavelet Transform (d) Instantaneous frequency of the response (e) Wavelet Transform of the response using low-oscillation Morlet wavelet (f) Ridge of the Wavelet Transform (g) Instantaneous frequency of the response.

during the adjacent negative motion, equations (3.36) and (3.38). The non-oscillatory locus of the frequency obtained through the standard Morlet wavelet depends on the sign of ϵ_3 as discussed earlier. In absence of ϵ_3, the frequency obtained by the standard Morlet wavelet remain in the close vicinity of unity.

Figure 4.6 belongs to case (3). Here too, the two wavelets give different plots for the instantaneous frequency. The standard Morlet wavelet yields a non-oscillatory curve, while the complete Morlet wavelet shows oscillatory behavior of the frequency. The sign of ϵ_2 determines the oscillating locus of frequency. For negative ϵ_2, the frequency locus maxima occur during the negative motion. The presence and sign of ϵ_3 governs the non-oscillatory locus of the frequency obtained through the standard Morlet wavelet as discussed earlier.

To investigate the robustness of the procedure against external noise, white Gaussian noise of different magnitude is added to the response signal. Response of the system with parameter $\epsilon_2 = 0.1$ and $\epsilon_3 = 0.1$ is corrupted with signal to noise ratio (SNR) = 40, 30 and 20 dB. The procedure for the classification is applied and the results are shown in Figure 4.7. It is found that for low noise level i.e. SNR = 40 dB, results and its interpretation for the nonlinearity classification are not affected by noise. In presence of moderate noise i.e. SNR = 30 dB, the results are not affected qualitatively but oscillations in frequency locus are little distorted. At higher noise level of SNR = 20 dB, the distortion in the frequency locus is high and the oscillations in response signal and oscillations in frequency locus start losing correspondence.
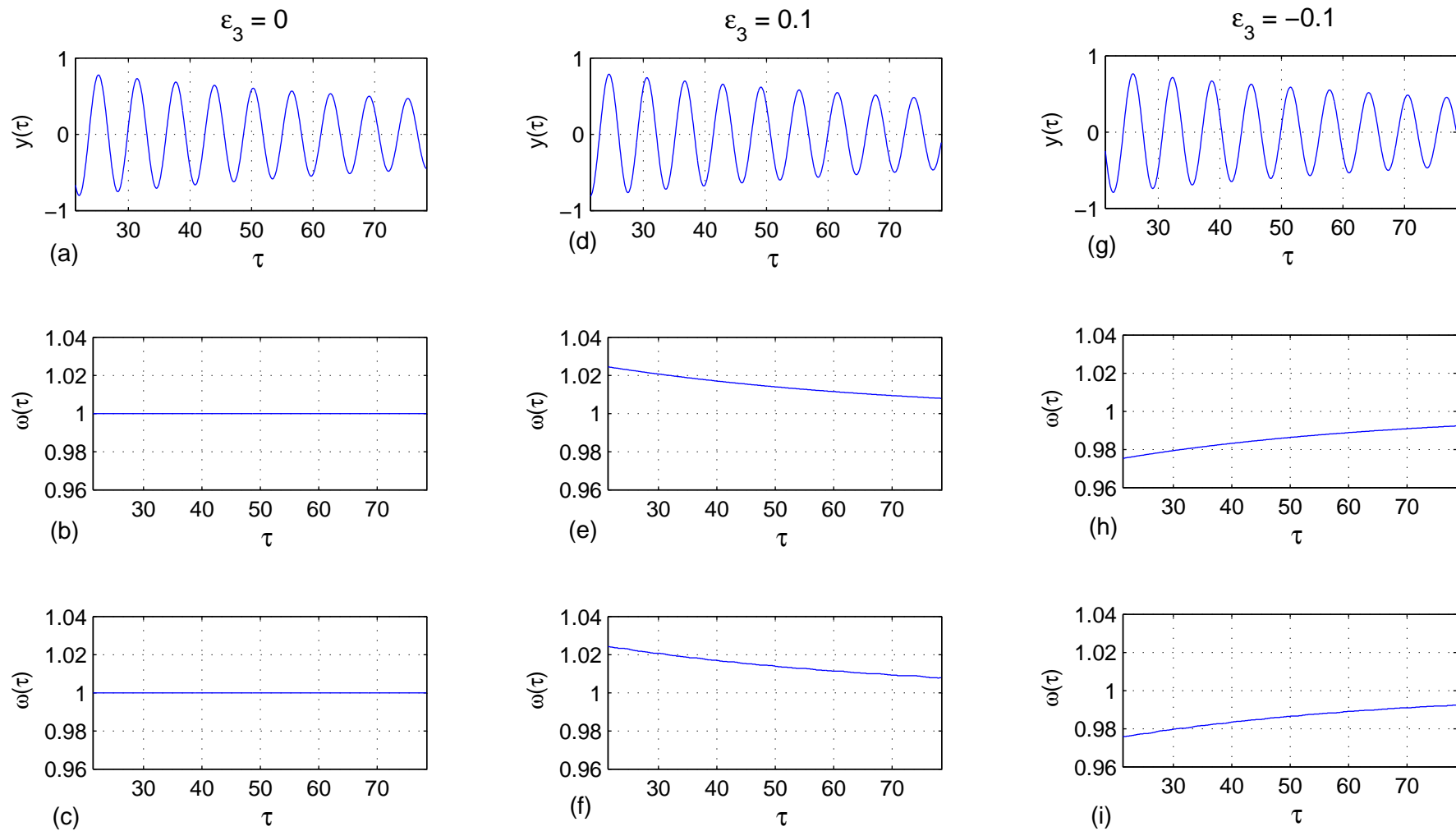
Figure 4.4: Results of Case (1) $\epsilon_2 = 0$. Simulated response (Row 1), Instantaneous frequency using standard Morlet wavelet (Row 2), Instantaneous frequency using low-oscillation Morlet wavelet (Row 3).
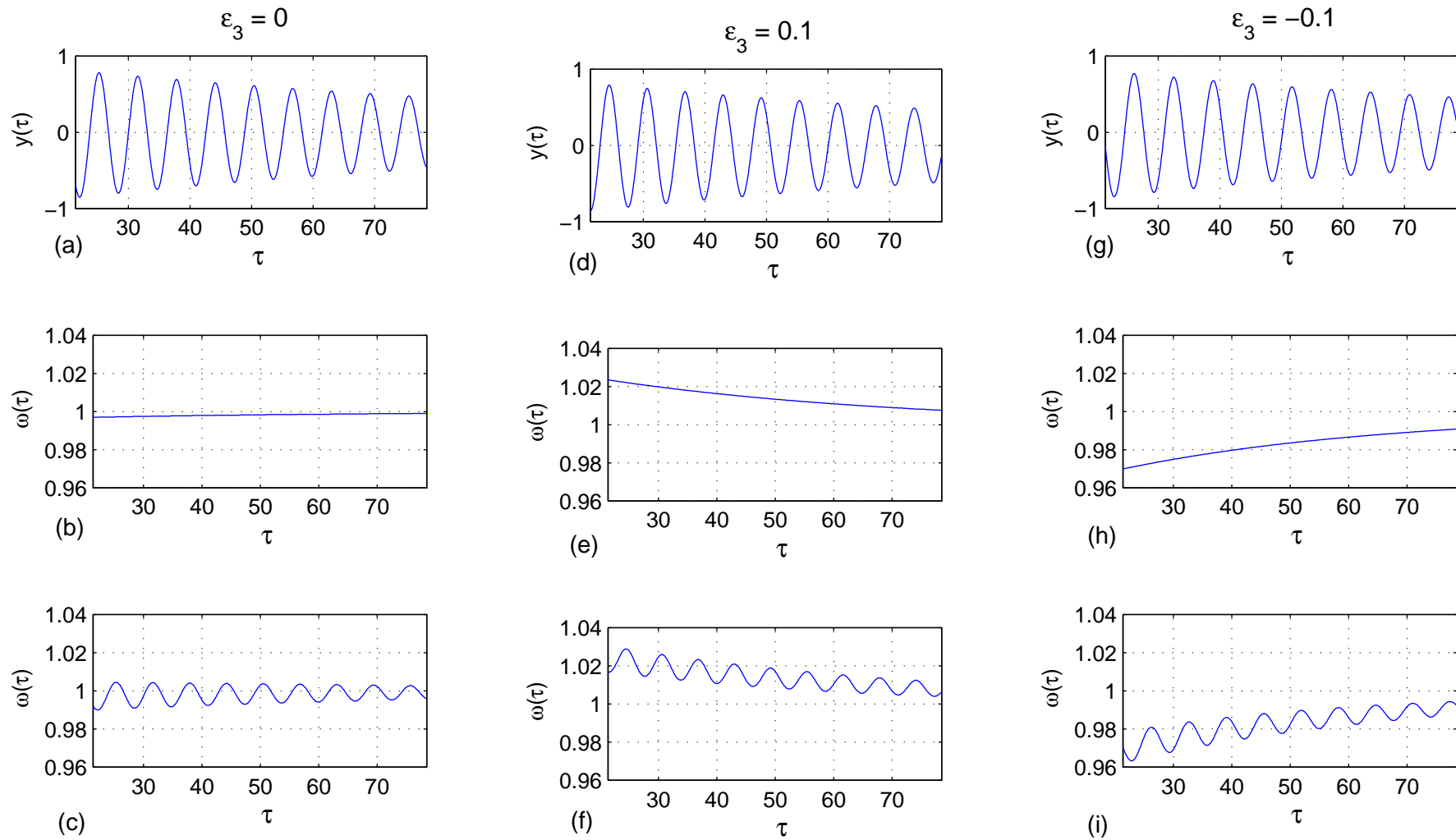
Figure 4.5: Results of Case (2) $\epsilon_2 = 0.1$. Simulated response (Row 1), Instantaneous frequency using standard Morlet wavelet (Row 2), Instantaneous frequency using low-oscillation Morlet wavelet (Row 3).

Figure 4.6: Results of Case (3) $\epsilon_2 = -0.1$. Simulated response (Row 1), Instantaneous frequency using standard Morlet wavelet (Row 2), Instantaneous frequency using low-oscillation Morlet wavelet (Row 3).

Figure 4.7: Effect of noise. $\epsilon_2 = 0.1$, $\epsilon_3 = 0.1$. Simulated response (Row 1), Instantaneous frequency using standard Morlet wavelet (Row 2), Instantaneous frequency using low-oscillation Morlet wavelet (Row 3).
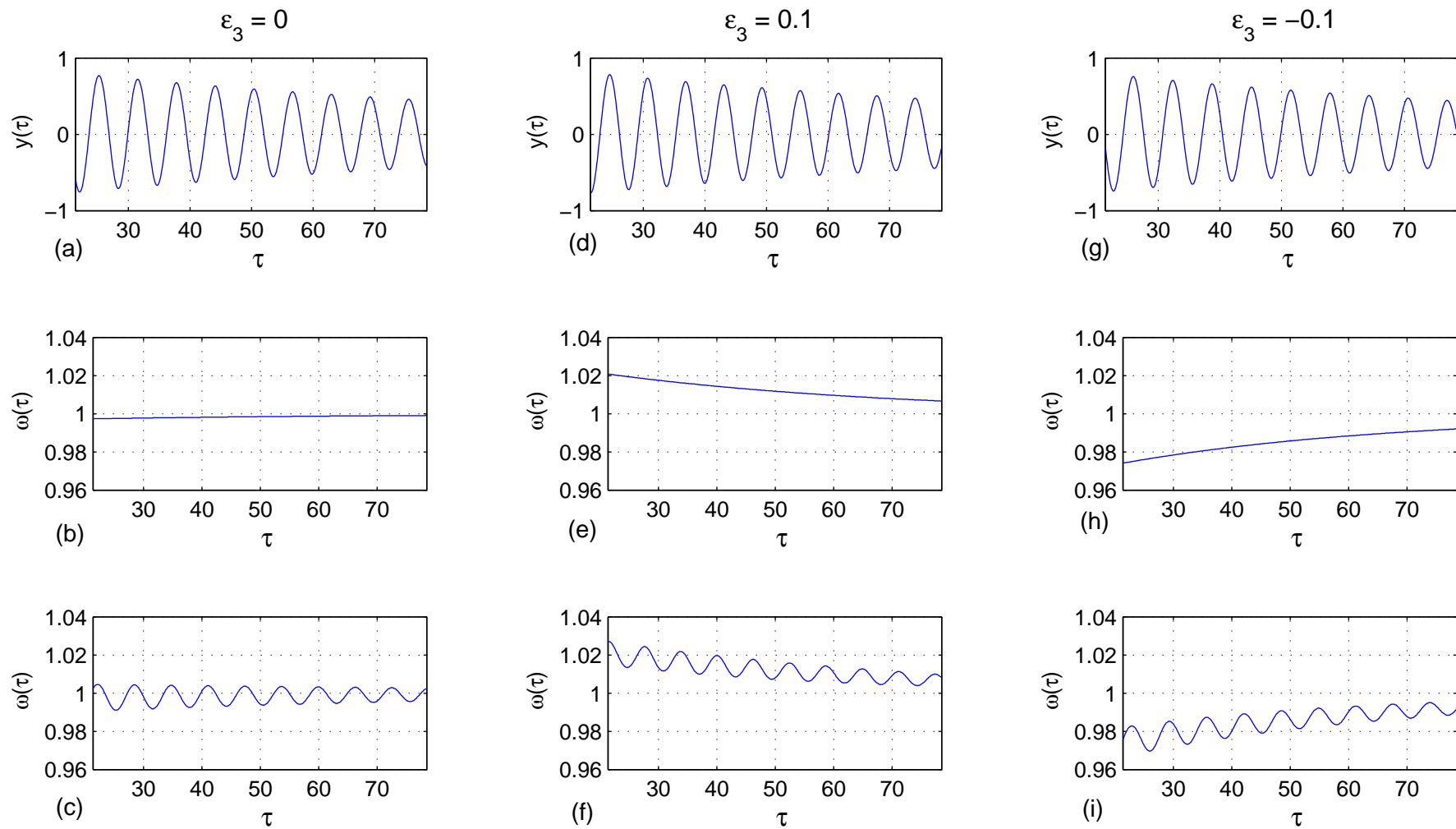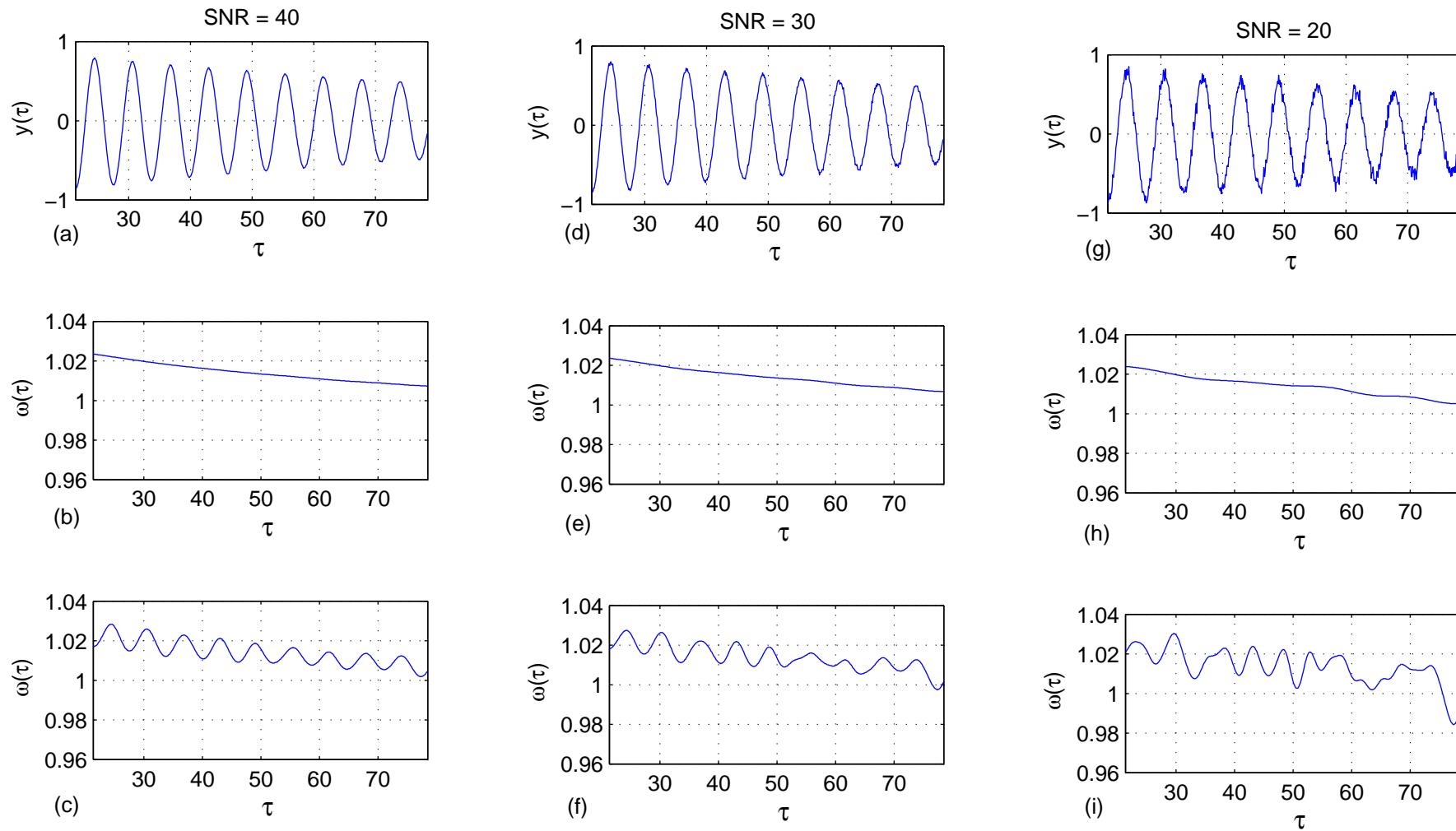
4.3   Remarks

Nonlinear stiffness represented by a third degree polynomial form is classified in two categories - symmetric and asymmetric and further sub-classification is carried out depending on the signs of nonlinearities. In case of symmetric polynomial forms, the frequency changes smoothly with amplitude of oscillation and this fact is evident from the governing equation, which is same for positive and negative motion. In case of asymmetric polynomial forms, the frequency shows oscillating behavior due to the different governing equation for positive and negative motion. The characteristics of frequency loci also depend on the signs of nonlinearities.

The frequency loci obtained through standard Morlet wavelet are non-oscillatory. Locus of frequency in this case is better explained by considering corresponding symmetric case i.e. the equation (3.30). Standard Morlet wavelet averages out the effect of asymmetric nonlinearity over a number of response cycles due to its higher time spread. This averaged out results can be used to find the presence and sign of ϵ_3. For positive ϵ_3, instantaneous frequency is more than unity and approaches unity as the amplitude decays.

For negative ϵ_3, the instantaneous frequency is less than unity and approaches unity as the amplitude decays. In absence of ϵ_3, frequency remains in the close vicinity of unity.

Complete Morlet wavelet, due to its ability to capture the temporal phenomenon, is able to distinguish between the symmetric and asymmetric forms easily. It gives non-oscillatory frequency locus for symmetric nonlinearity while for asymmetric nonlinearity the frequency locus is oscillatory. The oscillatory locus of frequency is better explained by the equations (3.36) and (3.38). The loci of frequency also help in deciding the signs of asymmetric nonlinearity (ϵ_2). The frequency locus maxima occur during the positive motion for positive ϵ_2 while for negative ϵ_2, frequency locus maxima occur during the negative motion.

The procedure also gives good results in presence of moderate noise i.e. up to SNR = 30.

The classification of nonlinearities in this way is useful to decide the form of system equation from its free vibration response. This leads to a better mathematical representation of the system which can be used further for the system parameter estimation.

Chapter 5

Parameter Estimation and Error Analysis in Single Degree of Freedom Systems

Nonlinear parameter estimation is carried out here using analytical results from Krylov-Bogoliubov method (refer Chapter 3) in conjunction with numerical results from Wavelet Transform procedure. As seen in earlier chapters, both involve approximations. The Krylov-Bogoliubov method assumes the system to have weak nonlinearity, while Wavelet Transform of the response signal assume the signal to be asymptotic. Therefore, errors are expected in the estimation of nonlinear parameters. A study on these errors is also attempted here. Most of the previous work on nonlinear system identification, using Wavelet Transforms, pertains to Duffing type of system, with linear or nonlinear damping of polynomial type. In the present study, parameter estimation is carried out on two oscillators: one having cubic stiffness nonlinearity, known as Duffing oscillator and the other is a self excited oscillator having nonlinear damping of the van der Pol type.

5.1 Duffing System

Since the Krylov-Bogoliubov method assumes weak nonlinearities, the estimation error is expected to depend on the magnitude of nonlinearities. An analysis of errors is carried out here for the system represented by the Duffing oscillator with viscous damping.

5.1.1 Response of the Duffing System

A Duffing system executing free vibrations, initiated by giving some initial displacement, can be represented by

$$mx''(t) + cx'(t) + k_1 x(t) + k_3 x^3(t) = 0; \qquad x(0) = X_0, \quad x'(0) = 0 \tag{5.1}$$

where ($'$) represents the differentiation with respect to time t. Defining the following non-dimensional parameters

$\tau = \omega_n t \qquad\qquad \omega_n = \sqrt{k_1/m} \qquad\qquad \zeta = c/2m\omega_n$

$y = x/X_0 \qquad\qquad \epsilon_3 = k_3 X_0^2/k_1 \qquad\qquad \dot{x} = \mathrm{d}x/\mathrm{d}\tau$

equation (5.1) becomes

$$\ddot{y}(\tau) + 2\zeta\dot{y}(\tau) + y(\tau) + \epsilon_3 y^3 \;=\; 0 \qquad y(0) = 1 \quad \dot{y}(0) = 0 \tag{5.2}$$

The above non-dimensional equation contains two non-dimensional system parameter i.e. damping factor (ζ) and non-dimensional nonlinearity parameter (ϵ_3). Parameter estimation exercise is carried out on these two non-dimensional parameters, (ζ) and (ϵ_3).

The Krylov-Bogoliubov method provides the solution of above equation (5.2) as (Mickens, 1995)

$$y(\tau) \;=\; A_0 \mathrm{e}^{-\zeta\tau} \cos\left[\tau + \int_0^\tau \frac{3}{8}\epsilon_3 A^2(\tau)\mathrm{d}\tau + \theta_0\right] \tag{5.3}$$

where amplitude envelope $A(\tau)$ and instantaneous frequency $\omega(\tau)$ are given by the following expressions

$$A(\tau) = A_0 e^{-\zeta\tau} \tag{5.4}$$

$$\omega(\tau) = 1 + \dot{\theta}(\tau)$$
$$= 1 + \frac{3}{8}\epsilon_3 A^2(\tau) \tag{5.5}$$

The above relationship shows the dependence of the frequency of oscillations on the amplitude of oscillations. This characteristic is utilized to estimate the nonlinear parameter (ϵ_3) and subsequently estimation error is calculated.

5.1.2   Wavelet Transform of the Response

Wavelet Transform of the response signal is carried out using standard Morlet wavelet. Ridges and skeleton of the transform are determined. Subsequently instantaneous frequency $(\omega(b))$ and amplitude envelope $(A(b))$ of the signal are determined.

5.1.3   Estimation of System Parameters

According to equation (5.5), an expression of the form

$$\omega(b) = 1 + c_2 A^2(b) \tag{5.6}$$

is fitted over the instantaneous frequency $\omega(b)$ and amplitude envelope $A(b)$ data. The coefficient c_2 is calculated using the least square error criterion. Value of the coefficient c_2 is $3\epsilon_3/8$ and this fact is used to estimate the nonlinear parameter ϵ_3. The corresponding percentage error in estimation is calculated The amplitude envelope $A(b)$ can be used to determine the damping factor ζ. The logarithm of amplitude envelope $A(b)$ is given by

$$\log A(b) = \log A_0 - \zeta b \tag{5.7}$$

Hence the damping factor ζ is determined as negative of the slope of the logarithm of $A(b)$ v/s b line and subsequently estimation error is determined.

5.1.4 Illustration

Figures 5.1 (a-i) illustrate the steps involved in nonlinear system parameter estimation. The nonlinear system equation (5.2) with the parameters $\zeta = 0.01$ and $\epsilon_3 = 0.1$ is simulated through fourth order Runge-Kutta method and the response is shown in Figure 5.1 (a). The response of the system is wavelet transformed and represented as modulus of Analytic Wavelet Transform (AWT) in Figure 5.1 (b). At this step Wavelet Transform is obtained over the wide range of scale ($a=3-7$) with the coarse incremental step size of 0.02. Figure 5.1(c) shows the ridge of the AWT. The ridge decides the range of scale over which the modulus of AWT attains the maximum value. This useful range of scale is finely divided in 300 equal parts and the wavelet transformation is performed over the response again. The corresponding modulus of AWT is shown in Figure 5.1 (d), while the corresponding ridge, after discarding the data influenced by edge effects, is shown in Figure 5.1 (e). The length of edge effect is considered as six times the time spread of wavelet function i.e. ($6\sigma_{\tau_{b,a}}$). Locus of the ridge is converted to frequency variation with time and represented in Figure 5.1(f). Figure 5.1(g) shows the envelope of the response obtained through skeleton of the Wavelet Transform. Information about the instantaneous frequency and amplitude envelope is used to draw the backbone curve ($\omega(b)$ v/s $A(b)$) in Figure 5.1(h). Equation (5.6) is fitted over the backbone data using least square error method to estimate nonlinear parameter ϵ_3 and the same is shown as a dotted curve in Figure 5.1 (h). The parameter estimation error is calculated further. The slope of the logarithm of amplitude envelope is used to determine the damping factor ζ. The logarithm of amplitude envelope is plotted in Figure 5.1(i), the best fit line is estimated and drawn as a dotted line in the same figure. The slope of this best fit line is reported as the damping factor of the system.
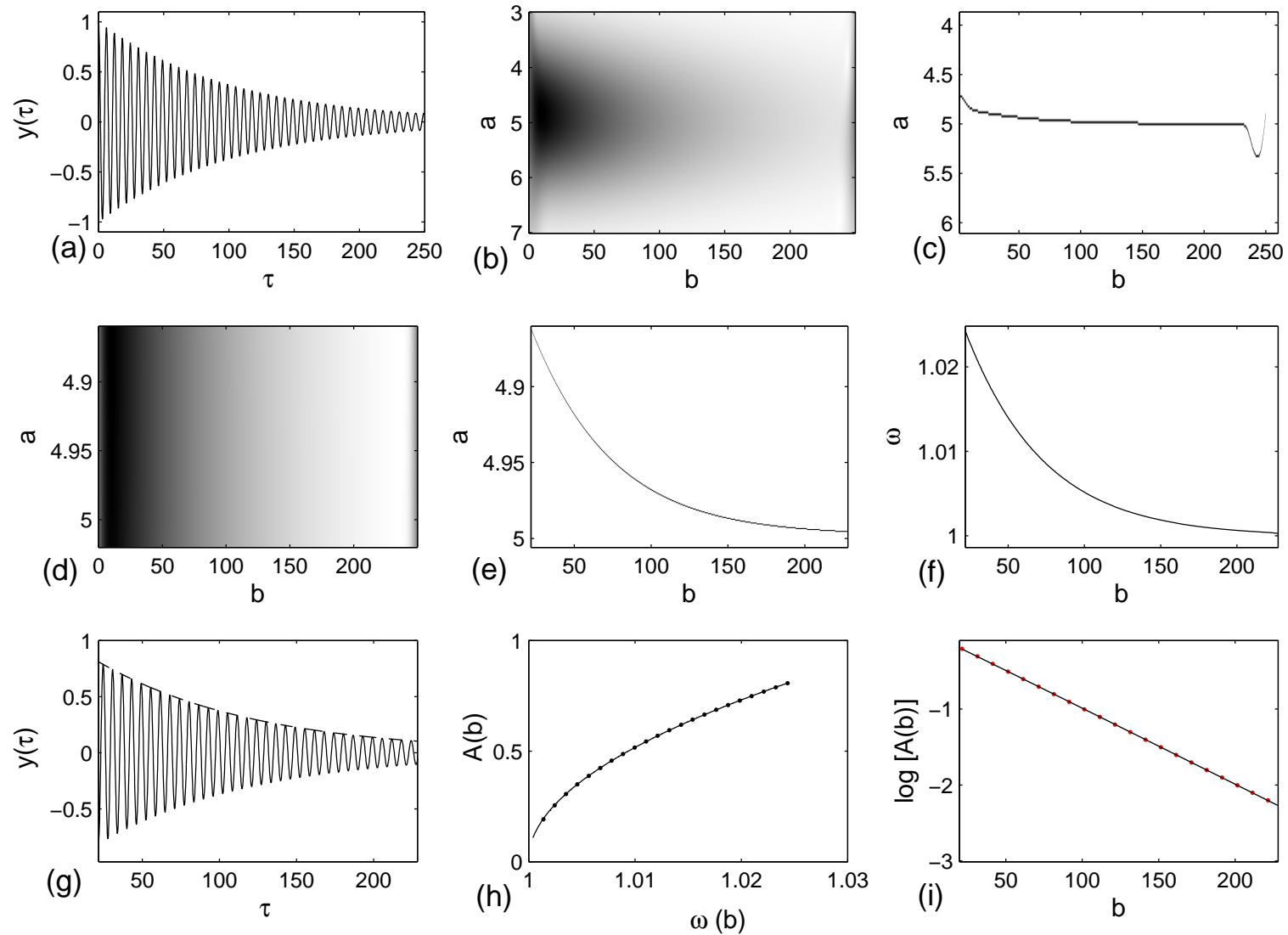
Figure 5.1: Various steps involved in the estimation of system parameters (a) Simulated response (b) Wavelet Transform ($a = 3$–7) (c) Ridge (d) Wavelet Transorm for finer resolution over scale (e) Ridge (f) ω v/s time (g) Amplitude envelope A(b) (h) ω(b) v/s A(b) (i) log A(b) v/s b

The above procedure is repeated for low to moderate values of system parameters. The range of ϵ_3 considered is from 0.05 to 0.25 and range of ζ is from 0.005 to 0.015. Estimation errors are calculated by changing ϵ_3 and ζ in steps of 0.01 and 0.001 respectively. The results obtained are shown in Figure 5.2 as the error surfaces. Figure 5.2(a) shows variation of nonlinear parameter estimation errors with the system parameters and Figure 5.2(b) shows the cross section of the surface for fixed damping factor $\zeta = 0.012$. Figure 5.2(c) shows variation of damping factor estimation errors with the system parameters and Figure 5.2(d) shows the cross section of the surface for a fixed damping factor $\zeta = 0.012$. The estimated parameters and estimation errors for the selected values of ϵ_3 for $\zeta = 0.012$ are tabulated in Table 5.1. The symbols ϵ_{3a}, ϵ_{3e} and e_3 represent the actual nonlinear system parameter, the estimated nonlinear parameter, and the error in the nonlinear parameter estimation respectively. ζ_e and e_ζ are the estimated damping factor and its estimation error respectively.

5.2   Remarks

It is found that the error in estimation of nonlinear parameter depends on the magnitude of nonlinear system parameters for specific wavelet. For a fixed value of damping, the estimation errors are low for a range of nonlinear parameters. For example, for a fixed value of $\zeta = 0.012$, estimation errors are low (-0.15 to -0.49 %), for ϵ_3 in the range of 0.05-0.15. For values of ϵ_3 beyond this range, the estimation errors are considerably higher. The fact can be used to design the experiments. The nonlinear parameter ϵ_3 is defined as $k_3 X_0^2/k_1$ and therefore, initial condition X_0 can be controlled such that ϵ_3 lies in the range where estimation errors are low.

In general, high estimation errors are obtained at higher nonlinearities. The analytical results obtained from Krylov-Bogoliubov method are based on the assumption of small nonlinearity and therefore analytical results at higher nonlinearities do not represent the system response truly.
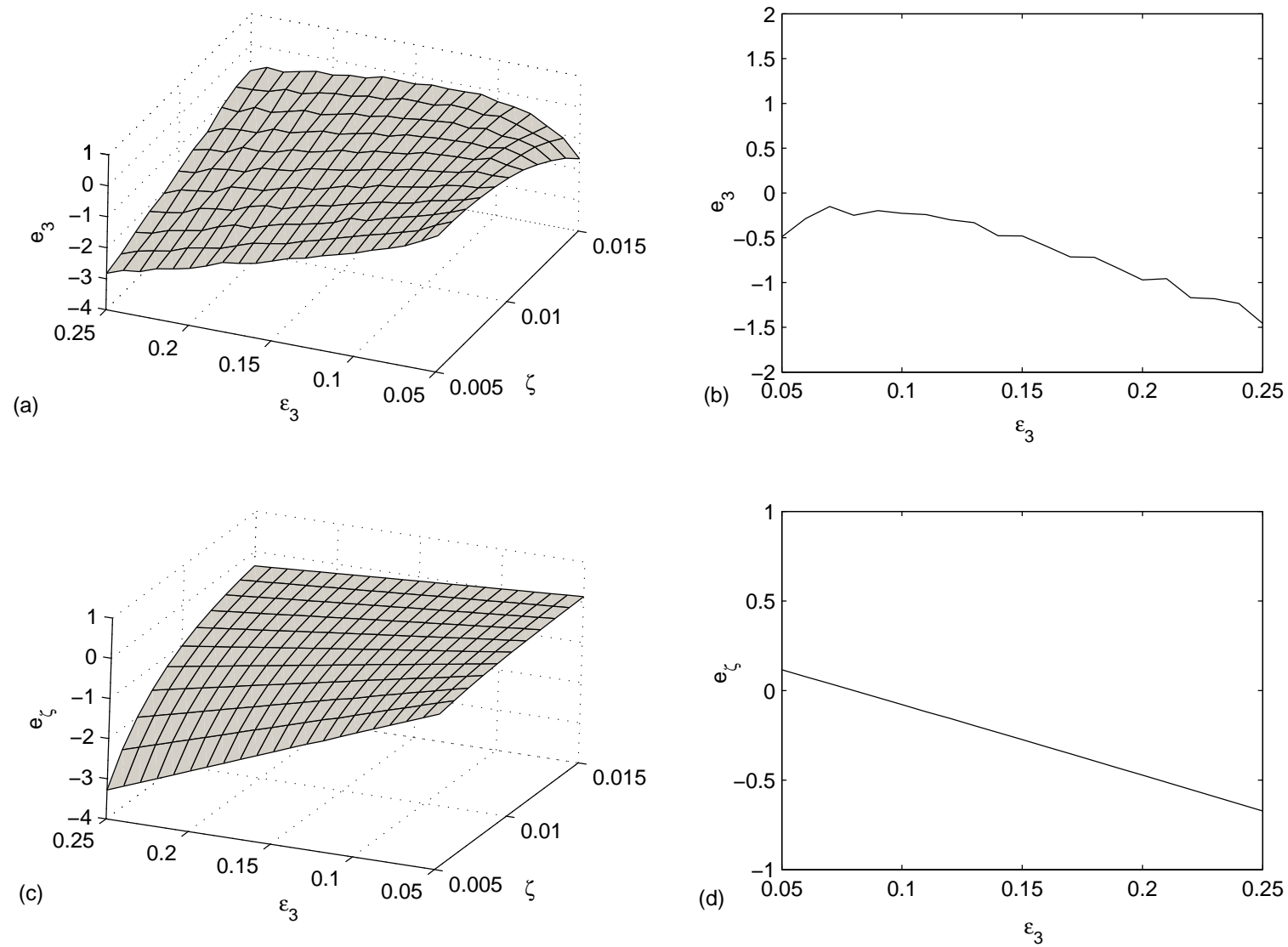
Figure 5.2: (a) Error surface for nonlinear parameter (b) Cross section of the nonlinear parameter error surface at $\zeta = 0.012$ (c) Error surface for damping factor and (d) Cross section of the damping error surface at $\zeta = 0.012$

Table 5.1: Estimated parameters and estimation errors

ϵ_{3a}	ϵ_{3e}	$e_3(\%)$	ζ_e	$e_\zeta(\%)$
0.05	0.0498	-0.489	0.01201	0.115
0.10	0.0998	-0.227	0.01199	-0.079
0.15	0.1493	-0.481	0.01197	-0.274
0.20	0.1980	-0.971	0.01194	-0.473
0.25	0.2463	-1.459	0.01192	-0.673

The estimation error is also high at higher damping values. The oscillations decay rapidly at higher damping and a short duration response signal is available for the analysis. A considerable portion of the Wavelet Transform of the short response signal is affected by the edge effect which gives rise to higher estimation errors.

5.3 A Self-Excited System : van der Pol System

The van der Pol system is a classical nonlinear system representation which has been used extensively in physical and biological sciences. It is used as a basic model in mechanical and electrical engineering also, where self sustained oscillations occur (Stoker, 1957). It has been used to model aortic blood flow (Atlas and Desiderio, 2006). Some other examples related to self-sustaining systems include flutter, a violin string, a block moving on a belt etc (Nayfeh, 1979). The free vibration response of a van der Pol system initiated by small disturbance shows transient vibrations for some duration before attaining steady state limit cycle oscillations. Analytical results known from the Krylov-Bogoliubov method show that the initial transient response depends on linear and nonlinear part of the system damping while amplitude of limit cycle oscillation

depends on the linear part of system damping. The amplitude envelope is obtained numerically using the ridge and skeleton method of Wavelet Transform. The analytical results and numerical results are used in conjunction to find the system parameters. The effect of linear and nonlinear part of damping on parameter estimation is studied here to establish the limitation of the procedure. Minimum sampling frequency required to obtain the better estimates of the system parameter is discussed. The algorithm is also checked in presence of moderate signal noise.

5.3.1 Response of van der Pol System

The van der Pol system executing free vibration under some initial disturbance can be modeled by the following equation

$$\ddot{x} + \epsilon_1(x^2 - \mu_1)\dot{x} + \omega_n^2 x = 0 \qquad\qquad x(0) = X_0\,;\ \dot{x}(0) = \dot{X}_0 \qquad\qquad (5.8)$$

The approximate analytic solution of this system is known from Krylov-Bogoliubov technique (Nayfeh, 1973), as

$$x(t) \quad = \quad A(t)\cos[\phi(t)] \qquad\qquad (5.9)$$

It assumes that for small values of the system parameters, the amplitude, $A(t)$ and phase, $\phi(t)$ change slowly so that

$$A(t) \quad = \quad \frac{2\sqrt{\mu_1}}{\sqrt{1 + (\frac{4\mu_1}{A_0^2} - 1)\mathrm{e}^{-\epsilon_1\mu_1 t}}} \qquad\qquad (5.10)$$

and

$$\phi(t) \quad = \quad \omega_n t + \theta_0 \qquad\qquad (5.11)$$

where A_0 and θ_0 are constants and depend on the initial conditions of the system. The instantaneous frequency is constant and equal to ω_n due to linear stiffness term in the system while amplitude envelope $A(t)$, changes with time in accordance with equation (5.10), due to the presence of damping in the system (Nayfeh, 1973).

5.3.2 Wavelet Transform of the Response Signal

For the response of van der Pol oscillator given by equation (5.10) the Wavelet Transform can be written as

$$W_x(a,b) = \frac{\sqrt{a}}{2} \frac{2\sqrt{\mu_1}}{\sqrt{1 + (\frac{4\mu_1}{A_0^2} - 1)e^{-\mu_1\epsilon_1 b}}} e^{j\omega_n b}(4\pi\sigma^2)^{1/4}e^{-\sigma^2(a\omega_n - \omega_0)^2/2} \qquad (5.12)$$

5.3.3 Estimation of System Parameters

Frequency of the response (ω_n) for the van der Pol oscillator is constant and therefore, the locus of the ridge in time-frequency plane will be a horizontal line parallel to the time axis.

The value of Wavelet Transform restricted to its ridge is known as the skeleton of the Wavelet Transform. Hence the skeleton of the asymptotic signal is

$$W_x(a_r(b),b) = \frac{\sqrt{a_r(b)}}{2}A(b)e^{j\omega b}(4\pi\sigma^2)^{1/4} \qquad (5.13)$$

$$= C(b)A(b)e^{j\omega b} \qquad (5.14)$$

where $C(b) = \frac{\sqrt{a_r(b)}}{2}(4\pi\sigma^2)^{1/4}$.

The modulus of skeleton is

$$|W_x(a_r(b),b)| = C(b)A(b) \qquad (5.15)$$

$$|W_x(a_r(b),b)| = C(b)\frac{2\sqrt{\mu_1}}{\sqrt{1 + (\frac{4\mu_1}{A_0^2} - 1)e^{-\mu_1\epsilon_1 b}}} \qquad (5.16)$$

The factor $C(b)$ is a correction factor and it is known. Hence the envelope of the signal $A(b)$ can be determined by equation (5.15).

The above two equations with some algebraic manipulation can be written as

$$\ln Z = \mu_1\epsilon_1 b \qquad (5.17)$$

where

$$
\begin{aligned}
Z &= Num/Den \\
Num &= \left(\frac{|W_x(a_r(b),b)|}{C(b)}\right)^2 \Big/ \left(4\mu_1 - \left(\frac{|W_x(a_r(b),b)|}{C(b)}\right)^2\right) \\
Den &= \left(\frac{|W_x(a_r(0),0)|}{C(0)}\right)^2 \Big/ \left(4\mu_1 - \left(\frac{|W_x(a_r(0),0)|}{C(0)}\right)^2\right)
\end{aligned}
$$

The logarithm of Z and time b are related by straight line relationship during the initial transient phase. The slope of the line is $\mu_1\epsilon_1$. The response amplitude will approach a limiting value of $2\sqrt{\mu_1}$ after a certain time, depending on the value of system parameters. This fact is used to estimate the system parameters.

5.3.4   Illustration

Using the following nondimensional substitutions

$$
\tau = \omega_n t \qquad\qquad \epsilon = \frac{\epsilon_1}{\omega_n} \qquad\qquad \mu = \mu_1
$$

equation (5.8) can be rewritten as

$$
\ddot{x} + \epsilon(x^2 - \mu)\dot{x} + x = 0 \qquad\qquad x(0) = X_0; \ \dot{x}(0) = \dot{X}_0 \tag{5.18}
$$

The above equation (5.18) contains two parameters (ϵ and μ)), to be estimated.

Application of the procedure has been numerically illustrated. The various steps involved in the parameter estimation procedure are explained in Figure 5.3. The assumed system parameters are $\epsilon = 0.05$ and $\mu = 1$. Figure 5.3(a) shows a portion of the simulated transient response through fourth order Runge-Kutta method with $x(0) = 0.1$ and $\dot{x}(0) = 0$. The scalogram over the scale of interest, using Gabor wavelet function, is shown in Figure 5.3(b). The Gabor wavelet function parameter $\sigma = 1$ and $\omega_0 = 5$ are used in the present work. These wavelet parameters meet the admissibility criterion (Carmona and Torresani, 1998) and provide equal and optimal resolution in time and frequency plane.

Since our signal involves single frequency a wavelet function having equal resolution in time and frequency plane is considered. The data affected by edge effects are discarded to minimize the error. The length of edge effect is considered as six times the standard deviation of the wavelet function. The estimated ridge is shown in Figure 5.3(c). The corresponding variation of frequency with time is shown in Figure 5.3(d). The horizontal ridge in Figure 5.3(c) can be taken as an indicator of the fact that the stiffness term in the system is linear (Nayfeh, 1973; Ta and Lardies, 2006). The ridge is along the scale $a = 5$ which corresponds to oscillating frequency equal to one, as expected. Figure 5.3(e) shows the estimated amplitude envelope of the response signal obtained using skeleton of the Wavelet Transform and the plot of logarithm of Z v/s time for initial transient response is shown in Figure 5.3(f). The linearity of the plot of logarithm of Z v/s time in Figure 5.3(f) also provides a tool to confirm that the nonlinearity in damping is of van der Pol type. The parameter μ is calculated by the limit cycle amplitude which is $2\sqrt{\mu}$ while slope in Figure 5.3(f) gives the product $(\mu\epsilon)$ and therefore, the two parameter can be calculated. Errors in estimation of parameters are calculated.

The above procedure is repeated for a range of parameters. Value of μ is varied from 0.5 to 2 in the steps of 0.25, while value of ϵ is changed from 0.01 to 0.1 in steps of 0.01. The parameter estimation errors are represented by error surfaces as a function of the system parameters. Figure 5.4 shows errors in estimation of μ i.e. (e_μ) while Figure 5.5 shows the estimation errors for ϵ i.e. (e_ϵ). The error increases with increase in the value of system parameters. It seems the estimation error depends on the product $(\mu\epsilon)$. Figure 5.6 and Figure 5.7 shows the variation of estimation error with $(\mu\epsilon)$ for μ and ϵ respectively. The error in estimation of linear parameter μ ranges from 0.015% to 0.77%, while the error in estimation of nonlinear parameter ϵ ranges from 0.08% to 8.54% over the range of parameter considered.

Good estimates are also obtained in the presence of nominal measurement noise. The response in a case with $\mu = 1$ and $\epsilon = 0.05$ was corrupted with white Gaussian noise, with signal to noise ratio (SNR) of 40 dB. The results of simulation are shown in Figure

5.8(a)-(f). The noise affects the detection and estimation of nonlinear parameter ϵ. The plot of logarithm of Z v/s time slightly deviates from straight line relationship. The error for noisy data is 1.04 % which is marginally higher as compared to 0.48 % in absence of noise.

Sampling frequency of the response signal affects the estimated value of nonlinear parameter ϵ. There should be a minimum required sampling frequency as dictated by the Nyquist sampling theorem (Carmona and Torresani, 1998) for accurate estimation of the nonlinear parameter. In order to establish a criterion, the sampling frequency is varied from 2 rad/sec to 10 rad/sec in the steps of 1 rad/sec for ($\mu\epsilon = 0.04$) and ($\mu\epsilon = 0.1$). The variation of error in the estimate of the parameter with sampling frequency is shown in Figure 5.9. The error in estimation attains almost a fixed lowest value at a sampling frequency equal to 5 rad/sec. It can therefore be said that the sampling frequency should be at least 5 times the oscillating frequency of the transient response in order to achieve minimum error status. Oversampling of the response signal may provide more detailed signal description but it does not help in reducing the estimation error.

5.4 Remarks

Parameter estimation error is high for higher value of the product ($\mu\epsilon$). The growth of the transient response is higher for higher value of the product and the response signal does not remain truly asymptotic. The underlying assumption of weak nonlinearity in Krylov-Bogoliubov method is also violated. Hence the procedure is applicable to weakly nonlinear system having low value of the product ($\mu\epsilon$) . Moreover fast growth of transient response gives very small signal length for the analysis, out of which significant portion is affected by end effect resulting in higher estimation error.
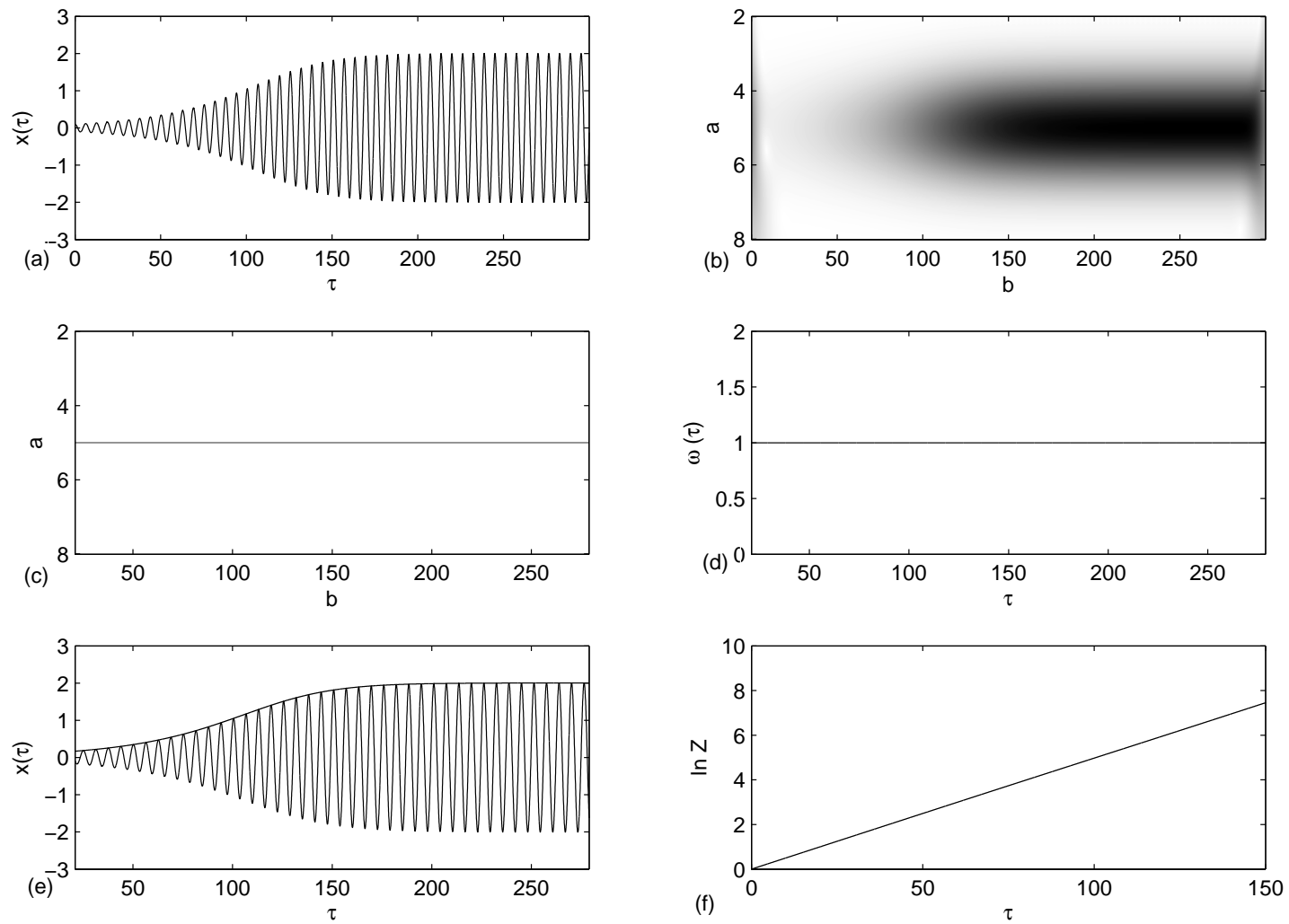
Figure 5.3: (a) Simulated response (b) Normalized scalogram (c) Ridge (d) frequency v/s time (e) Envelope of the response (f) $\ln Z$ v/s time, for $\mu = 1 \, \epsilon = 0.05$
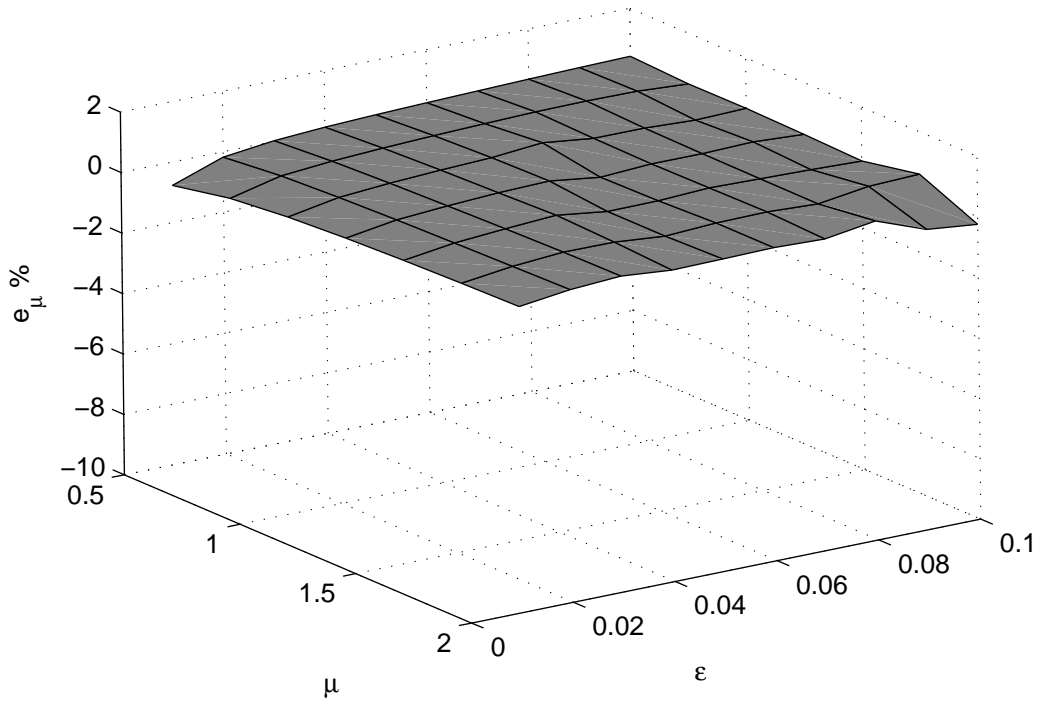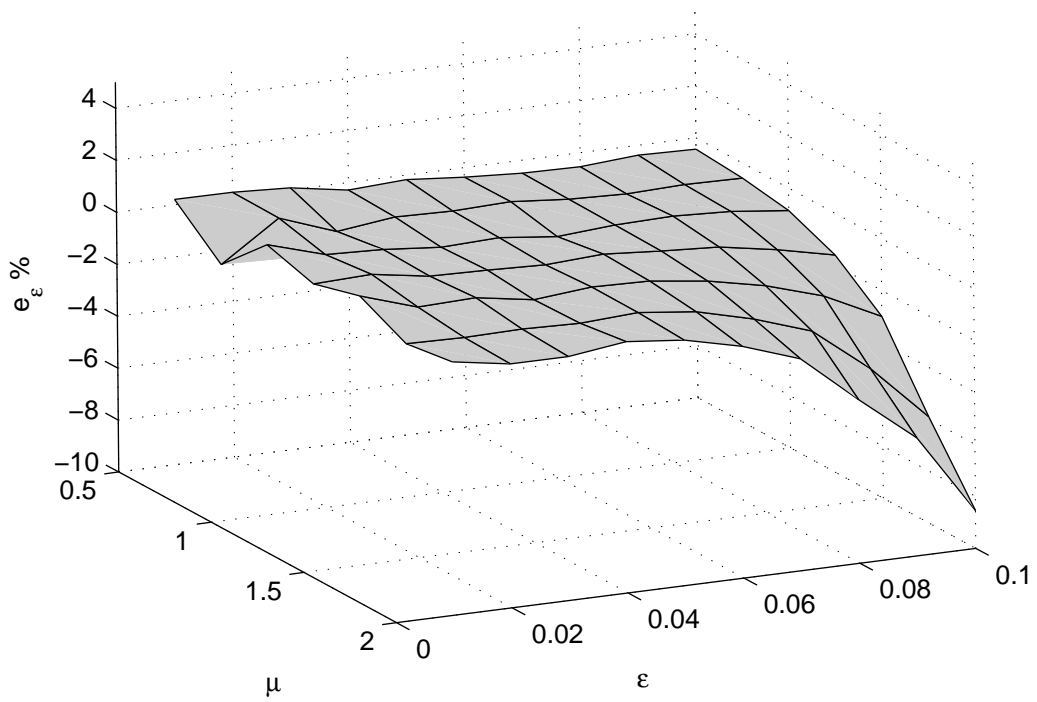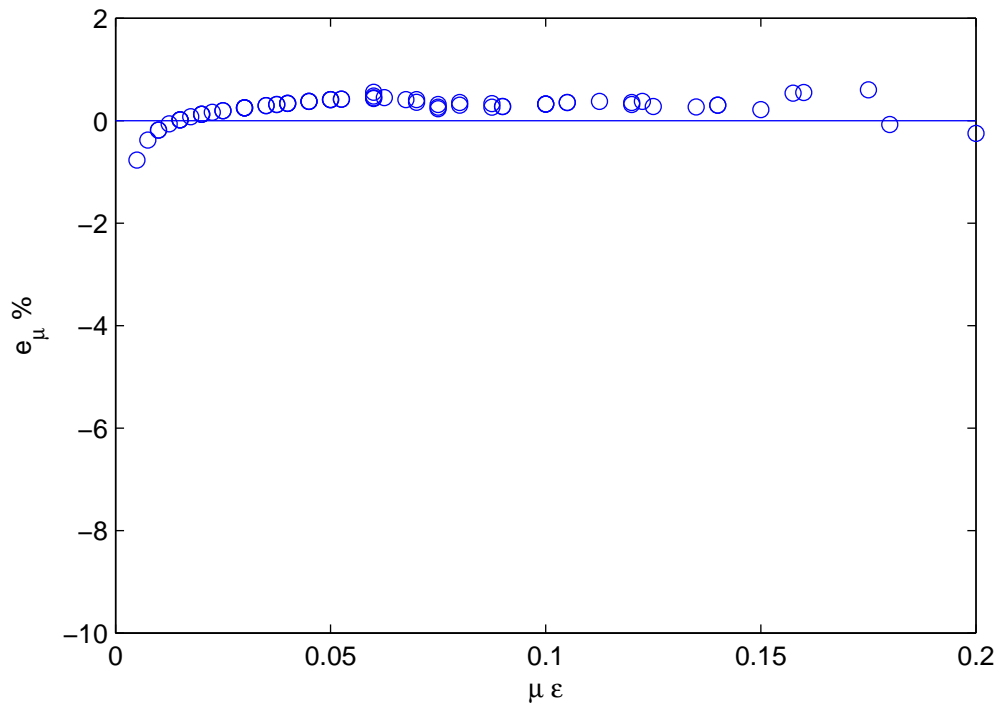
Figure 5.4: Error surface for the parameter μ
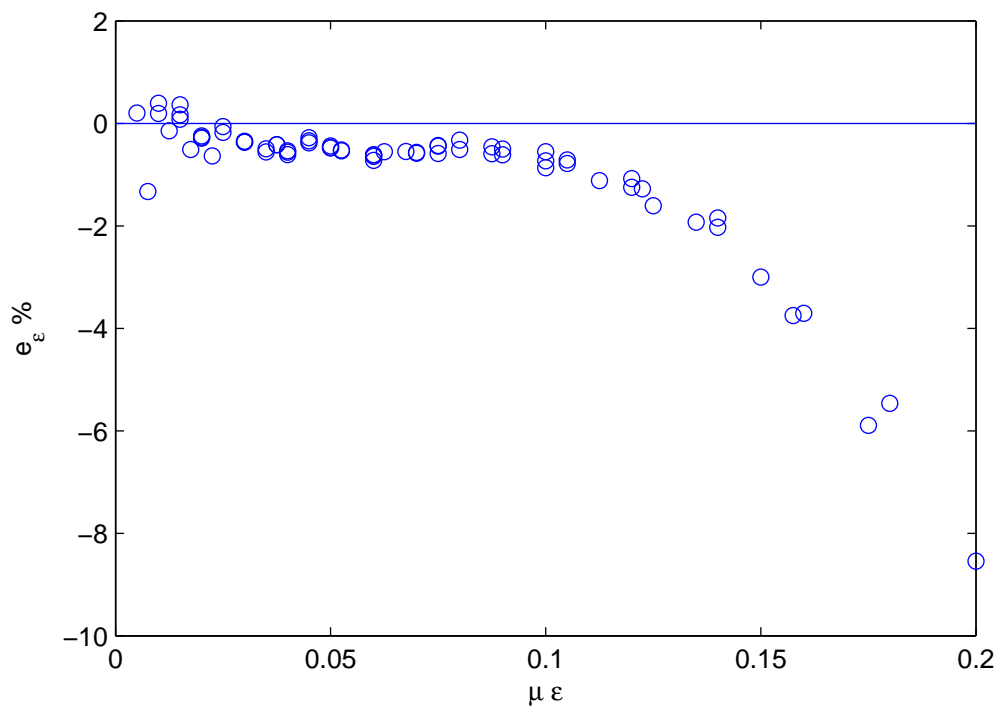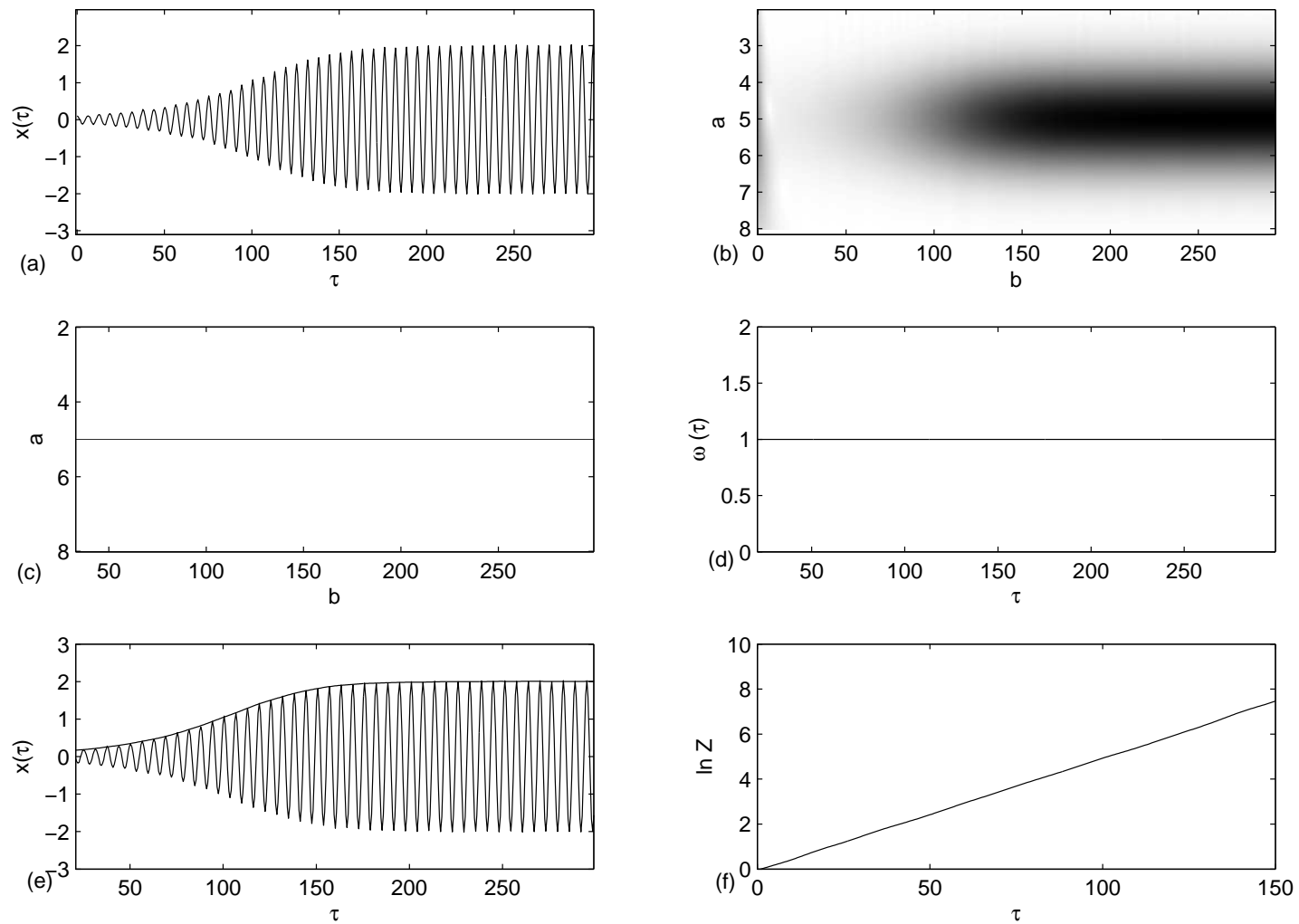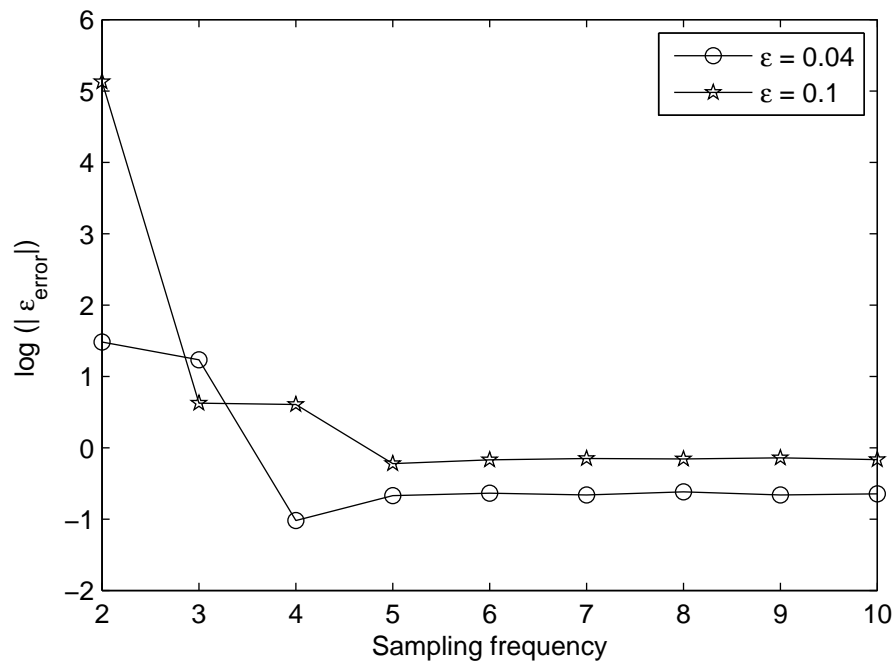

Figure 5.5: Error surface for the parameter ϵ

Figure 5.6: Variation of error in μ with the product of parameters $\mu\epsilon$

Figure 5.7: Variation of error in ϵ with the product of parameters $\mu\epsilon$

Figure 5.8: (a) Simulated response (b) Normalized scalogram (c) Ridge (d) frequency v/s time (e) Envelope of the response (f) $\ln Z$ v/s time, for $\mu = 1\,\epsilon = 0.05$, SNR=40dB

Figure 5.9: Variation of errors in nonlinear parameter estimation with sampling frequency

It is evident from these results that the methodology is able to detect the van der Pol type of nonlinearity in the given response signal and provides good estimate of nonlinear parameter for small product of system parameters. The estimation error in ϵ remains within 1 % for $\mu\epsilon < 0.12$

The proposed method provides a tool based on free vibration response and does not require measurement of the excitation force. Also, measurement of only one of the response quantities is sufficient (i.e. displacement or velocity or acceleration), in contrast to some non-parametric methods which require simultaneous measurement of all the three parameters.

Chapter 6

Parameter Estimation in Multi-Degree of Freedom Systems

Multi-Degree of Freedom (MDOF) systems have been analyzed, in this study, using Fourier-Bessel (FB) expansion and Wavelet Transforms. Fourier-Bessel expansion is used to separate the individual n- modal components from the response of n-DOF system and then system parameters are estimated using Wavelet Transforms of the separated signal. A multi-component signal can be dissected in time-frequency plane, using Wavelet Transforms and distinct ridges for each component can be obtained. Subsequently each ridge can be analyzed to estimate the modal parameters. The method, however, fails for close modes (with modal frequencies separated by small amount) due to presence of cross-terms in the scalogram representation of the Wavelet Transforms. Usage of Fourier-Bessel expansion in conjunction with Wavelet Transforms is suggested here. The proposed methodology is shown in Figure 6.1.

A multicomponent signal can also be separated in its individual components by proper design of band-pass filters. However, the optimum choice of the centre frequency and that of bandwidth of filter may be complicated if the signal contains close frequencies. The filtered signal components also have amplitude and phase distortions (Pachori and Sircar, 2006; Potamianos and Maragos, 1994). The proposed method using Fourier-Bessel expansion is performing better in such situations.
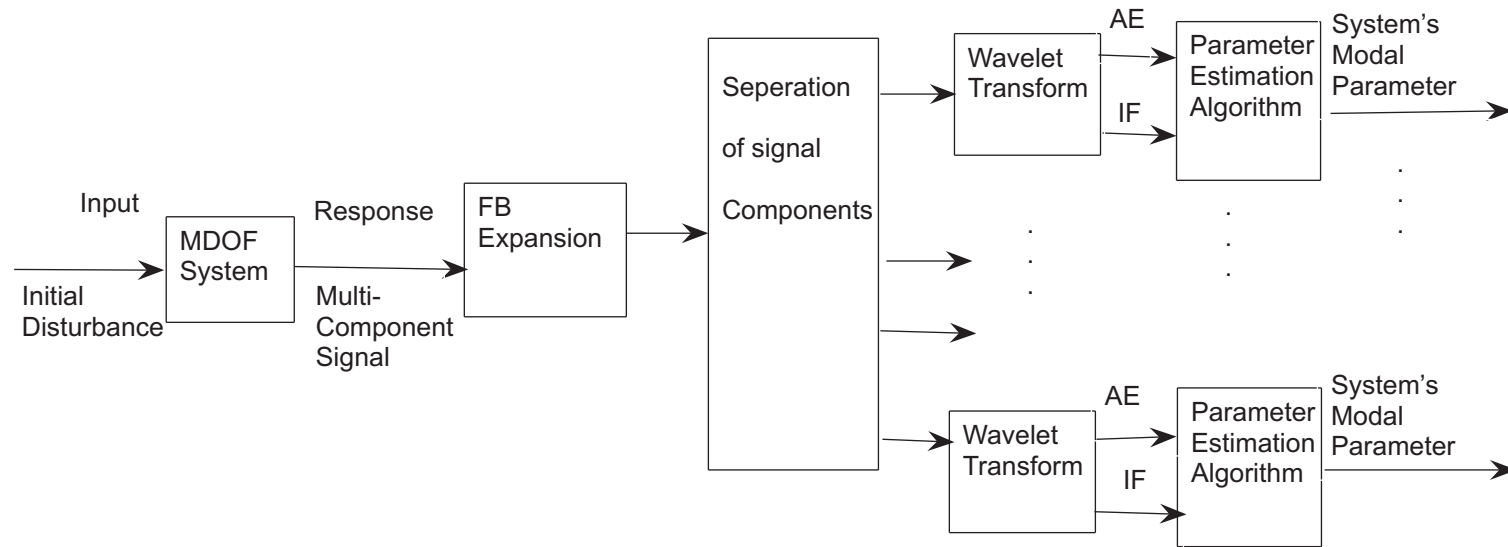
Figure 6.1: Schematic representation of the proposed scheme for MDOF system parameter estimation. AE = Amplitude envelope, IF = Instantaneous Frequency

6.1 Nonlinear Multi-Degree of Freedom System

A nonlinear MDOF system executing free vibration can be represented as

$$[M]\ddot{X} + F(X, \dot{X}) = 0 \qquad X(0) = X_0; \ \dot{X}(0) = \dot{X}_0 \qquad (6.1)$$

where $F(X, \dot{X})$ is a function which models the damping and stiffness terms. A system containing cubic stiffness nonlinearity, for example, can be represented as

$$[M]\ddot{X} + [C]\dot{X} + [K]X + [K_3]X^3 = 0 \qquad X(0) = X_0; \ \dot{X}(0) = \dot{X}_0 \qquad (6.2)$$

Free vibration response of a damped nonlinear n-DOF system with weak nonlinearities can be represented as summation of n-nonlinear modes (Staszewski, 1998).

$$x(t) = \sum_{i=1}^{n} A_i(t) \sin\left(\omega_i(t) + \phi\right) \qquad (6.3)$$

Due to presence of damping the response will be multi-component nonstationary signal. The time decay of these nonstationary components depends on the damping present in the system. Also, the frequency changes with change in the instantaneous amplitude, as the signal decays with time.

Separation of the individual components of the multi-component signal is a crucial step in the estimation of modal parameters of the system.

The proposed method along with its limitations is described in the next section.

6.2 Multi-Component Signal in Time-Frequency Plane

Capability and limitations of Wavelet Transforms to separate the ridges of multi-component signal are illustrated here through numerical simulations. A signal is synthesized from two individual components and their ridges are obtained.

The two components of the signals are taken as

$$x_1(t) = A_1 e^{-\zeta_1 \omega_1 t} \sin\left[(\omega_1 - 0.01t)t\right] \tag{6.4}$$

$$x_2(t) = A_2 e^{-\zeta_2 \omega_2 t} \sin\left[\omega_2 t\right] \tag{6.5}$$

and the composite signal is obtained by combining the above two components

$$x_3(t) = x_1(t) + x_2(t) \tag{6.6}$$

These two components of the signal, $x_1(t)$ and $x_2(t)$, are such that their amplitudes are decaying exponentially and the frequency of the first component is changing continuously. Therefore, the composite signal $x_3(t)$ can be considered as a typical free vibration response signal for a nonlinear two degree of freedom system.

The parameters are $A_1 = 1, \zeta_1 = 0.002, A_2 = 1.2, \zeta_2 = 0.003$. Following three cases are considered for simulation

Case I

Frequencies far apart i.e. $\omega_1 = 5, \omega_2 = 2$

Case II

Frequencies close i.e. $\omega_1 = 5, \omega_2 = 3$

Case III

Frequencies very close i.e. $\omega_1 = 5, \omega_2 = 4$

The simulated results for the above three cases are shown in Figures 6.2 - 6.4. Individual component signals and composite signals consist of band of frequencies because of their continuously changing amplitudes and frequencies.

Figure 6.2 represents Case I, when the frequency bands of two components of a composite signal are well separated and therefore we get two distinct ridges without any ambiguity. In this figure the first column shows simulated signals, second column represents Wavelet

Transforms of the signals and the third column represents the ridges of the Wavelet Transforms. The first row is for the first component of the signal, second row for the second component of the signal while the third row represents the composite signal consisting of the above two components of the signal. Here in the last row the composite signal consists of signal components whose frequency bands are well separated. Hence, we get two distinct ridges and therefore Wavelet Transform technique helps in successful analysis of the signal.

Figure 6.3 corresponds to the Case II with component signals having closer frequency bands. It can be seen that in the last row, the ridges of the composite signal are not proper (as in Case I, in Figure 6.2). There is a very high degree of waviness in the ridges. This is due to the presence of cross-terms, in the Wavelet Transform. The waviness renders the ridges, inappropriate for parameter estimation.

Figure 6.4 corresponds to Case III, in which component signals will have their frequency bands overlapping each other. It can be seen that the Wavelet Transform and the two ridges of the composite signal, in the last row are blurred and ambiguous.

In order to overcome the problem of close modes in MDOF system analysis an alternative procedure using Fourier-Bessel expansion has been suggested in the next section. Fourier-Bessel expansion helps in separating the components of a multi-component signal.

Fourier-Bessel expansion method is introduced in the beginning of the next section and its suitability to separate the components of a multi-component signal is verified through numerical simulations.
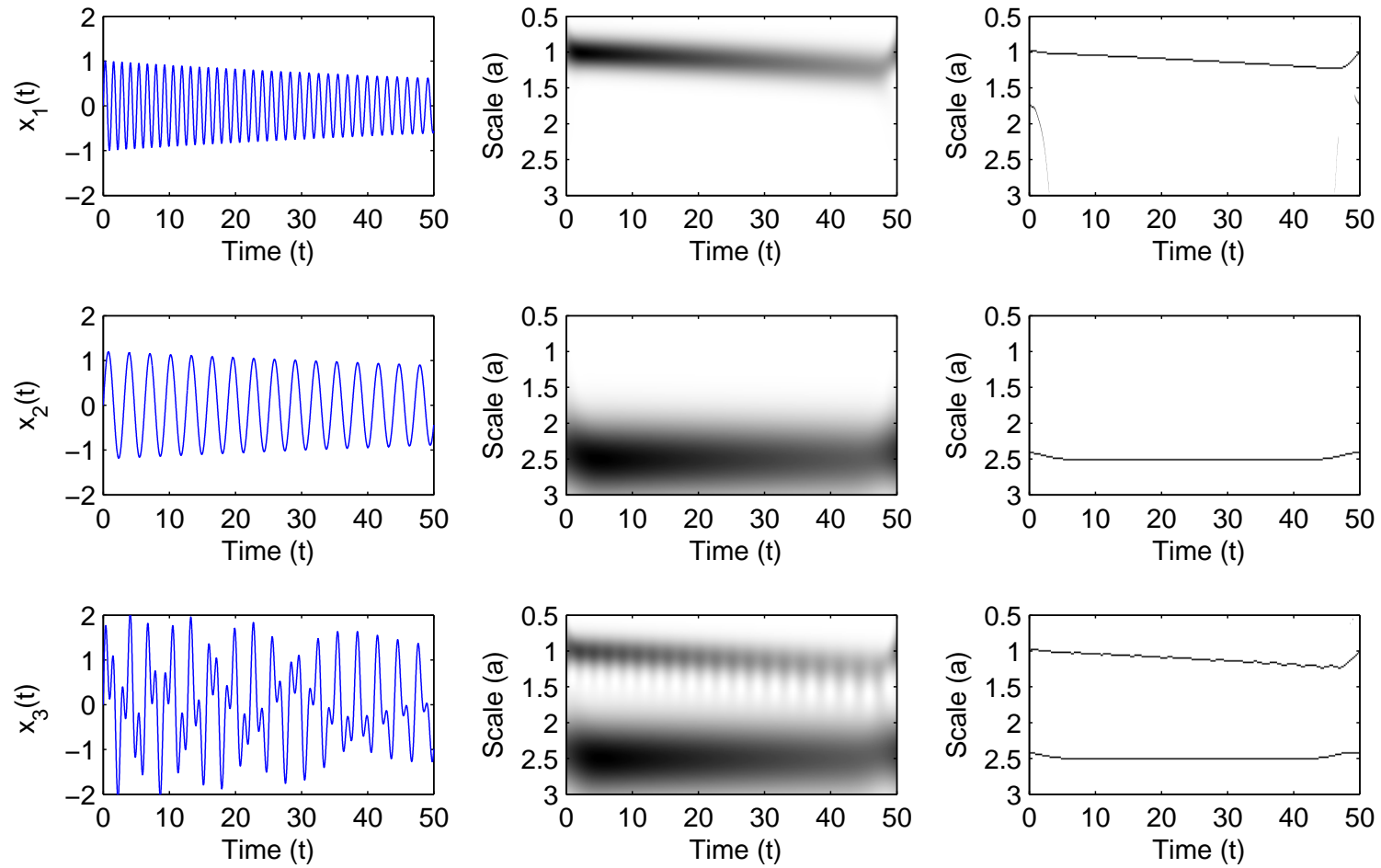
Figure 6.2: *Case I*   Signal components, composite signal and corresponding Wavelet Transforms and ridges
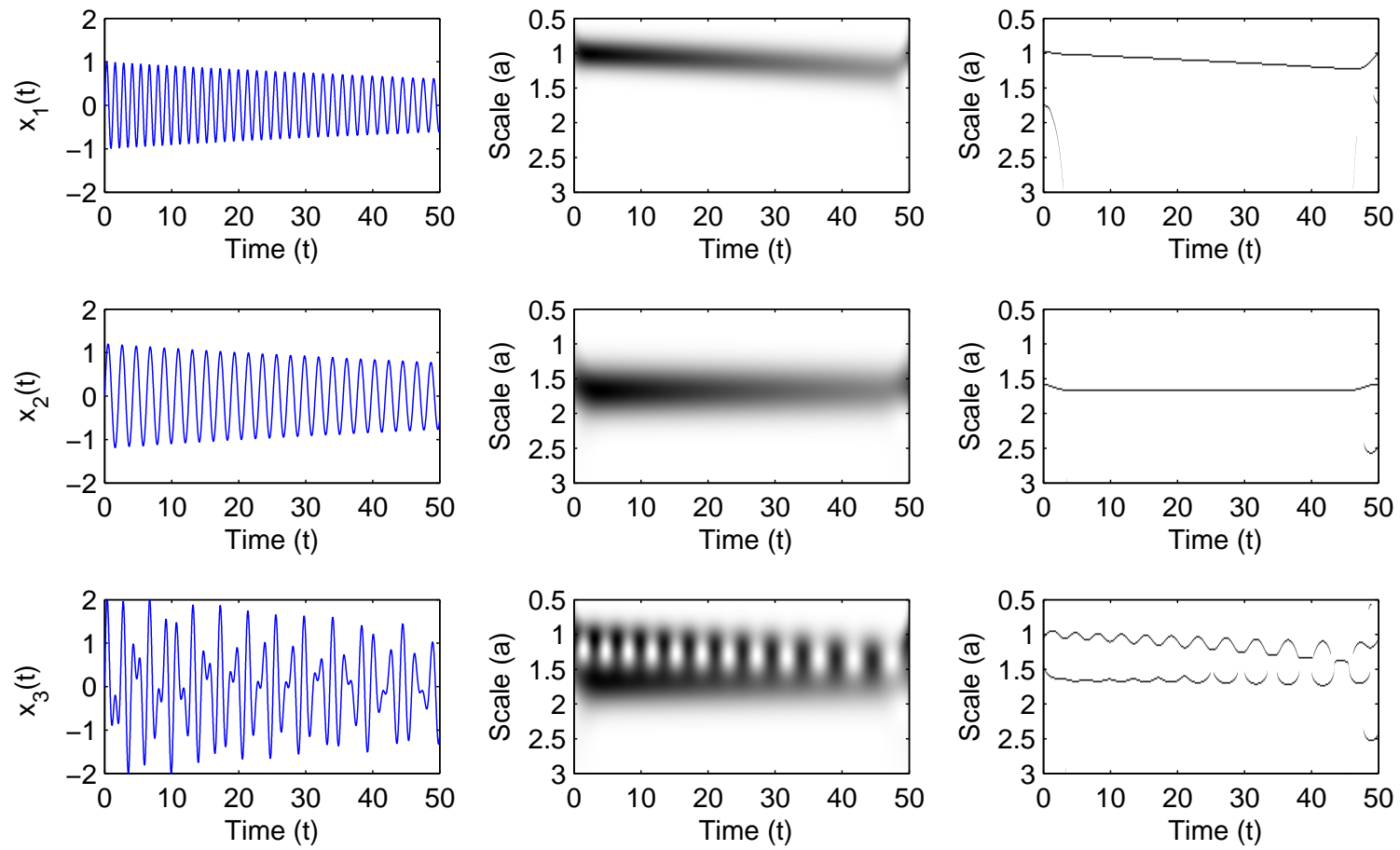
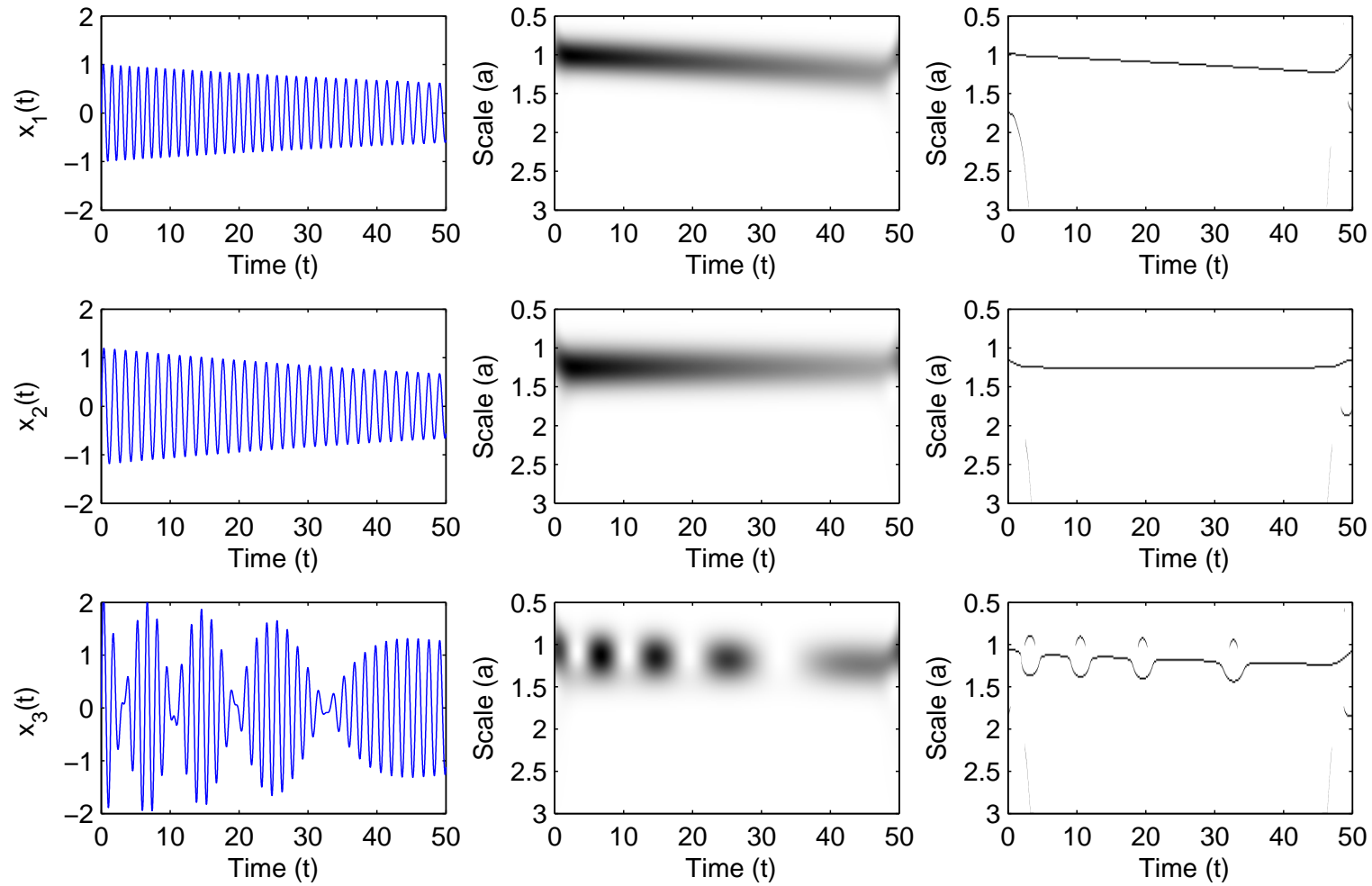Figure 6.3: *Case II* Signal components, composite signal and corresponding Wavelet Transforms and ridges

Figure 6.4: *Case III*   Signal components, composite signal and corresponding Wavelet Transforms and ridges

6.3 Fourier Bessel Expansion

Bessel Functions are very briefly described here for the sake of continuity. Bessel functions are obtained as the solution of the following differential equation (O'Neil, 2003)

$$t^2\ddot{y} + t\dot{y} + (t^2 - n^2)y = 0, \qquad n \geq 0 \tag{6.7}$$

which is called n^{th} order Bessel's differential equation. The general solution of this equation is

$$y = C_1 J_n(t) + C_2 Y_n(t) \tag{6.8}$$

where $J_n(t)$ is called the Bessel function of the first kind of order n and $Y_n(t)$ is called the Bessel function of the second kind of order n. The order n can be any real number. Bessel functions can be expressed in series form as follows

$$J_n(t) = t^n \sum_{r=0}^{\infty} \frac{(-1)^r (\frac{t}{2})^2 r}{2^n r! \Gamma(n + r + 1)} \tag{6.9}$$

The zero order Fourier-Bessel series expansion of a signal $x(t)$ considered over some arbitrary interval (0,d) is given by (O'Neil, 2003)

$$x(t) = \sum_{p=1}^{N} C_p J_0 \left(\frac{\lambda_p}{d} t \right) \tag{6.10}$$

where $\lambda = \lambda_p, p = 1, 2, 3, ...$ are the ascending positive roots of $J_0(\lambda)$ and $J_0 \left(\frac{\lambda_p}{d} t \right)$ are the zero order Bessel functions. The Bessel function for p=1 to 20 is shown Figure 6.5

The sequence of the Bessel functions $\left\{ J_0 \left(\frac{\lambda_p}{d} t \right) \right\}$ forms an orthogonal set on the interval $0 \leq t \leq d$ with respect to the weight t, that is,

$$\int_0^d t J_0 \left(\frac{\lambda_p}{d} t \right) J_0 \left(\frac{\lambda_q}{d} t \right) dt = 0 \tag{6.11}$$
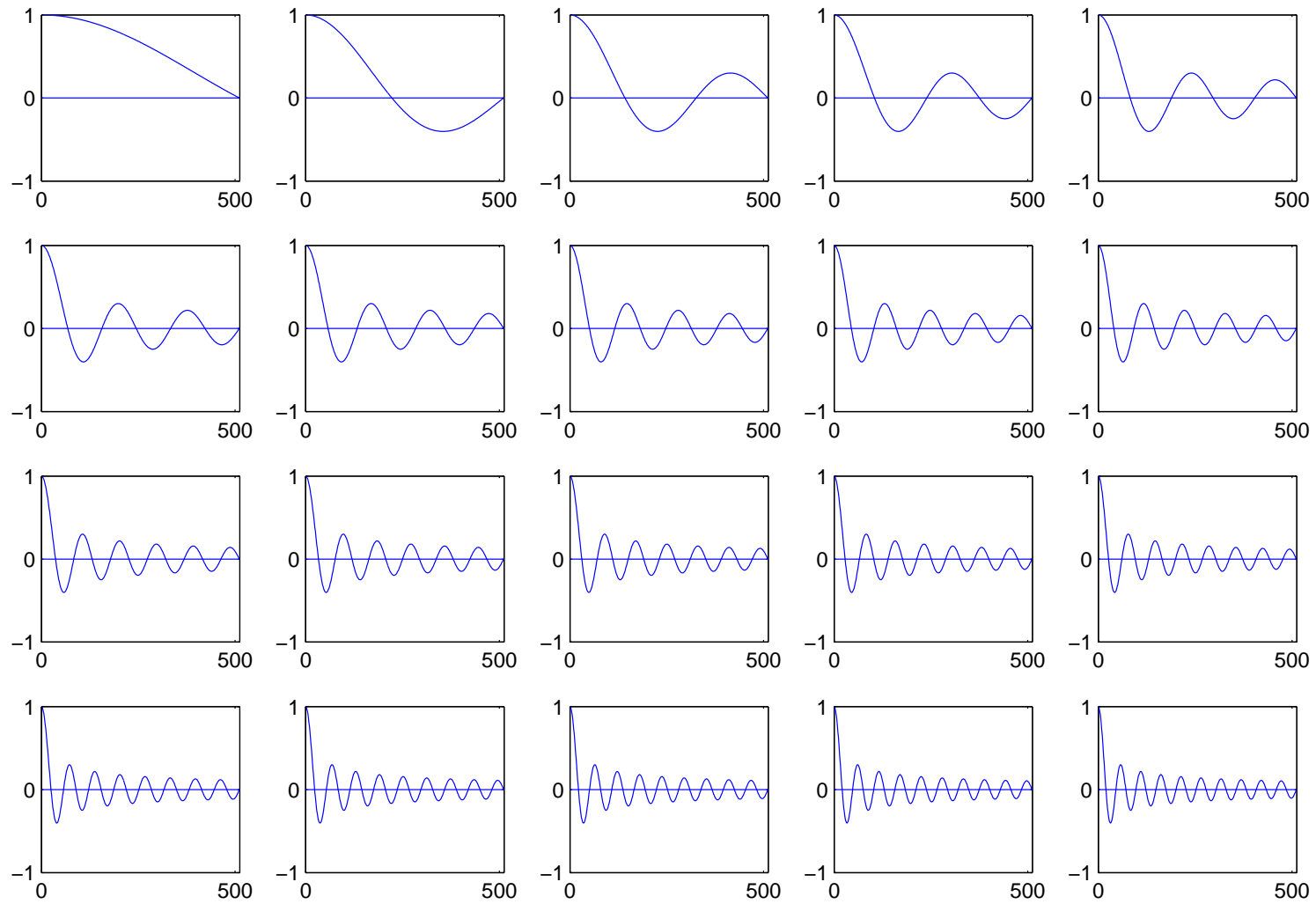
for $p \neq q$

Figure 6.5: Bessel functions of the first kind of order zero $J_0\left(\frac{\lambda_p}{d}t\right)$ for $p = 1$ to 20

Using the orthogonality of the set $\left\{ J_0 \left(\frac{\lambda_p}{d} t \right) \right\}$, the Fourier-Bessel coefficient are computed by using the following equation

$$C_p = \frac{2 \int_0^d t x(t) J_0 \left(\frac{\lambda_p}{d} t \right) dt}{d^2 \left[J_1(\lambda_p) \right]^2} \tag{6.12}$$

with $1 \leq p \leq N$, where N is the order of Fourier-Bessel expansion and $J_1(\lambda_p)$ are the first order Bessel functions.

It was shown analytically that for a given sinusoidal signal $cos(\omega t)$, the Fourier-Bessel coefficients will have peak at $\omega = \frac{\lambda_p}{d}$ (Pachori, 2007). Therefore the relation between the frequency and the order of the Fourier-Bessel expansion is given by

$$\lambda_p = 2\pi f d$$

where f is the frequency in Hz and d is the size of the window.

This illustrates that the frequency content of a signal and the order of the Fourier-Bessel expansion, where the coefficient attains peak magnitude, are related. The Fourier-Bessel expansion, therefore, represents the spectrum of a signal in a manner similar to that in Fourier expansion. The advantage lies in the fact that, unlike a Fourier coefficient which represents only a single frequency, each Fourier-Bessel coefficient represents a band of frequencies. Thus only a fewer Fourier-Bessel coefficient are sufficient to represent a band pass signal adaquately, compared to the number of Fourier coefficients.

When $x(t)$ is the superposition of M cosine signals $cos(\omega_i t)$, i.e.

$$x(t) = \sum_{i=1}^{M} \cos(\omega_i t) \tag{6.13}$$

the Fourier-Bessel coefficients are given as (Pachori, 2007)

$$C_p = \sum_{i=1}^{M} \frac{2\lambda_p}{J_1(\lambda_p)} \left(\frac{\cos(\omega_i a - \psi_i)}{\sqrt{\left[(\lambda_p^2 - \omega_i^2 d^2)^2 + \omega_i^2 d^2 \right]}} \right) \tag{6.14}$$

where

$$\psi_i = \arcsin \left(\frac{\omega_i d}{\sqrt{\left[(\lambda_p^2 - \omega_i^2 d^2)^2 + \omega_i^2 d^2 \right]}} \right) \tag{6.15}$$

then it can be shown that for well-separated circular frequencies ω_i, each term on the right-hand side of equation (6.14) will represent a region where the Fourier-Bessel coefficients are non-zero corresponding to a sub-signal of the composite signal $x(t)$. Since coefficients are real, each cosine component can be directly reconstructed from the Fourier-Bessel coefficient plot (Pachori, 2007).

6.4   Multi-Component Signal Analysis using Fourier-Bessel Expansion

If a multicomponent transient signal is expanded into Fourier-Bessel series, then each component of the composite signal will have clusters of the peaks in the Fourier-Bessel coefficients plot (Pachori, 2007). If every component of a multicomponent signal has non-overlapping cluster of the Fourier-Bessel coefficients, and since the Fourier-Bessel coefficients are real, then each component of the composite signal can be directly reconstructed from the coefficient versus order plot.

The proposed scheme can be called Fourier-Bessel-Wavelet Transform technique for nonlinear parameter estimation. Here, Fourier-Bessel expansion is utilized to separate the multiple components of any MDOF system response; thereafter Wavelet transformation is applied to estimate instantaneous frequency (IF) and the amplitude envelope (AE) of separated components.

The technique is illustrated here through numerical simulations. The three cases discussed in the section 6.2 is once again taken for analysis.

Case I pertains to the composite signal having component signals whose frequency bands are far apart. This signal is successfully analyzed in Time Frequency plane (Figure 6.2) using wavelet transform. We get two distinct ridges for the composite signal without ambiguity. Hence no preprocessing using Fourier-Bessel expansion is required for the separation of the components of composite signal.

The composite signal in Case II consists of signal components whose frequency bands are close. Presence of close frequency give rise to cross term in Wavelet Transform (Figure 6.3) and subsequently we do not get two distinct ridges. Now the Fourier-Bessel expansion is used to separate the individual components and the separated components are analyzed to obtain separate ridges. The simulated results are shown in Figures 6.6 - 6.9. Fourier-Bessel expansion of the composite signal and its component are obtained in Figure 6.6. Fourier-Bessel coefficients occupy two distinct zones for the component signals. These coefficients are further used to reconstruct the individual components of the signal in Figure 6.7. Figure 6.8 compares the reconstructed signal (shown as dots) and the original signal (solid lines). It can be observed that the reconstructed signals matches very well with the original signals. These isolated components of the signal are wavelet transformed and the two separate distinct ridges are obtained in Figure 6.9. This illustrates that a composite signal whose ridges does not occupy distinct regions in time-frequency plane (Figure 6.3), can be separated by Fourier-Bessel expansion and distinct ridges for each component of the signal can then be obtained through Wavelet transformation of individual components.

Case III belongs to the composite signals whose component frequency bands are overlapping. The Wavelet Transforms and ridges due to the two components are merged together and are distorted (Figure 6.4). Therefore, further analysis of the signal in Time-Frequency plain is not possible. Fourier-Bessel expansion of the composite signal and its component are obtained in Figure 6.10. It can be seen here that the Fourier-Bessel coefficients of the component signals do not occupy two distinct zones. Therefore it is not possible to distinguish between the coefficients of the individual components of the composite signal. This happens due to the overlapping of frequency bands, which is due to the change in the frequency of the first signal (eqn 6.4), with time.
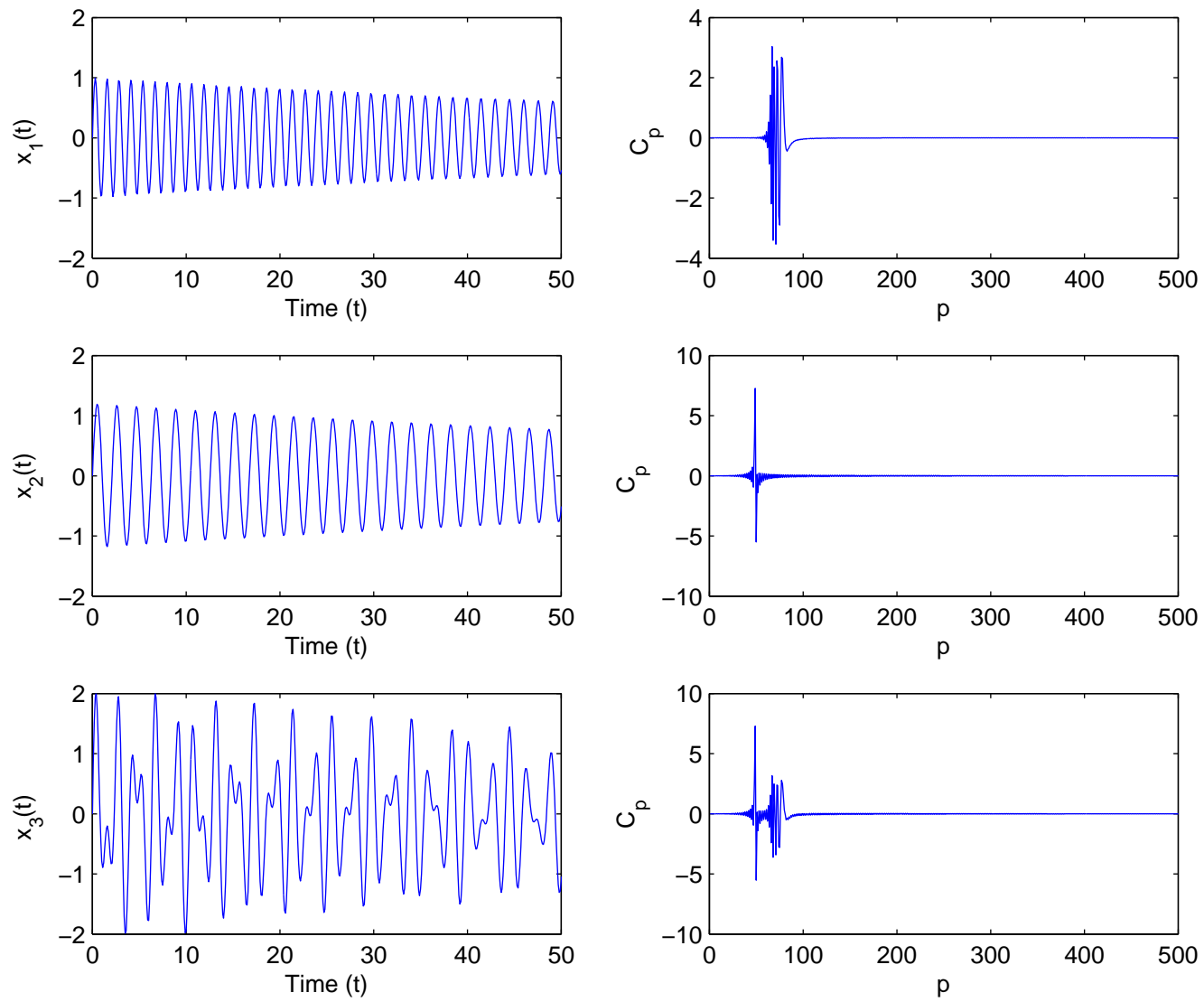
Figure 6.6: Case II Signal components, composite signal and their corresponding Fourier-Bessel coefficients
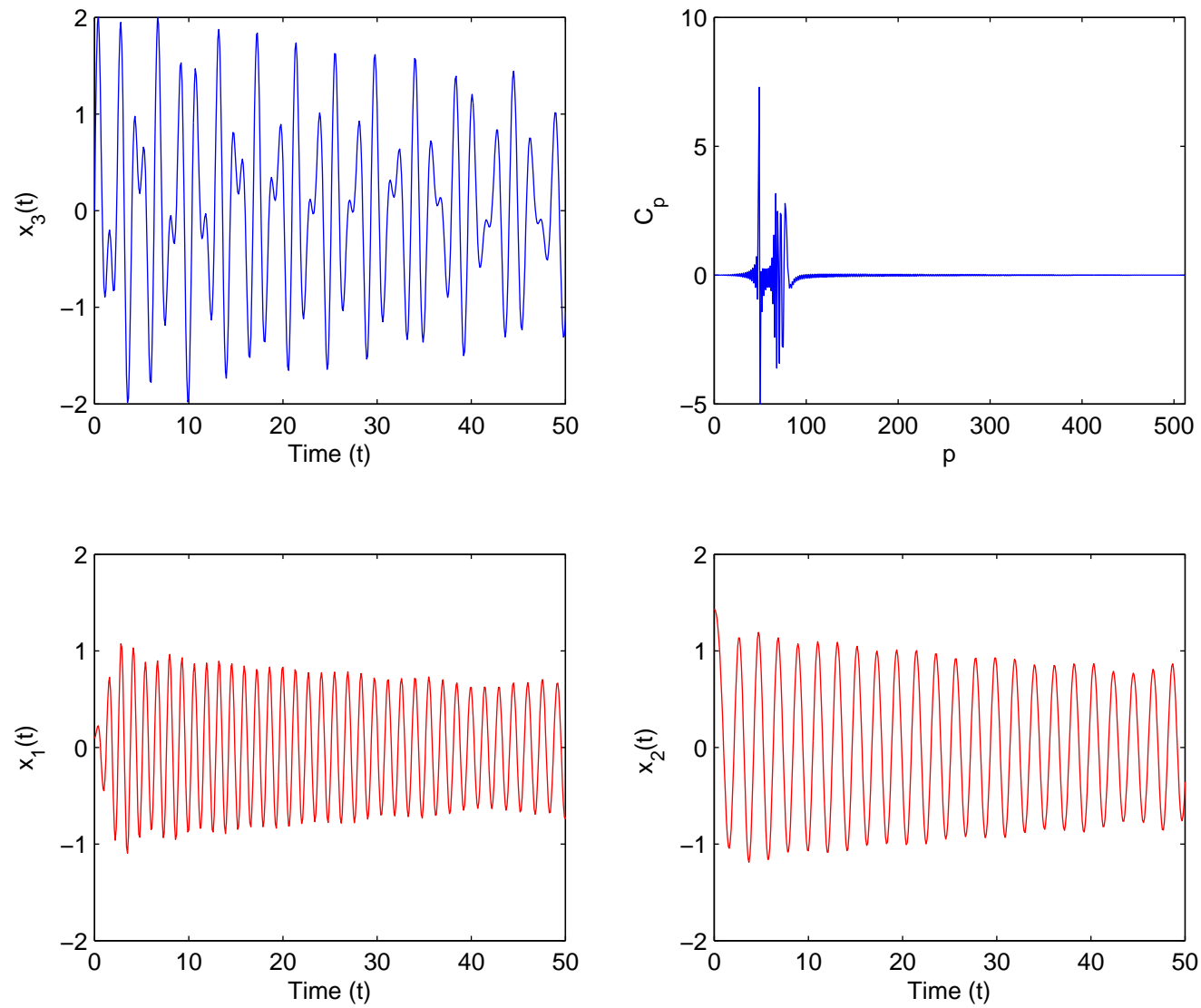
Figure 6.7: Case II Reconstruction of the components of the signal using Fourier-Bessel expansion (a) Composite signal (b) Fourier-Bessel coefficients (c) First component and (d) Second component of the signal
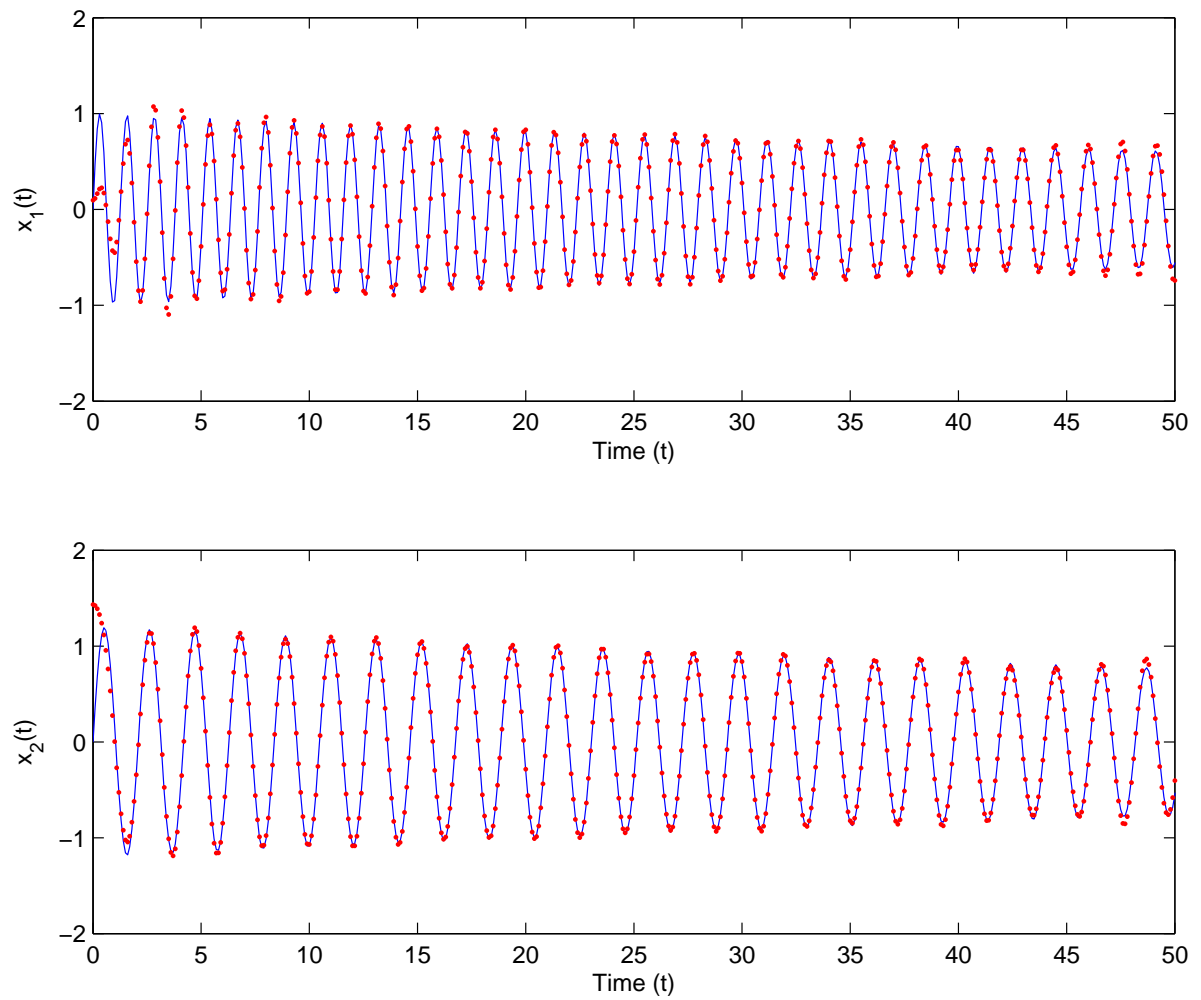
Figure 6.8: Case II Reconstructed (dots)signals and the original (solid lines) signals (a) First compoment and (b)Second component of the composite signal
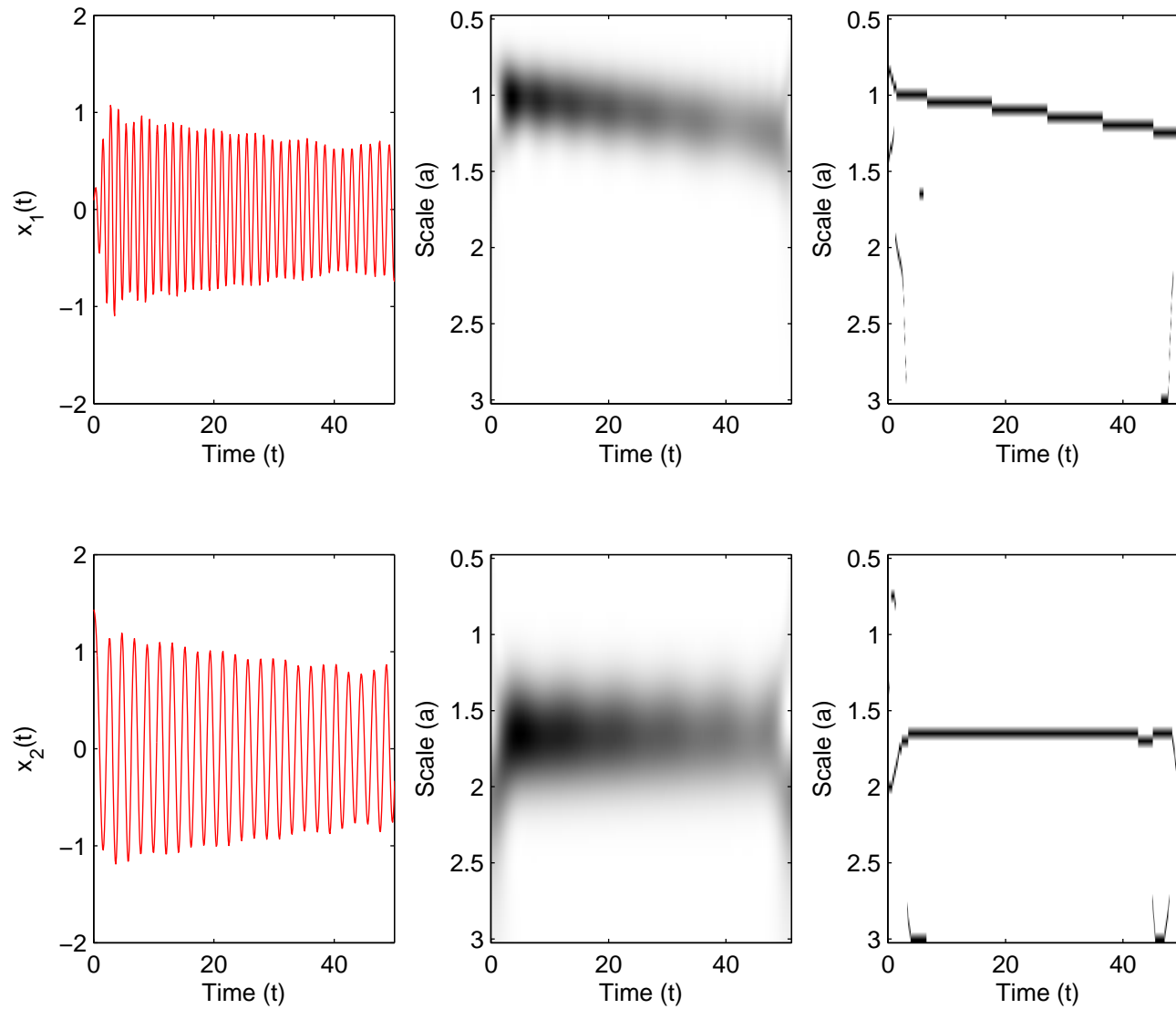
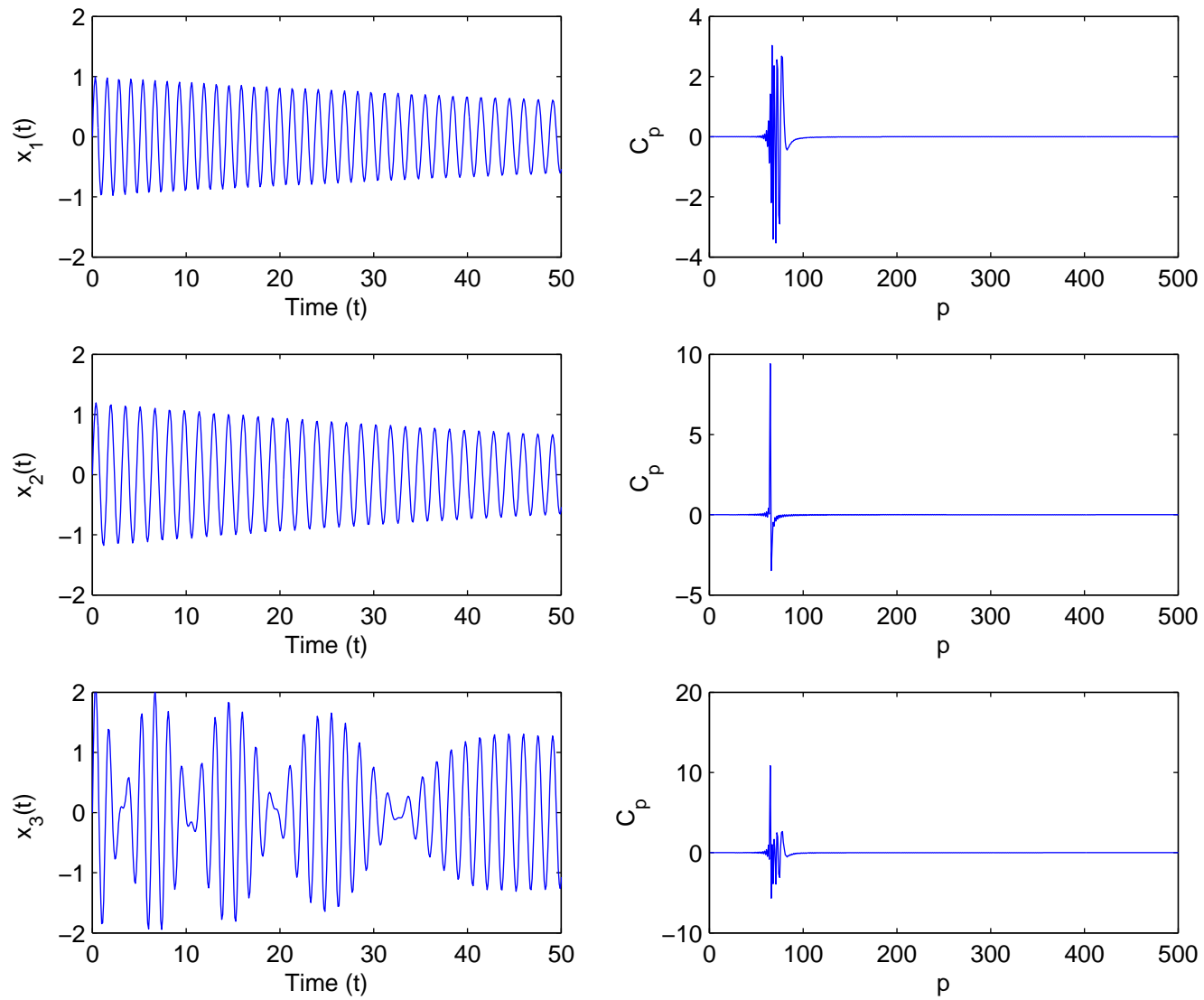Figure 6.9: Case II Reconstructed signal components, their Wavelet Transforms and ridges

Figure 6.10: Case III Signal components, composite signal and their corresponding Fourier-Bessel coefficients

On the basis of the simulations carried out usage of Fourier-Bessel expansion to separate individual component can be suggested as a pre-processing step, prior to the analysis in Time-Frequency plane using Wavelet Transform. However, if the frequency bands of component signal overlap over the time period of the transient data under analysis, the Fourier-Bessel expansion will be unable to separate the individual components.

6.5 Parameter Estimation for a Nonlinear Two Degree of Freedom System

The proposed procedure is illustrated in this section for a two degree of freedom system with cubic stiffness nonlinearity as shown in Figure 6.11
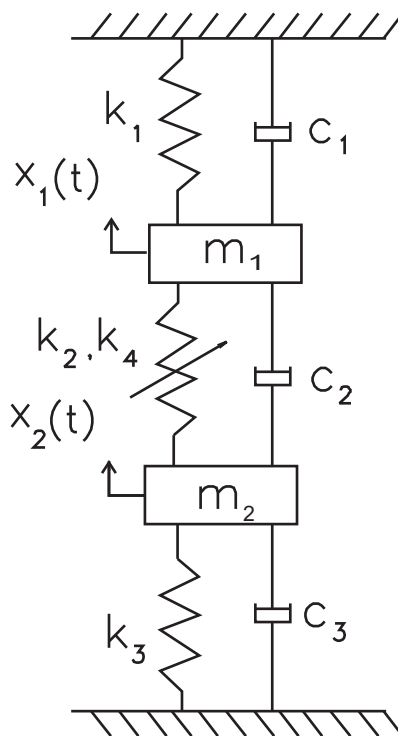

Figure 6.11: Two degree of freedom system with cubic stiffness nonlinearity

The governing equations of motion for free vibration of the system are given by the

following two coupled differential equations

$$m_1 x_1'' + (c_1 + c_2)x_1' - c_2 x_2' + (k_1 + k_2)x_1 - k_2 x_2 + k_4(x_1 - x_2)^3 = 0 \qquad (6.16)$$

$$m_2 x_2'' + (c_2 + c_3)x_2' - c_2 x_1' + (k_2 + k_3)x_2 - k_2 x_1 - k_4(x_1 - x_2)^3 = 0 \qquad (6.17)$$

where ($'$) represents the differentiation with respect to time t. Initial conditions are $x_1(0) = x_{10}$; $x_2(0) = x_{20}$; $\dot{x}_1(0) = \dot{x}_{10}$; $\dot{x}_2(0) = \dot{x}_{20}$.

For a simplified case with $k_1 = k_3 = k$; $c_1 = c_3 = c$; $c_2 = 0$, the above two equations become

$$m_1 x_1'' + cx_1' + (k + k_2)x_1 - k_2 x_2 + k_4(x_1 - x_2)^3 = 0 \qquad (6.18)$$

$$m_2 x_2'' + cx_2' + (k + k_2)x_2 - k_2 x_1 - k_4(x_1 - x_2)^3 = 0 \qquad (6.19)$$

Defining the following nondimensional parameters

$$\tau = \sqrt{\frac{k}{m_1}}t \qquad \zeta = \frac{c}{2\sqrt{km_1}} \qquad y_1 = \frac{x_1}{x_{10}} \qquad y_2 = \frac{x_2}{x_{10}}$$

$$\alpha = \frac{k_2}{k} \qquad \alpha_N = \frac{k_4 x_{10}^2}{k} \qquad \mu = \frac{m_2}{m_1} \qquad \dot{y} = \frac{dy}{d\tau}$$

the equations (6.18) and (6.19) can be written as

$$\ddot{y}_1 + 2\zeta\dot{y}_1 + y_1 + \alpha(y_1 - y_2) + \alpha_N(y_1 - y_2)^3 = 0 \qquad (6.20)$$

$$\mu\ddot{y}_2 + 2\zeta\dot{y}_2 + y_2 - \alpha(y_1 - y_2) - \alpha_N(y_1 - y_2)^3 = 0 \qquad (6.21)$$

Initial conditions become $y_1(0) = y_{10} = 1$; $y_2(0) = y_{20}$; $\dot{y}_1(0) = \dot{y}_{10}$; $\dot{y}_2(0) = \dot{y}_{20}$. The following values are taken for numerical simulation -

$\mu = 1$; $\zeta = 0.02$; $\alpha = 1$; $\alpha_N = 0.3$

The free vibration response of the system was simulated using fourth order Runge-Kutta method with initial displacement $y_{10} = 1$. The response of the system $y_1(\tau)$ and $y_2(\tau)$ is shown in Figure 6.12. The response $y_1(t)$ is analyzed further for estimation of modal parameters. Figure 6.13 shows the response, its wavelet transform and ridges. Since frequency bands are close, Wavelet transform shows cross terms and the ridges are wavy.
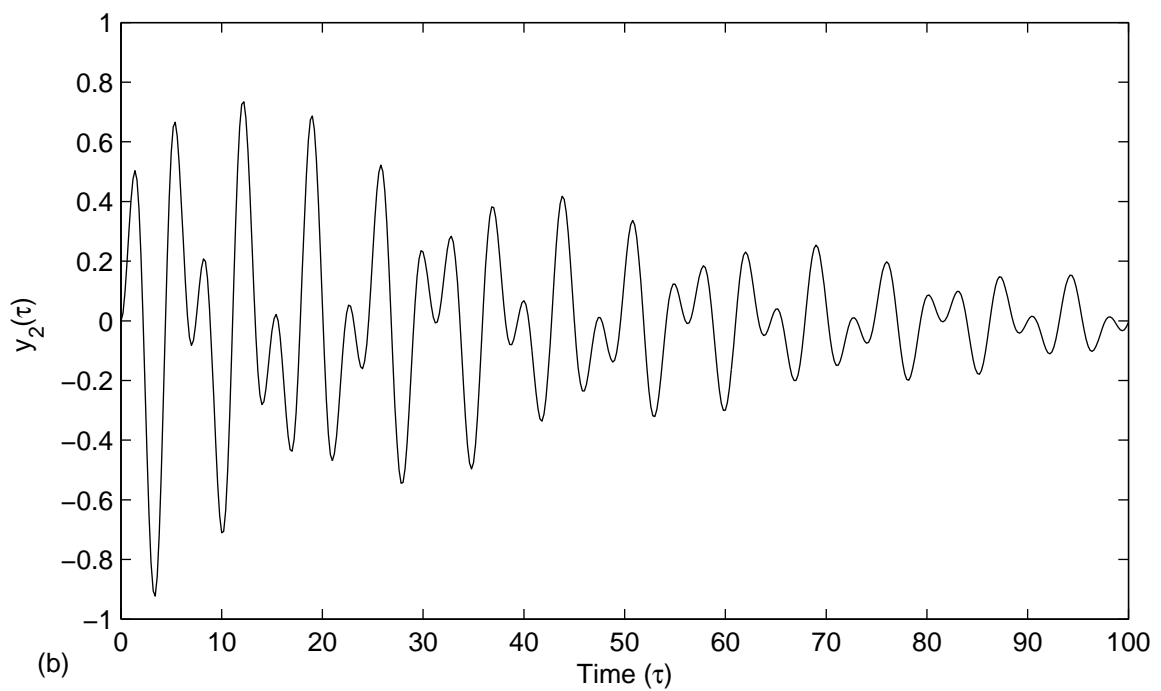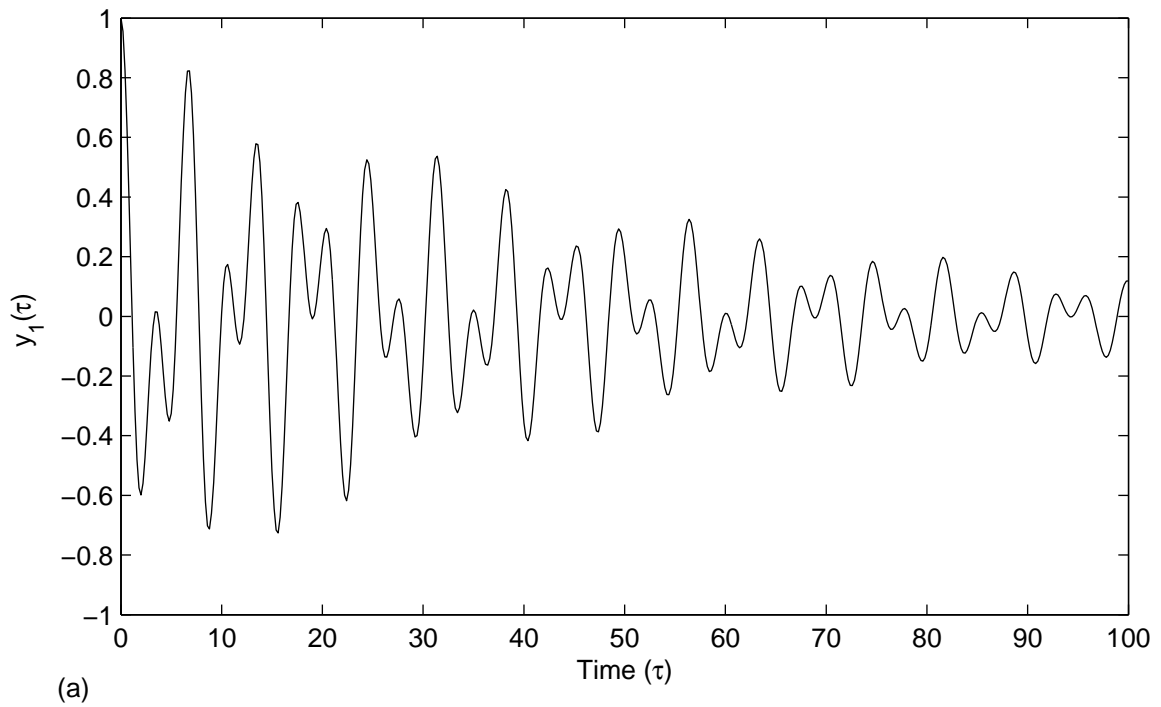
Figure 6.12: Free vibration response of the system (a) $y_1(\tau)$ and (b) $y_2(\tau)$
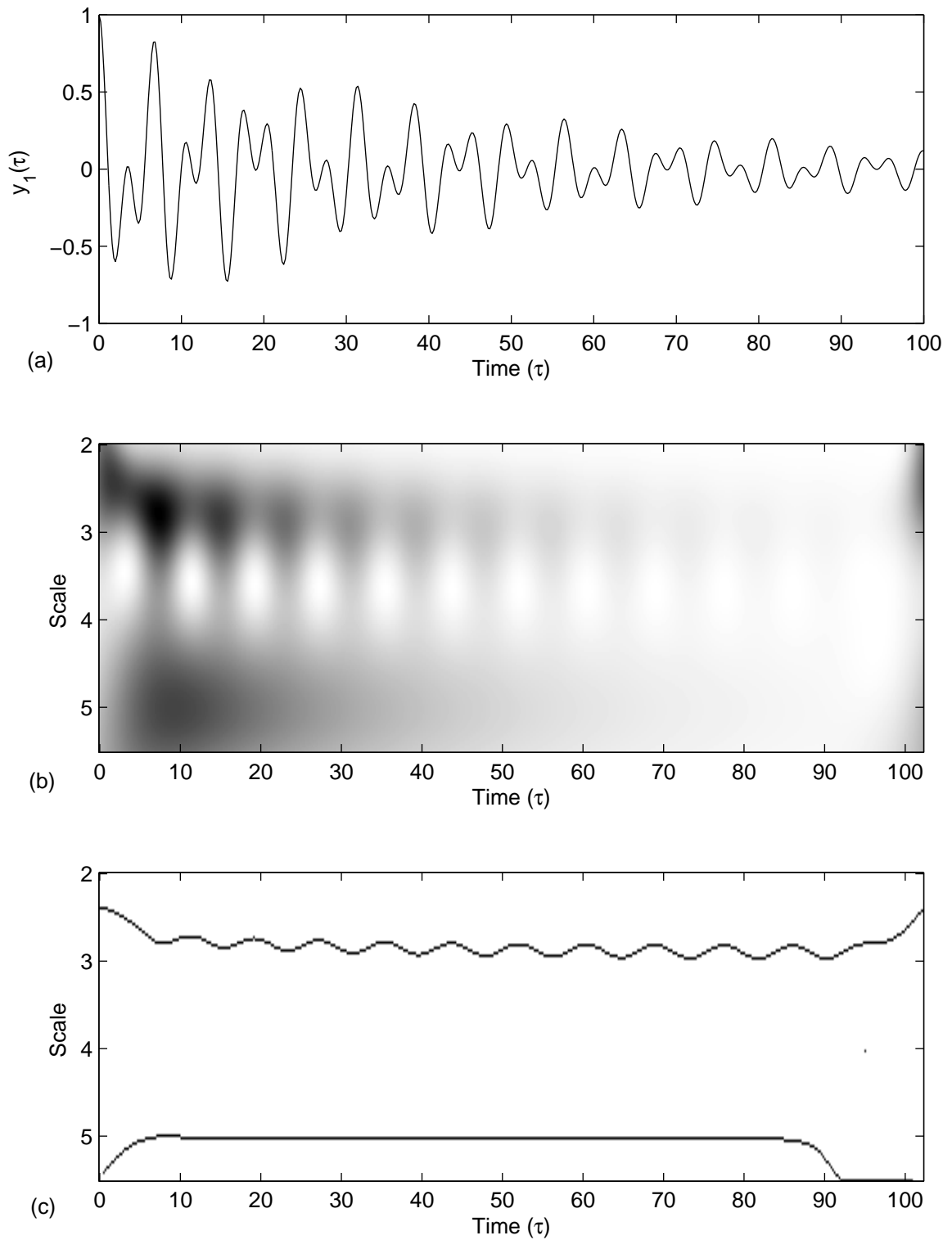
Figure 6.13: (a) response $y_1(\tau)$ of the system (b) Wavelet Transform (c) Ridges

Figure 6.14 shows the Fourier-Bessel expansion of the signal and here two distinct clusters of the Fourier-Bessel coefficients are obtained. Using these Fourier-Bessel coefficients components of the signal are reconstructed as in Figure 6.15. The separated signals are wavelet transformed and subsequently ridges are obtained in Figure 6.16. These ridges are used further to find the modal parameters. The first mode does not show presence of stiffness nonlinearity because its ridge indicates the constant frequency with amplitude of oscillations. It is observed that the second mode contains stiffness nonlinearity as its ridge indicates that the frequency changes with amplitude of oscillations. The nonlinearity is of hardening type because the frequency of oscillation decreases with decrease in amplitude of oscillations.

Further both the modes are analyzed separately for estimation of modal parameters as described in chapter 5 (Refer Figure 5.1). Analysis of first mode is presented in Figure 6.17. Instantaneous frequency and amplitude envelope are obtained through ridge and skeleton data. The natural frequency (ω_{n1}) obtained is 1. The slope of the logarithm of amplitude envelope gives damping factor $\zeta_1 = 0.02$.

Figure 6.18 describes the analysis of second mode. To find natural frequency (ω_{n2}) and modal cubic stiffness nonlinearity (η_3), equation of the form (Nayfeh, 1973)

$$\omega \quad = \quad \omega_{n2} + \frac{3\eta_3}{8\omega_{n2}}A^2 \tag{6.22}$$

is fitted over the backbone curve (ω v/s A) using the least square method. Subsequently, we get natural frequency (ω_{n2}) as 1.7328 and modal cubic stiffness nonlinearity (η_3) equal to 2.3083. The slope of the logarithm of amplitude envelope gives damping factor $\zeta_2 = 0.0198$.
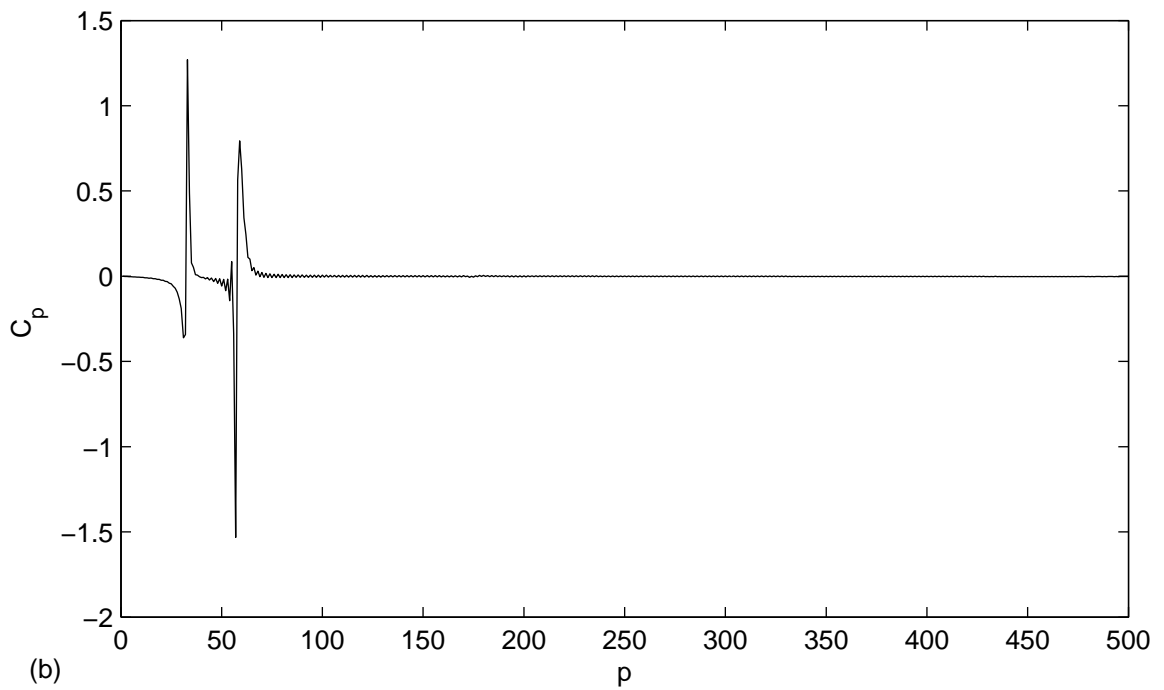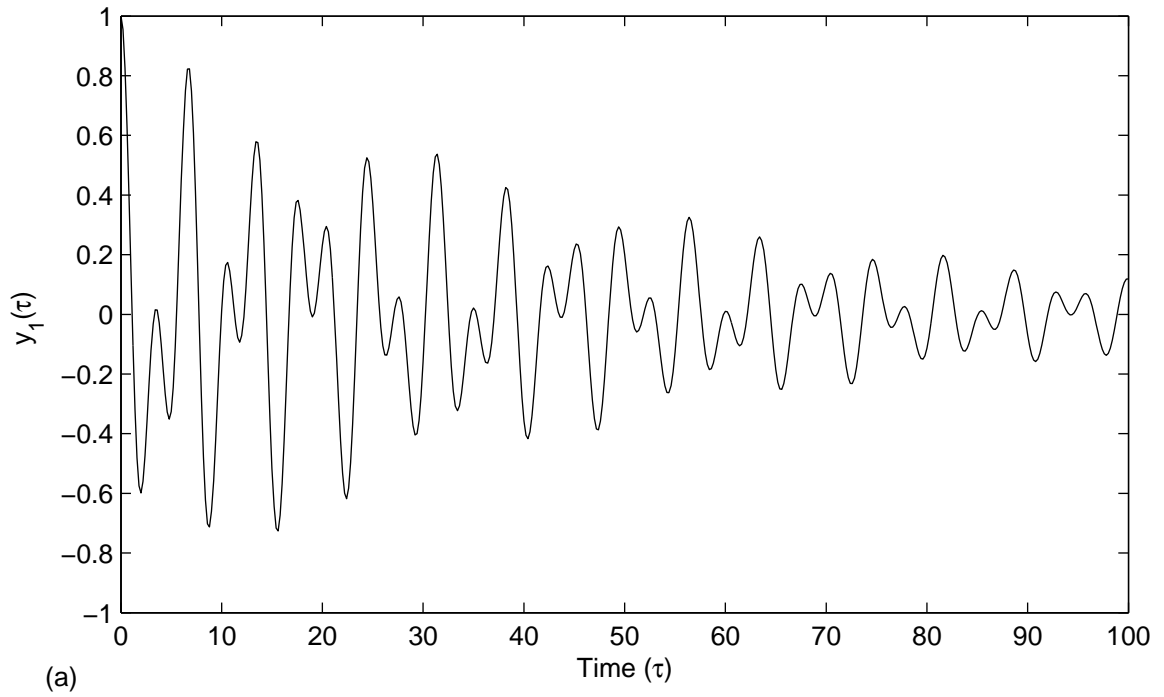
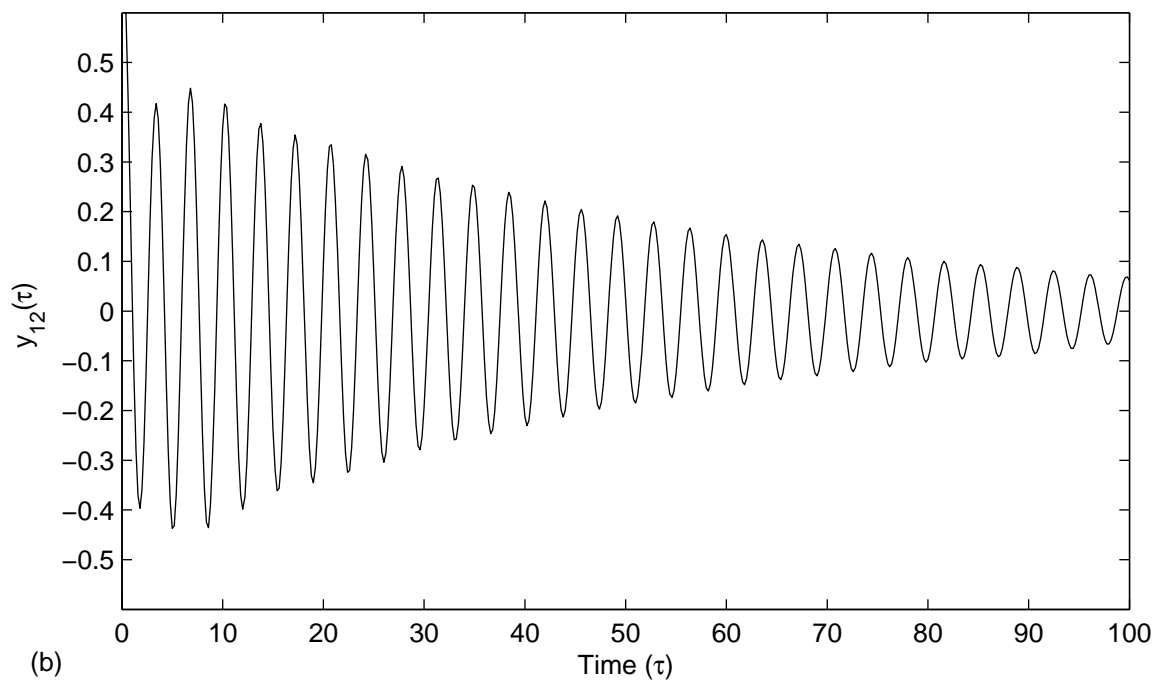Figure 6.14: (a) Free vibration response of the system $y_1(t)$ and (b) Fourier-Bessel coefficients
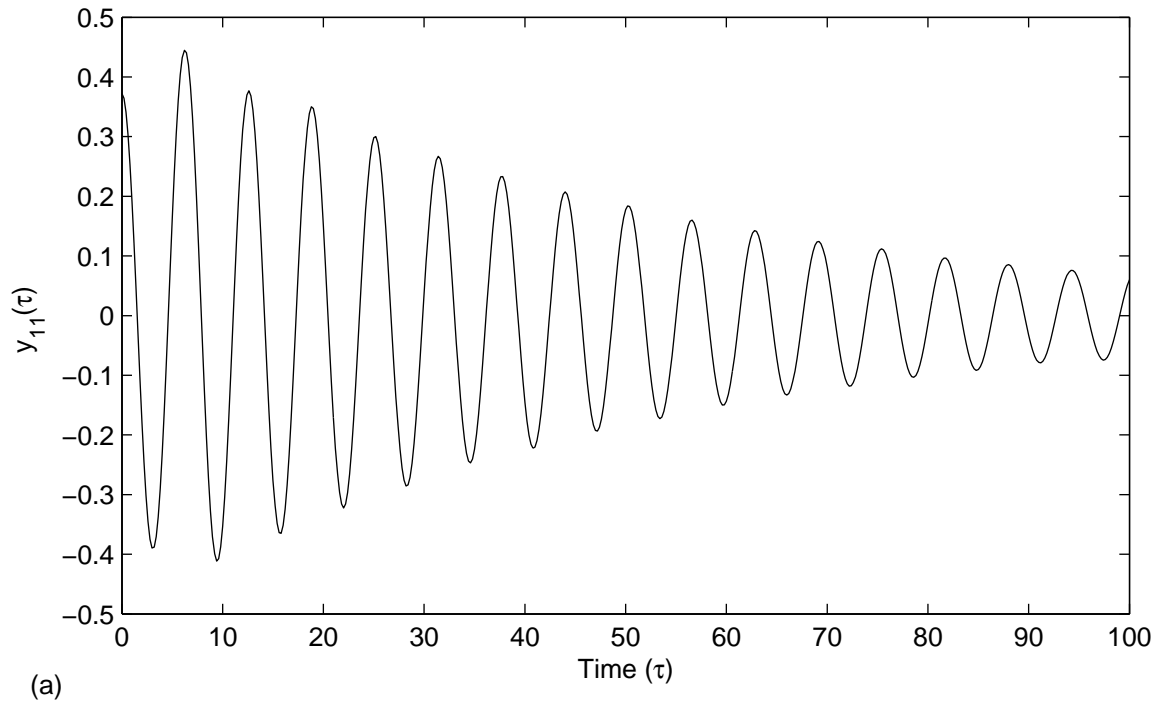
Figure 6.15: Reconstruction of the component signals from $y_1(t)$ (a) First mode $y_{11}(\tau)$ and (b) Second mode $y_{12}(\tau)$
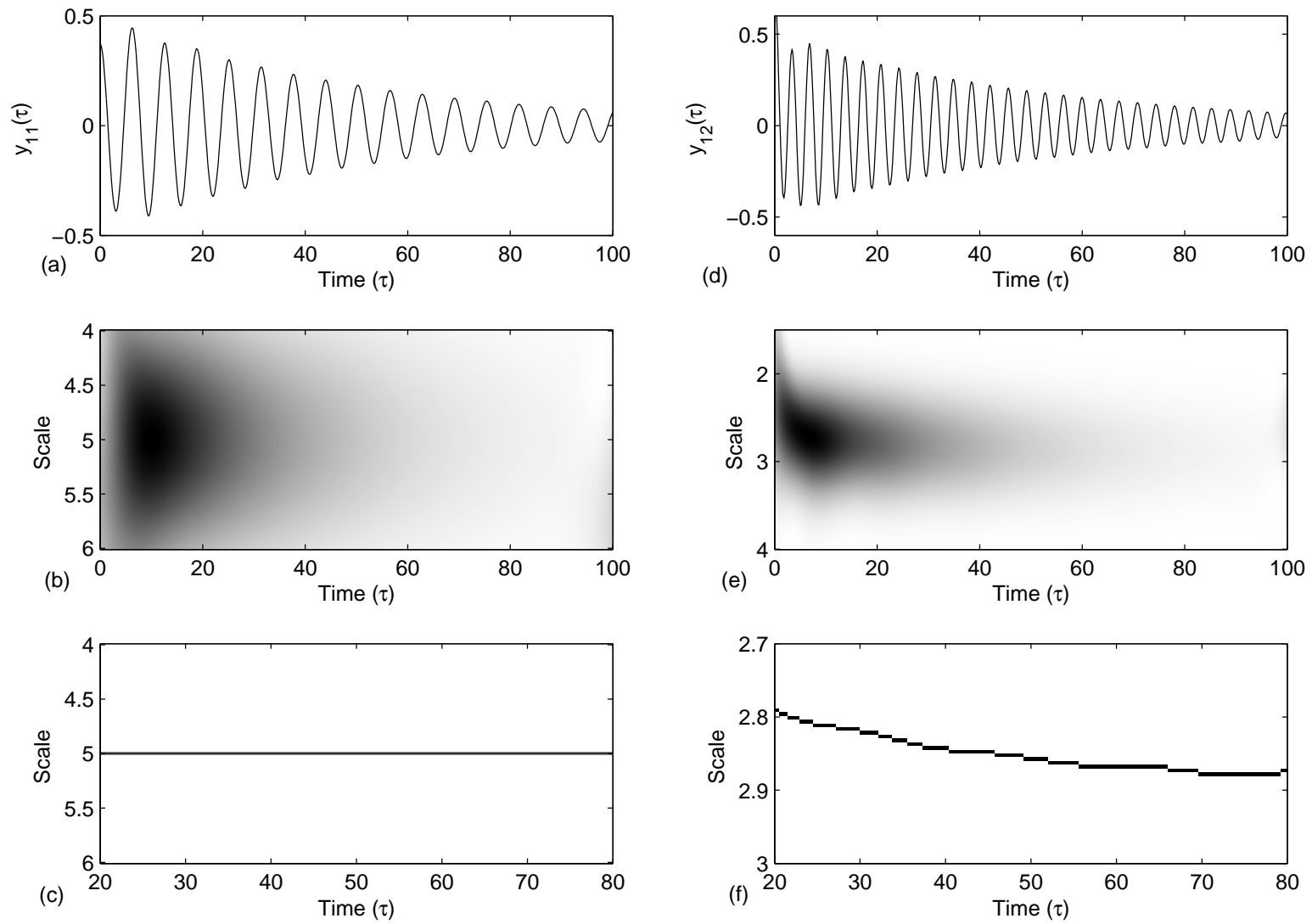
Figure 6.16: (a) First mode $y_{11}(\tau)$ (b) Wavelet Transform (c) Ridge (d) Second mode $y_{12}(\tau)$ (e) Wavelet Transform (f) Ridge

Figure 6.17: Parameter estimation in first mode (a) First mode $y_{11}(\tau)$ (b) Wavelet Transform (c) Frequency variation with time (d) Amplitude envelope $A(\tau)$ v/s t (e) $A(\tau)$v/s ω (f) $\log A(\tau)$ v/s τ
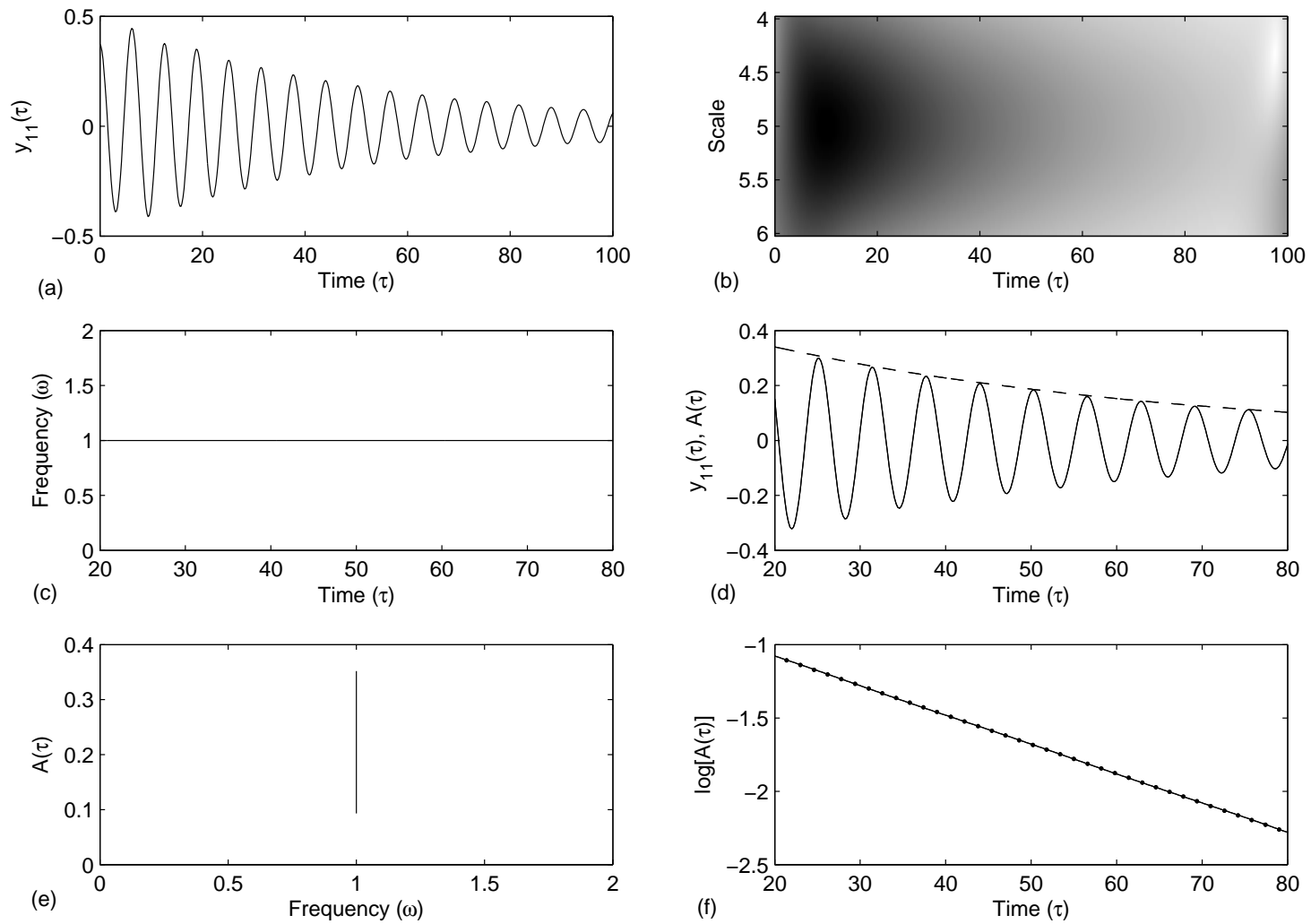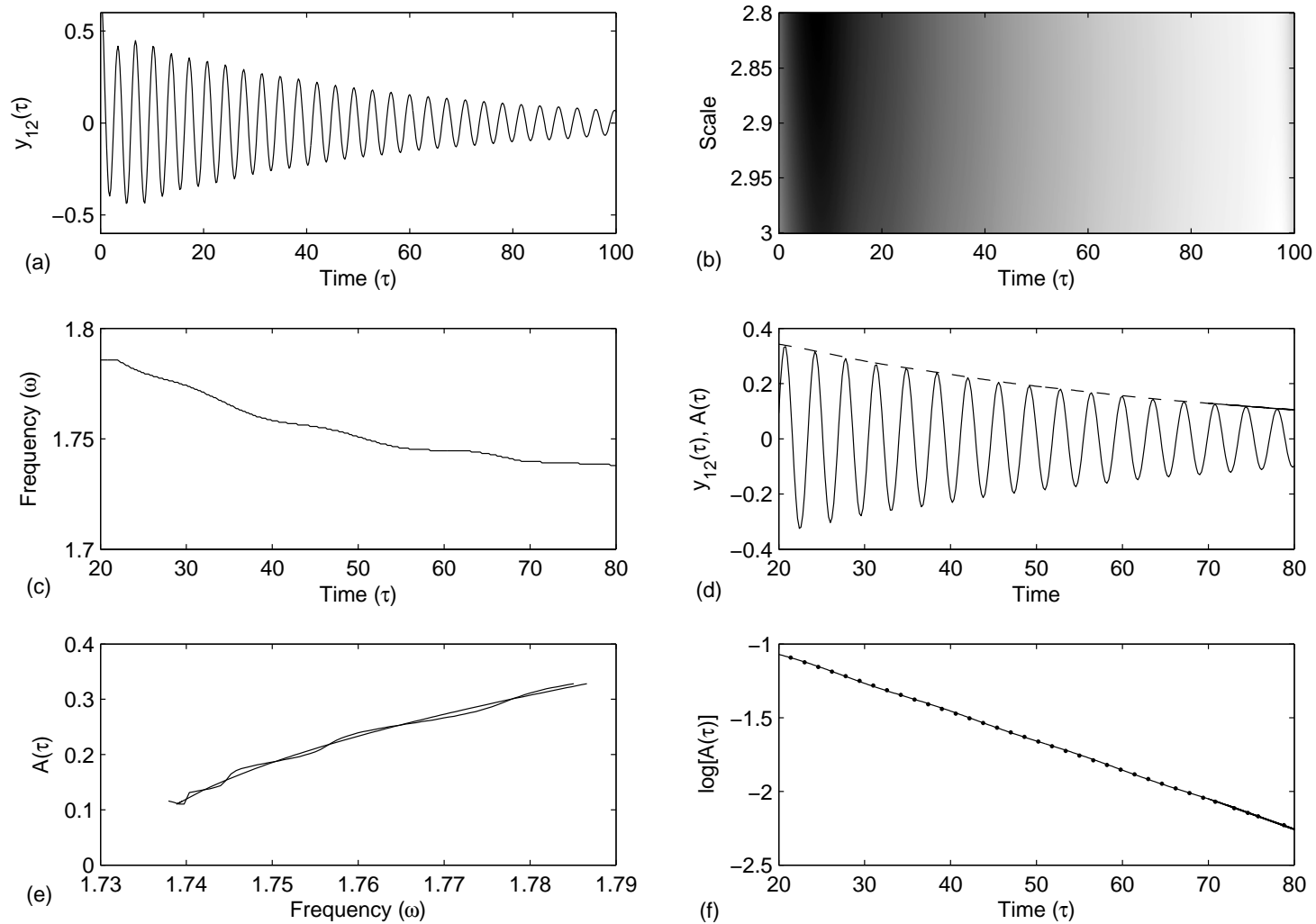
Figure 6.18: Parameter estimation in second mode (a) Second mode $y_{12}(\tau)$ (b) Wavelet Transform (c) Frequency variation with time (d) Amplitude envelope $A(\tau)$ v/s τ (e) $A(\tau)$ v/s ω (f) $\log A(\tau)$ v/s τ

6.6 Remarks

The Fourier-Bessel series coefficients are unique for a given signal, like the Fourier series coefficients. However, Bessel functions decay over time as compared to the sinusoidal basis functions in the Fourier series. This property of the Bessel functions makes the Fourier-Bessel series expansion suitable for non-stationary signals as obtained in nonlinear damped vibrations. Fourier-Bessel decomposition is defined in the time-domain, and the Fourier-Bessel coefficients contain all the necessary information for the synthesis of the signal. As illustrated in this chapter they can be used in conjunction with Wavelet Transforms, for parameter estimation in nonlinear systems.

Chapter 7

Experimental Investigations

Experimental investigations to illustrate the proposed nonlinear parameter estimation procedures have been carried out on a rotating machinery kit. The transient vibratory response of the rotor-bearing assembly, as its speed is accelerated, is measured and processed for parameter estimation.

Numerical simulation of such a response of the rotor, modeled as a single degree of freedom system, is initially carried out. It is then compared with experimentally obtained results, for parameter identification.

Various researchers have studied the transient behavior of rotors during acceleration. Frank M. (1932) quantified the relation between the amplitude of vibration with the acceleration rate. He observed that the critical speed appears higher than the true critical speed when the speed is increasing and lower when speed is decreasing. Baker (1939) numerically estimated the vibration amplitude of an accelerated unbalanced rotor to generate a knowledge base to design the system so as to have low amplitudes of vibration. Hassenpflug et al. (1981) critically examined the previous related investigations and presented a detailed study of a Jeffcott rotor (rigid circular disc fixed at the centre of massless shaft which is supported in rigid bearings) as it passes through critical speed. He

investigated the phenomenon experimentally also and showed good agreement between numerical and experimental results. He observed the beat frequency after rotor had passed through critical speed. This fact suggests the presence of two frequencies in the response signal as the rotor passes through the critical speed. Vyas et al. (1987) investigated a similar problem to analyze the vibratory stress response of a turbine blade during step-up / down operation of a turbo machinery.

In the present work, Wavelet Transform is applied to the nonstationary signal of the rotor as its speed is increased. The response signal frequencies are seperated in time frequency plane using Wavelet Transforms. The intial part here, deals with the numerical simulation of the phenomenon, while the later part deals with experimental investigations.

7.1   Numerical Simulation

Modeling the rotor system as a single degree of freedom system case, the response is initially simulated for a linear system and then for a nonlinear system. The difference in the behavior of accelerated linear and nonlinear rotor systems is highlighted.

7.1.1   Linear Rotor System

The linear accelerated rotor system is governed by following linear ordinary differential equation (Hassenpflug et al., 1981)

$$mx'' + cx' + kx = me\left[\omega^2 \cos\left(\omega_0 t + \frac{1}{2}\alpha t^2\right) + \alpha\sin\left(\omega_0 t + \frac{1}{2}\alpha t^2\right)\right] \qquad (7.1)$$

where e is unbalance eccentricity. ω, ω_0 and α represent instantaneous angular velocity, initial angular velocity and acceleration respectively. Using the following nondimensional

parameters

$$\omega_n^2 = \frac{k}{m} \qquad\qquad \zeta = \frac{c}{2m\omega_n} \qquad\qquad \tau = \omega_n t$$

$$\frac{x}{e} = y \qquad\qquad \dot{y} = \frac{\mathrm{d}y}{\mathrm{d}\tau}$$

equation(7.1) can be written as

$$\ddot{y} + 2\zeta\dot{y} + y = r_\omega^2 \cos\left(r_{\omega 0}\tau + \frac{1}{2}r_\alpha\tau^2\right) + r_\alpha \sin\left(r_{\omega 0}\tau + \frac{1}{2}r_\alpha\tau^2\right) \qquad (7.2)$$

where $r_\omega = \omega/\omega_n$, $r_{\omega 0} = \omega_0/\omega_n$ and $r_\alpha = \alpha/\omega_n^2$.

Closed form analytical solution of the above equation does not exist.

The response of equation is numerically simulated and wavelet transformed. The linear system is simulated with damping factor, $\zeta = 0.01$, initial angular speed $\omega_0 = 0$ and acceleration factor $r_\alpha = 0.003$. Fourth order Runge-Kutta method is used and the time response is shown in Figure 7.1(a). The response is wavelet transformed and subsequently ridges are obtained and the results are shown in Figure 7.1 (b) and Figure 7.1 (c) respectively. It can be seen that two separate ridges are obtained as the rotor passes through the critical speed. It shows the transient response during resonance is a multi-component signal having component signals with two different frequencies. One component of signal corresponds to forced vibration (due to residual unbalance) at rotating speed whose frequency is continuously increasing. The other component of the vibration signal corresponds to free vibration response of the system which is decaying continuously.

In the case of a linear system, the ridge corresponding to second component of the signal is horizontal, illustrating the fact that the natural frequency of the system is independent of the amplitude of vibration..

Figures 7.2 (a)-(c) also illustrate the same fact. However, here the rotor is allowed to attain a fixed speed after passing through critical speed. Therefore the ridge corresponding to force vibrations also becomes horizontal as it attains the fixed speed.
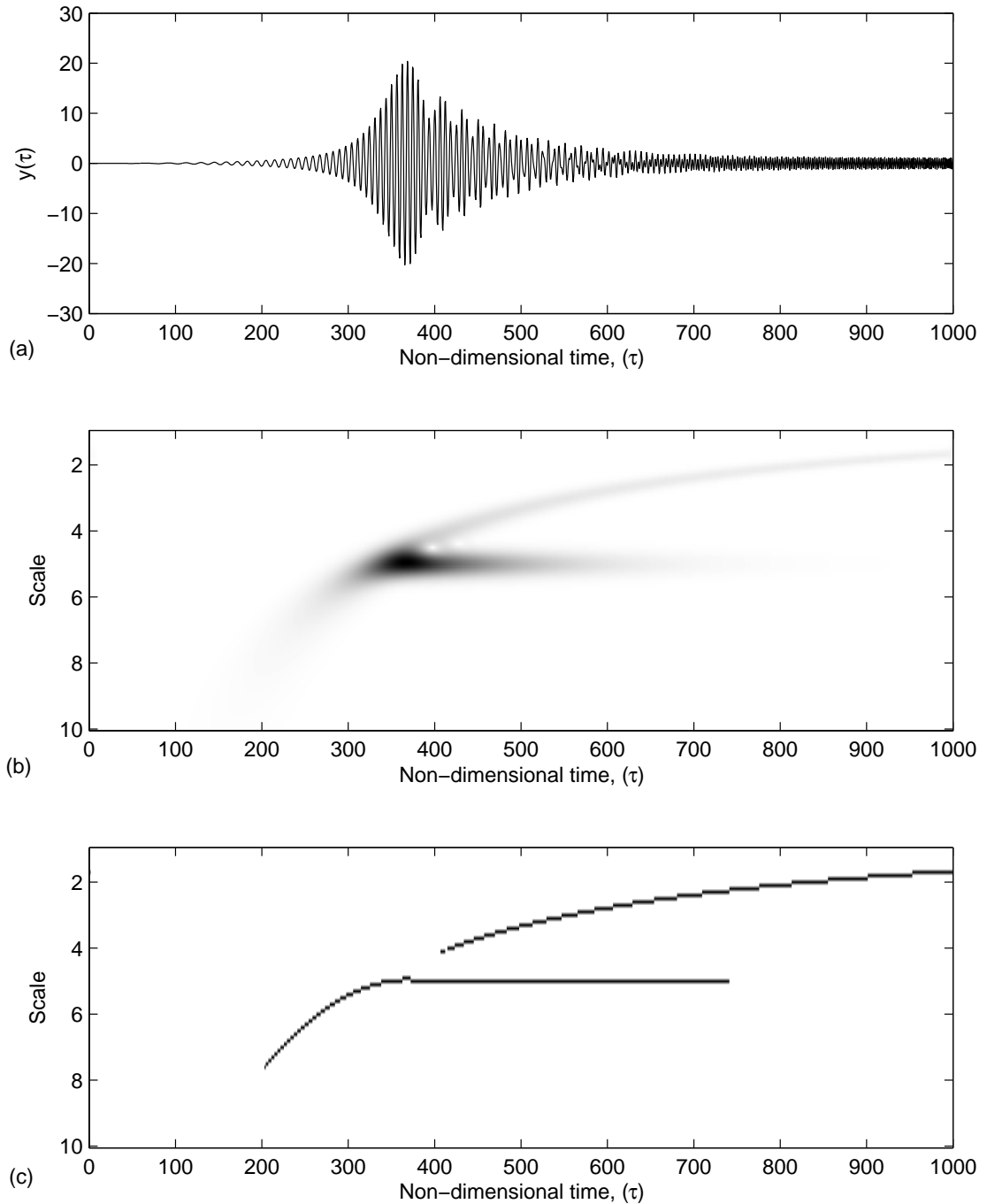
Figure 7.1: (a) Linear system response, (b) Wavelet Transform and (c) Ridges. Rotor speed is continuously increasing
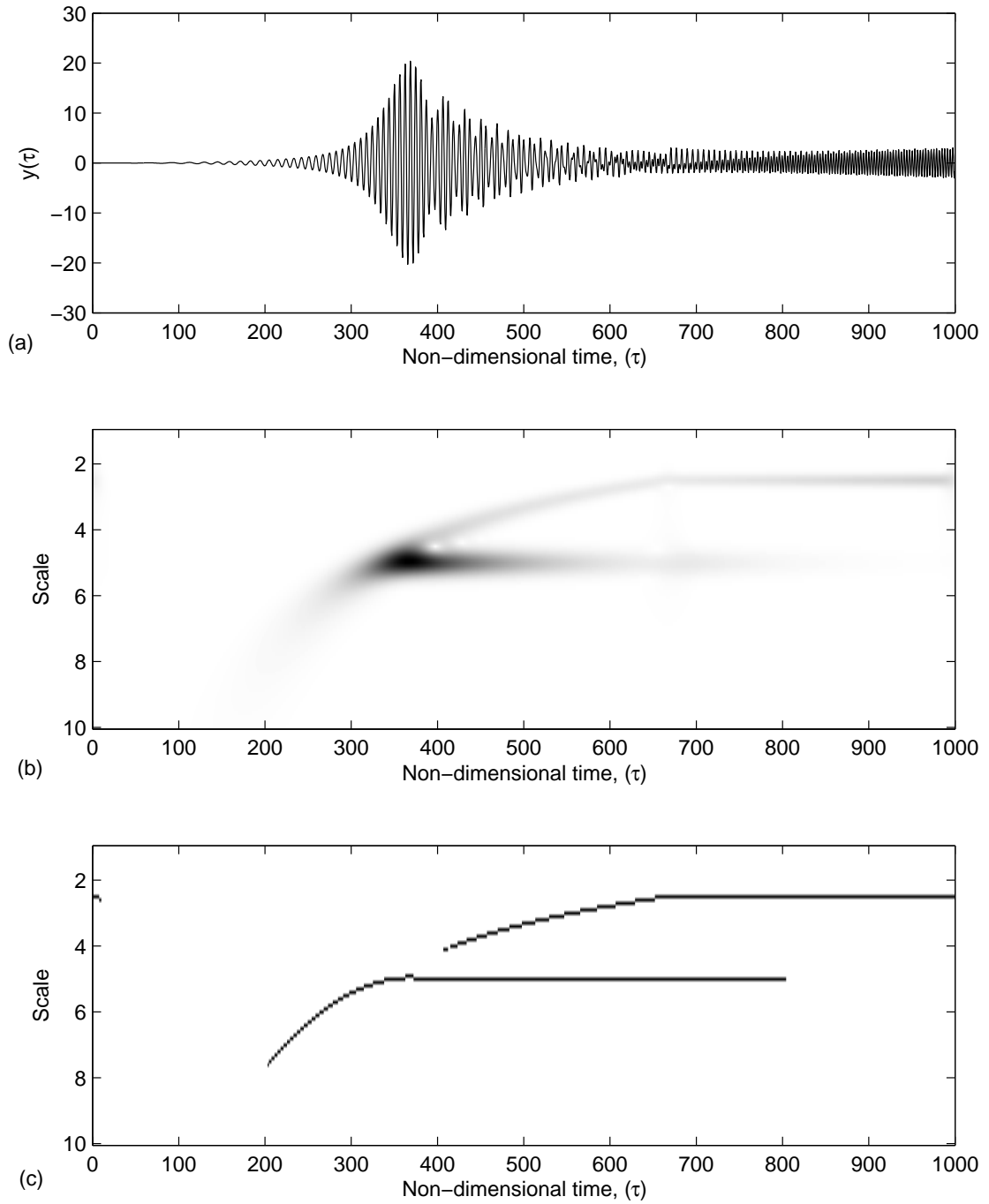
Figure 7.2: (a) Linear system response, (b) Wavelet Transform and (c) Ridges. Rotor attains constant speed after sometime

7.1.2 Nonlinear Rotor System

The case of a system with cubic stiffness nonlinearity is considered. The governing equation is given by the following nonlinear ordinary differential equation

$$mx'' + cx' + kx + k_3 x^3 = me\left[\omega^2 \cos\left(\omega_0 t + \frac{1}{2}\alpha t^2\right) + \alpha \sin\left(\omega_0 t + \frac{1}{2}\alpha t^2\right)\right] \quad (7.3)$$

The above equation can be nondimensionalized using the following substitution

$$\omega_n^2 = \frac{k}{m} \qquad\qquad \zeta = \frac{c}{2m\omega_n} \qquad\qquad \tau = \omega_n t$$

$$\frac{x}{e} = y \qquad\qquad \epsilon_3 = \frac{k_3 e^2}{k} \qquad\qquad \dot{y} = \frac{dy}{d\tau}$$

Using the above parameters the governing nondimensional can be written as

$$\ddot{y} + 2\zeta\dot{y} + y + \epsilon_3 y^3 = r_\omega^2 \cos\left(r_{\omega 0}\tau + \frac{1}{2}r_\alpha\tau^2\right) + r_\alpha \sin\left(r_{\omega 0}\tau + \frac{1}{2}r_\alpha\tau^2\right) \quad (7.4)$$

where $r_\omega = \omega/\omega_n$, $r_{\omega 0} = \omega_0/\omega_n$ and $r_\alpha = \alpha/\omega_n^2$.

Hardening Stiffness

The governing equation is numerically simulated. Its response is wavelet transformed and subsequently ridges are obtained. The nonlinear system is simulated with damping factor, $\zeta = 0.01$, nonlinear factor, $\epsilon_3 = 0.0006$, initial angular speed, $\omega_0 = 0$ and acceleration factor, $r_\alpha = 0.003$.

The results are shown in Figure 7.3 (a)-(c). The ridge corresponding to the free vibration response after critical speed shows a dip, indicating the presence of nonlinearity. The dip is illustrative of the fact that the frequency decreases as the amplitude of vibration decreases. It, clearly, is a case of hardening type stiffness.

Figures 7.4 (a)-(c) shows the same fact as above. However, here the rotor is allowed to attain the fixed speed after passing through critical speed.
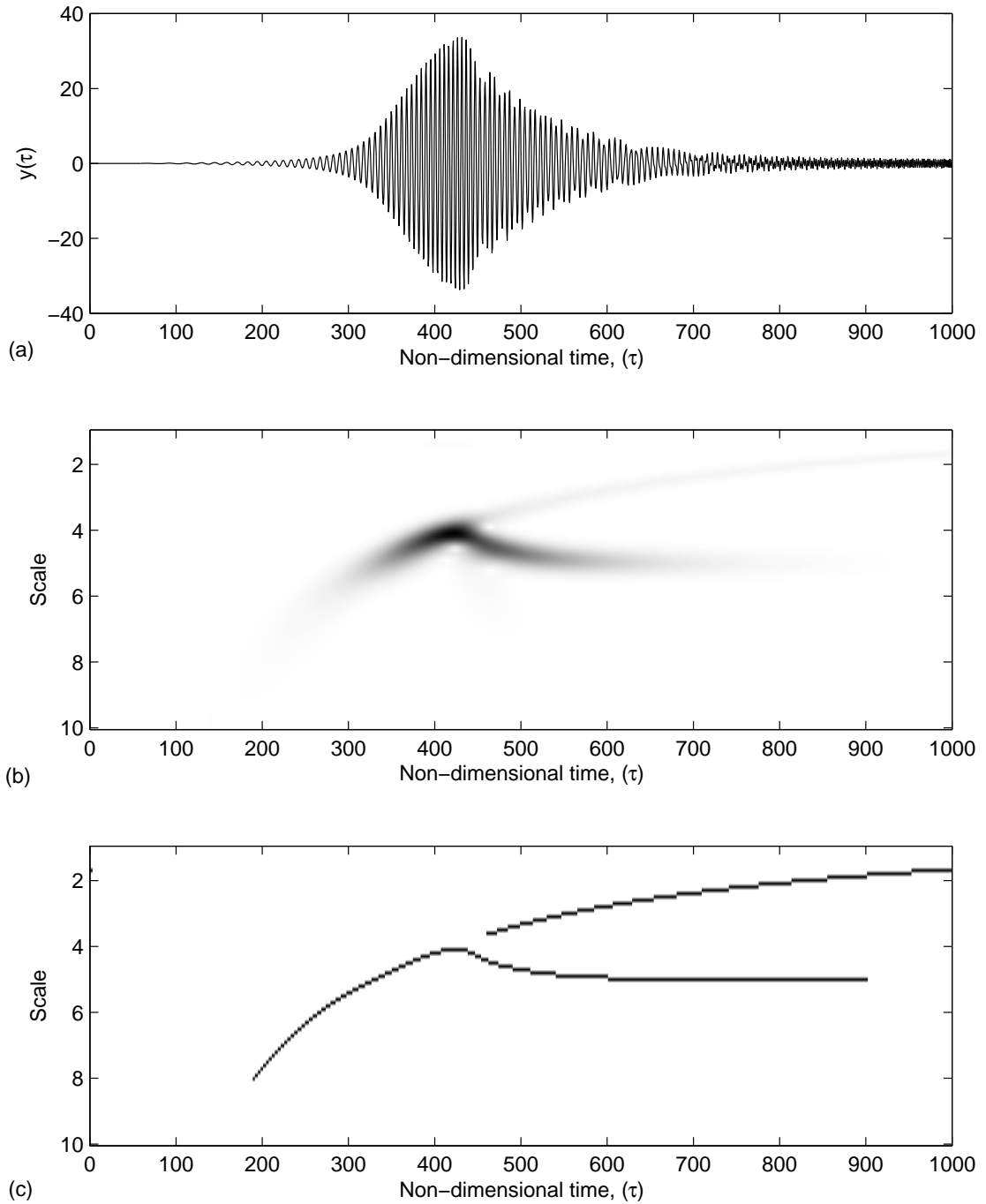
Figure 7.3: (a) Nonlinear system response (Hardening stiffness), (b) Wavelet Transform and (c) Ridges. Rotor speed is continuously increasing
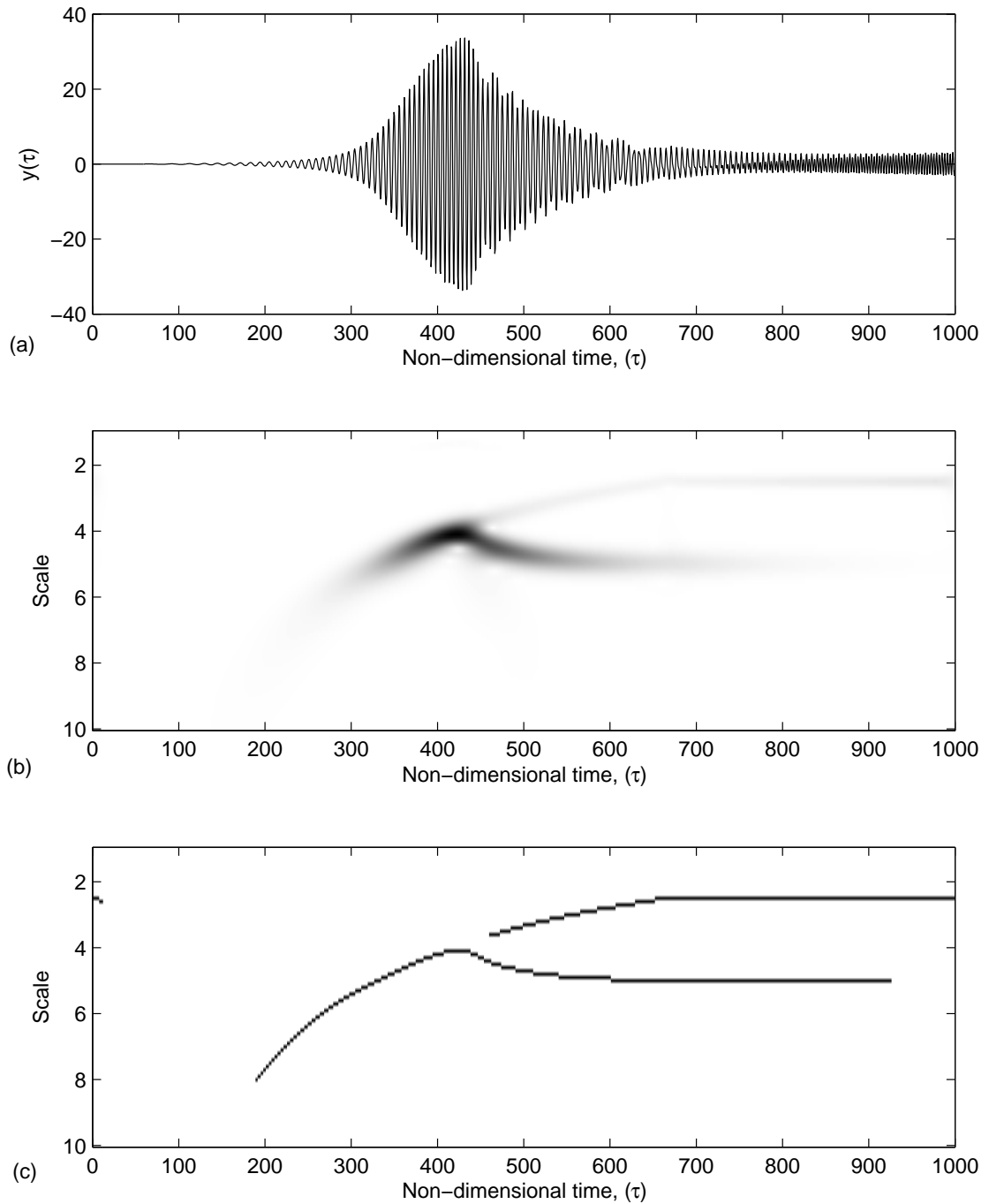
Figure 7.4: (a) Nonlinear system response (Hardening stiffness), (b) Wavelet Transform and (c) Ridges. Rotor attains constant speed after sometime

Softening Stiffness

Here the nonlinear system is simulated using negative value of ϵ_3 i.e. -0.002. Figures 7.5 (a)-(c) and Figures 7.6 (a)-(c) corresponds to the softening type of stiffness. Here the ridge corresponding to natural frequency confirms the fact that frequency increases with the decrease in amplitude of vibration as it should be for the softening type of stiffness.

7.2   Rotor System

Experimental studies have been carried out on a laboratory kit (Machine Fault Simulator, MFS, Spectra Quest Inc. USA). It is mainly used for studying signature of common machine faults and to train personnel for condition based predictive maintenance and diagnostics. The relevant schematic diagram of the experimental setup is shown in Figure 7.7. The MFS is also supplied with a resonance kit. The MFS is equipped with a electric Motor (1/2 HP, 3450 rpm which is controlled by a variable frequency drive (VFD). The acceleration / deceleration of the shaft rotor system can be programmed as required. The measurement scheme is also illustrated in Figure 7.7. The vibration signals of the accelerated rotor system are recorded as observed on the bearing housing, using accelerometers (Bruel & Kjaer, Type 4374). The vibration signal is fed to charge amplifier (Bruel & Kjaer, Type 2635). The vibration response output from charge amplifier is recorded in the PC (Pentium IV) using NI hardware and LabVIEW software (version 8.2). NI 9215 and NI cDAQ 9172 are used for data acquisition. Details of the experimental set up along with the instrumentation is shown in Figure 7.8. Initially, a rap test is performed on the shaft rotor system to estimate its natural frequency. The natural frequency is found to be around 32 Hz (Figure 7.9).

For the accelerated rotor test the VFD is programmed such that rotor is accelerated at constant rate of $20\text{Hz}/s^2$ till it achieves a maximum rotational speed of 50 Hz and data are logged into the PC.

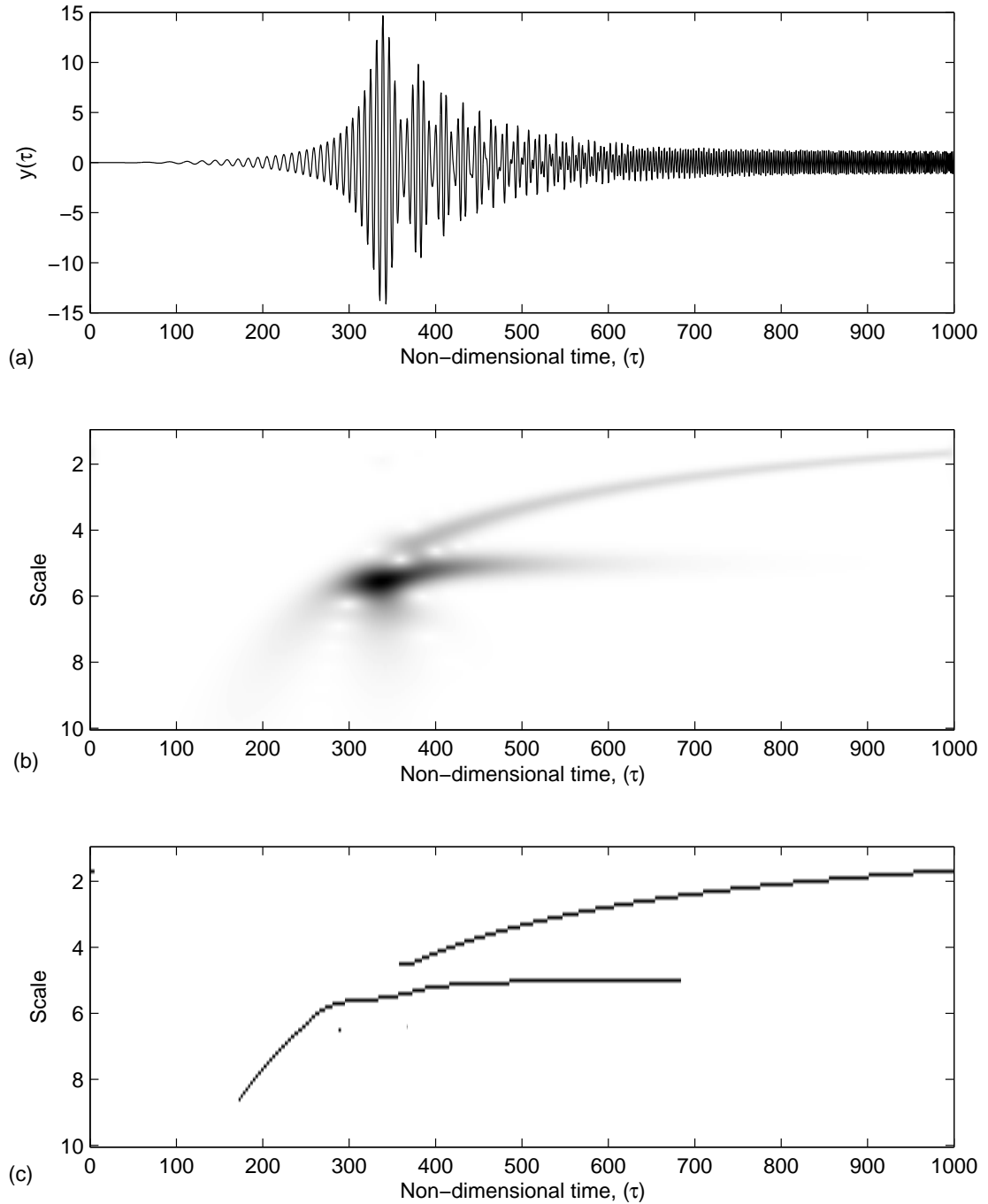Figure 7.5: (a) Nonlinear system response (Softening stiffness), (b) Wavelet Transform and (c) Ridges. Rotor speed is continuously increasing
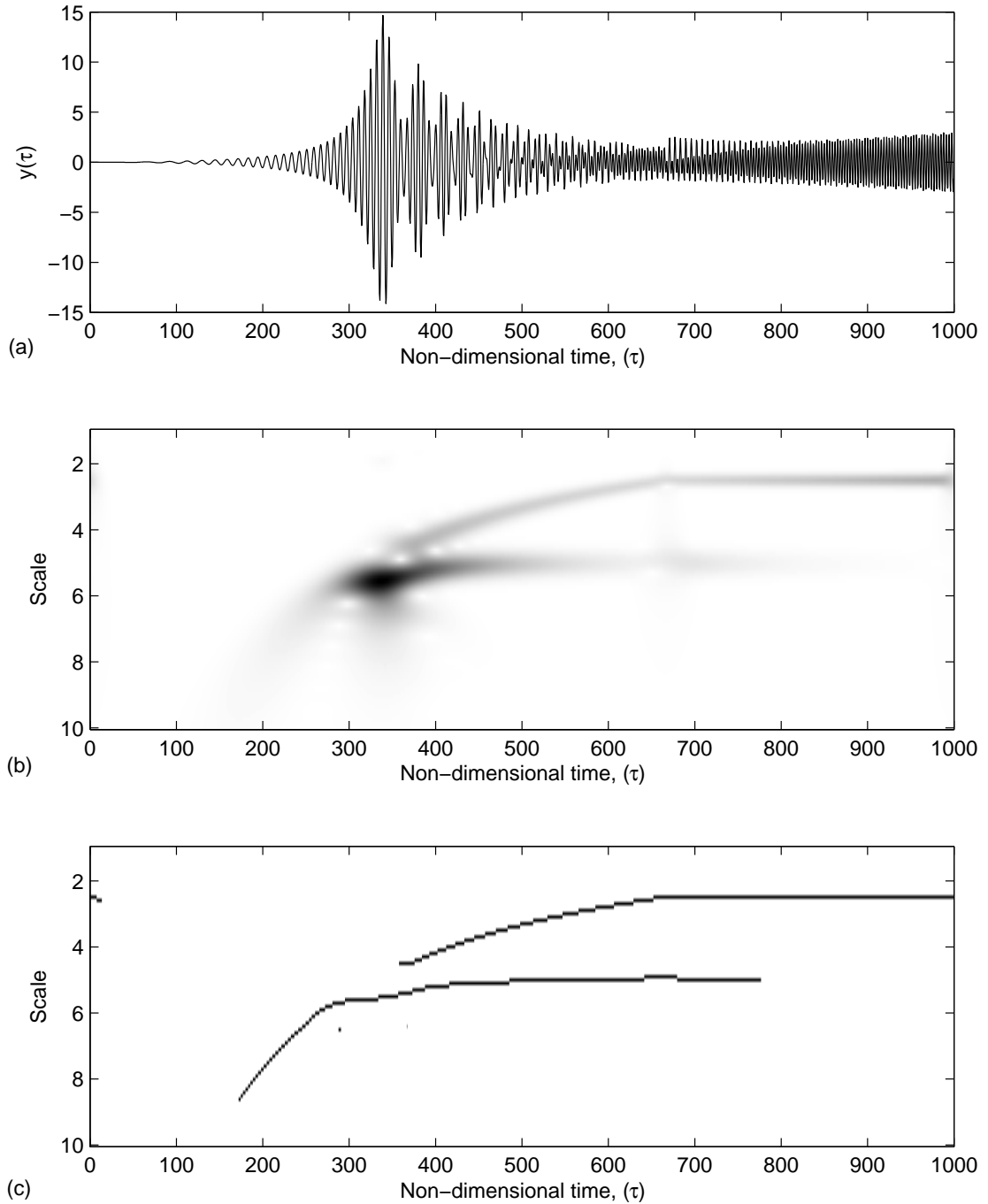
Figure 7.6: (a) Nonlinear system response (Softening stiffness), (b) Wavelet Transform and (c) Ridges. Rotor attains constant speed after sometime
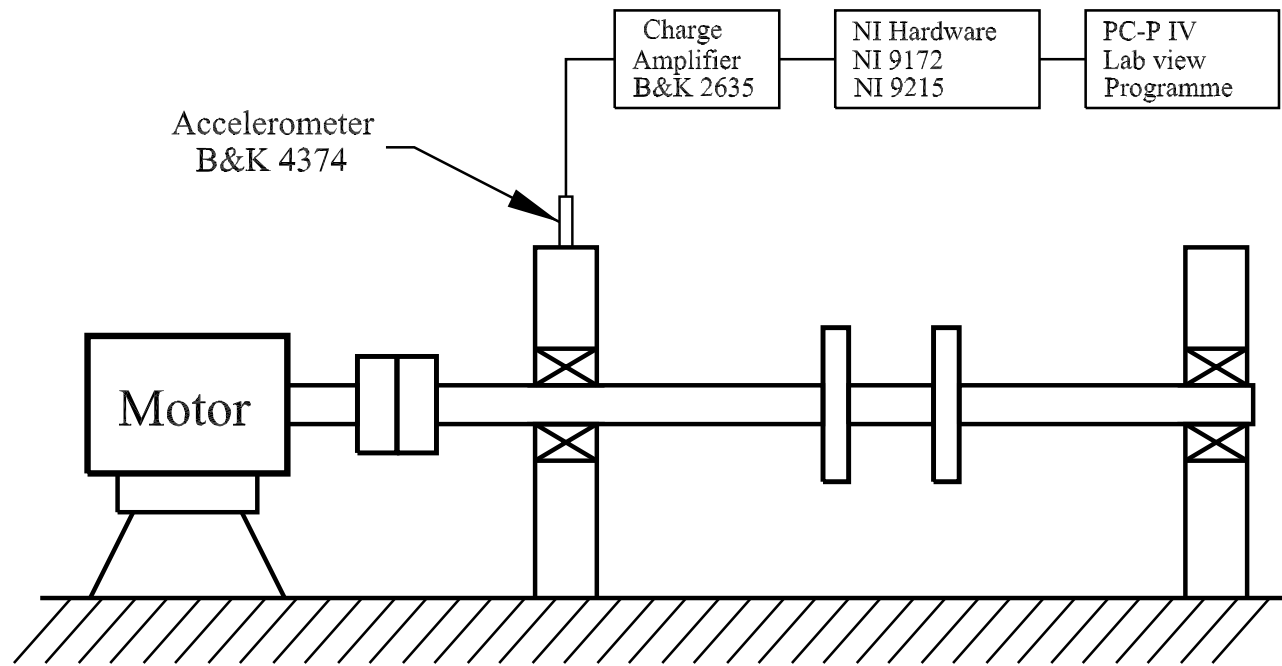
Figure 7.7: Schematic diagram of test setup with instrumentation

Figure 7.8: Experimental set up along with instrumentation
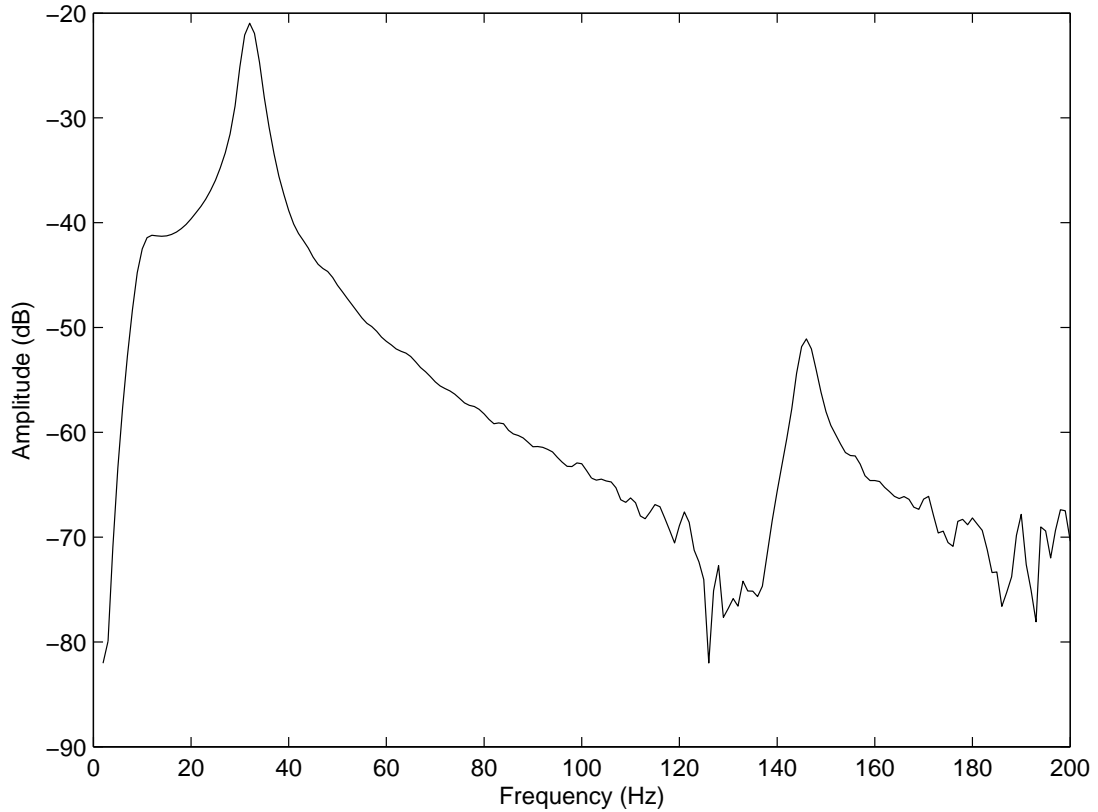
Figure 7.9: Response spectrum from rap test

The Wavelet Transform of the signal and its ridges are obtained (Figure 7.10) using the code developed. It can be seen from the ridge corresponding to the natural frequency immediately after passing critical speed the frequency decreases as the amplitude of vibration decreases. This is indicative of the presence of hardening type of nonlinearity.

Presence of hardening type of nonlinearity, in a similar system, has been reported earlier by Khan (1999) and Chatterjee (2001), who employed Volterra and Wiener theories for nonlinear parameter estimation in rotor-bearing systems.

In absence of an analytic closed form solution, quantitative estimate of the nonlinearity can only be made by creation of a knowledge base from numerical simulation and then template matching with the experimental results.
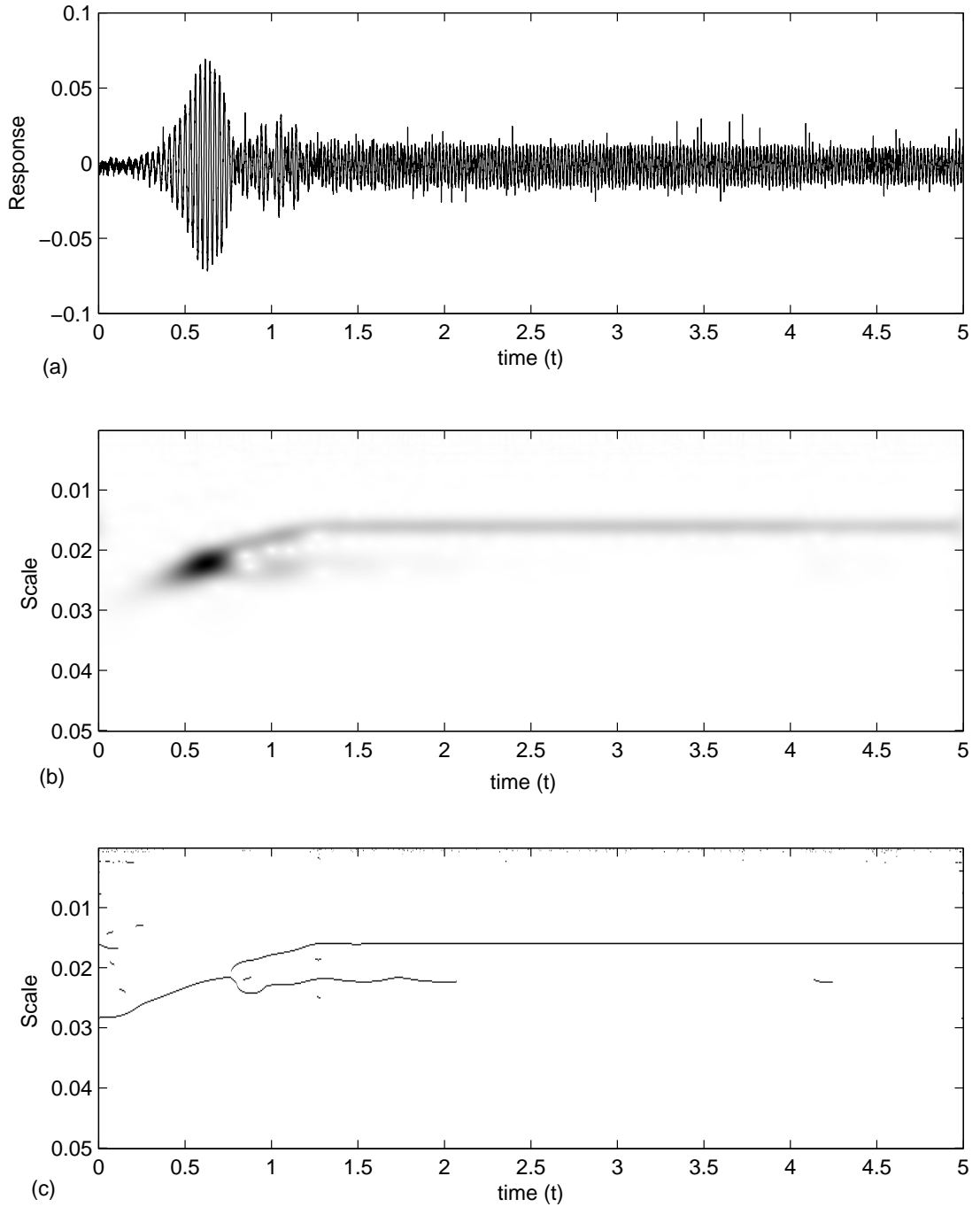
Figure 7.10: Experimental Results (a) Response (b) Wavelet Transform and (c) Ridges. Rotor attains constant speed after sometime

7.3   Remarks

While, quantitative estimation is not carried out in the present study, the following procedure is proposed for achieving it.

The ridges can be obtained for the test data from actual rotor system passing through the critical speed. Its natural frequency ω_n and approximate value of damping factor ζ can be determined using rap test. Numerical simulations can be performed in parallel, using suitable values of nonlinear parameter k_3 and a knowledge bank of ridges can be created. The best fit values of the experimental ridge with those of the knowledge bank ridges can be compared to make a statement about the quantitative value of the nonlinear parameter.

Chapter 8

Conclusion

The present study deals with the inverse problem of parameter estimation in nonlinear systems from the free vibration response of the system. Wavelet Transforms are employed for development of procedure for identification of the type of nonlinearity and parameter estimation.

A methodology for classifying the polynomial type of stiffness nonlinearity has been developed. The Krylov-Bogoliubov method is adopted to obtain analytically the free vibration response of a linearly damped quadratic and mixed parity oscillator. It has been shown that the analytical solutions agree well with the simulated results of system for low value of quadratic and cubic stiffness nonlinearities i.e. ($\epsilon_2 \leq 0.2, \epsilon_3 \leq 0.1$). Subsequently Wavelet Transforms of the free vibration response of the system, using Standard Morlet Wavelet and Complete Morlet Wavelet are obtained. Characteristics of the ridges of the transforms are used in conjunction with the analytical solutions to identify the type of nonlinearity present in the system. The proposed methodology is checked for the robustness against noisy data. It is concluded that the method work well for moderate signal to noise ratio up to 30.

The issue of errors in estimation of nonlinear parameters is extensively addressed. The

sources of errors are discussed and the limitations of the procedures are mentioned. Numerical simulations are carried out for the Duffing and van der Pol oscillators to illustrate the parameter estimation methodology. For the Duffing systems, the parameter estimation error is less than 1% for moderate system parameters ($\epsilon_3 \leq 0.2$, $\zeta \leq 0.012$). In case of van der Pol oscillator, the error in estimation of nonlinear damping parameter (ϵ) remains less than 1 % , if the product ($\mu\epsilon$) is less than 0.12.

Multi-degree-of-freedom (MDOF) systems are analyzed using Fourier-Bessel expansion in conjunction with Wavelet Transforms. Fourier-Bessel expansion is used as a pre-processor to separate the modal components of the system response and then Wavelet Transforms are employed to estimate the system parameters from each separated component. Wavelet Transform is capable of separating the multi-component signals in time-frequency plane. However, it can become ineffective if the modes are close due to presence of cross terms. Fourier-Bessel expansion along with the Wavelet Transform gives better parameter estimation. The procedure is numerically illustrated for a classical two degree of freedom system. The free vibration response signal having close modal frequencies ($\omega_{n1} = 1, \omega_{n2} = 1.7328$) is separated in its individual components successfully and modal parameters of the system are estimated.

Experimental investigations are carried out on a rotor-bearing system. Rotor resonance, as it passes through a critical speed during acceleration, is studied. The response is also numerically simulated for comparison with experimental data. Capability of Wavelet Transform to separate the multi component signal is utilized here to investigate this transient phenomenon. Nonlinearity is detected from the ridge of the Wavelet Transform.

The methods and procedures developed during the course of the study clearly demonstrate that Wavelet Transforms can be employed effectively as system identification and parameter estimation tools for mechanical systems. Unlike other existing procedures, like those based on like higher order frequency transforms (Volterra - Wiener Series) which require controlled and known excitation to be provided to the system, Wavelet Transforms based procedures can work on the transient free vibration response. The

scope of the present study has been restricted to polynomial form of stiffness nonlinearity. However, most of the non-polynomial forms can be approximated by suitable polynomial form. Therefore, estimation procedures can be suitably employed in these cases also. However, future studies can be carried out on non-polynomial forms. Their analytical solutions will have to be studied in conjunction with their Wavelet Transform for identification of the mathematical form of the governing equations and their parameters.

Methods other than Wavelet Transforms, which can work on transient free vibration response of mechanical systems, can be explored for estimation of the instantaneous frequency and amplitude envelope. Discrete Energy Separation Algorithms (DESA) is one such widely used method in the field of signal processing (speech analysis). Future studies can investigate such methods and provide comparison with the present study, to help in planning improved strategies for nonlinear parameter estimation. The mode seperation in case of MDOF system can also be achieved through Empirical Mode Decomposition procedures. The methodology based on Fourier-Bessel expansion can be compared with the Empirical Mode Decomposition procedures.

Studies on accelerated rotor passing through critical speed can be done in more exhaustive manner. Numerical simulations of linear and nonlinear accelerated rotors passing through critical speed can be performed over a wide range of system parameters to create a knowledge base. A dedicated resonance rotor kit can be developed and the vibration of accelerate rotor can be acquired through non- contacting type of proximity sensors. This arrangement may give cleaner response signal which can be analyzed along with the knowledge base of simulated results for the quantification of system parameters.

Appendix A

Response of damped mixed parity nonlinear oscillator

A damped mixed parity nonlinear oscillator is represented as

$$\ddot{y} + 2\zeta\dot{y} + y + \epsilon_2 y^2 + \epsilon_3 y^3 = 0 \tag{A.1}$$

Its motion during positive half cycle can be represented by following auxilliary equation

$$\ddot{y} + 2\zeta\dot{y} + y + \epsilon_2 y\,|y| + \epsilon_3 y^3 = 0 \tag{A.2}$$

Response of the system is obtained by Krylov-Bogoliubov method as described in section 3.2. Above equation can be written as

$$\ddot{y} + y = -2\zeta\dot{y} - \epsilon_2 y\,|y| - \epsilon_3 y^3 \tag{A.3}$$

Comparing the above equation (A.3) with the following general form of the equation

$$\ddot{y} + \omega_n^2 y = \epsilon f(y, \dot{y}) \tag{A.4}$$

we get $\omega_n = 1$ and

$$\epsilon f(y, \dot{y}) = -2\zeta\dot{y} - \epsilon_2 y\,|y| - \epsilon_3 y^3 \tag{A.5}$$

Therefore

$$\epsilon f(A\cos\phi, -A\omega_n\sin\phi) \quad = \quad 2\zeta A\sin\phi - \epsilon_2(A\cos\phi)\,|(A\cos\phi)| - \epsilon_3(A\cos\phi)^3 \tag{A.6}$$

Using standard formulae from the section 3.2, we get

$$\begin{aligned}
\epsilon f_1(A) &= \frac{1}{\pi}\int_0^{2\pi} \sin\phi\,\epsilon f(A\cos\phi, -A\omega_n\sin\phi)\mathrm{d}\phi \tag{A.7}\\
&= \frac{1}{\pi}\int_0^{2\pi} \sin\phi\left[2\zeta A\sin\phi - \epsilon_2(A\cos\phi)\,|(A\cos\phi)| - \epsilon_3(A\cos\phi)^3\right]\mathrm{d}\phi \tag{A.8}\\
&= 2\zeta A \tag{A.9}
\end{aligned}$$

and

$$\begin{aligned}
\epsilon g_1(A) &= \frac{1}{\pi}\int_0^{2\pi} \cos\phi\,f(A\cos\phi, -A\omega_n\sin\phi)\mathrm{d}\phi \tag{A.10}\\
&= \frac{1}{\pi}\int_0^{2\pi} \cos\phi\left[2\zeta A\sin\phi - \epsilon_2(A\cos\phi)\,|(A\cos\phi)| - \epsilon_3(A\cos\phi)^3\right]\mathrm{d}\phi \tag{A.11}\\
&= -\frac{8\epsilon_2 A^2}{3\pi} - \frac{3\epsilon_3 A^3}{4} \tag{A.12}
\end{aligned}$$

The amplitude envelope is obtained as

$$\begin{aligned}
\dot{A}(t) &= -\frac{\epsilon}{2\omega_n}f_1(A) \tag{A.13}\\
&= -\zeta A \tag{A.14}\\
A(t) &= A_{pi}\mathrm{e}^{-\zeta t} \tag{A.15}
\end{aligned}$$

and

$$\begin{aligned}
\dot{\theta}(t) &= -\frac{\epsilon}{2A\omega_n}g_1(A) \tag{A.16}\\
&= \left(-\frac{1}{2A}\right)\left(-\frac{8\epsilon_2 A^2}{3\pi} - \frac{3\epsilon_3 A^3}{4}\right) \tag{A.17}\\
&= \frac{4\epsilon_2 A}{3\pi} + \frac{3\epsilon_3 A^2}{8} \tag{A.18}
\end{aligned}$$

which gives instantaneous frequency as

$$\omega_{pi} = 1 + \dot{\theta}(t) \tag{A.19}$$

$$= 1 + \frac{4\epsilon_2 A}{3\pi} + \frac{3\epsilon_3 A^2}{8} \tag{A.20}$$

Hence the response of the system is

$$y_{pi}(t) = A_{pi}e^{-\zeta t}\cos\left[\omega_{pi}t + \theta_{pi}\right] \tag{A.21}$$

The motion during negative half cycle is given by the following auxilliary equation

$$\ddot{y} + 2\zeta\dot{y} + y - \epsilon_2 y\,|y| + \epsilon_3 y^3 = 0 \tag{A.22}$$

Its response can be analysed in a similar way and following relationship for amplitude envelope and instantaneous frequency can be obtained

$$A(t) = A_{nj}e^{-\zeta t} \tag{A.23}$$

$$\omega_{nj} = 1 - \frac{4\epsilon_2 A}{3\pi} + \frac{3\epsilon_3 A^2}{8} \tag{A.24}$$

Hence the response of the system is

$$y_{nj}(t) = A_{nj}e^{-\zeta t}\cos\left[\omega_{nj}t + \theta_{nj}\right] \tag{A.25}$$

References

Abbate, A., DeCusatis, C. M., Das, P. K., 2002. Wavelets and Subbands Fundamentals and applications. Birkhauser,Boston.

Addison, P. S., Watson, J. N., Feng, T., 2002. Low-oscillation complex wavelets. Journal of Sound and Vibration 254 (4), 733–762.

Argoul, P., Le, T.-P., 2003. Instantaneous indicators of structural behaviour based on the continuous cauchy wavelet analysis. Mechanical Systems and Signal Processing 17 (1), 243–250.

Atlas, G., Desiderio, M., Apr. 2006. Solutions to the van der pol equation : A model of the aortic blood flow. In: Bioengineering conference,2006. Proceeding of the IEEE 32nd Annual Northeast. pp. 143–144.

Baker, J. G., 1939. Mathematical-machine determination of the vibration of accelerated unbalanced rotor.

Boltezar, M., Slavic, J., 2004. Enhancement to the continuous wavelet transform for damping identification on short signals. Mechanical Systems and Signal Processing 18, 1065–1076.

Carmona, R.and Hwang, W., Torresani, B., 1998. Wavelet Analysis and Its Application : Practical Time Frequency Analysis, Vol. 9. Academic Press, San Diego.

Chatterjee, A., 2001. Ph.D. thesis on Nonlinear Parameter Estimation using Volterra Series. I.I.T., Kanpur.

Chui, C. K., 1992. An Introduction to Wavelets. Academic Press,INC.

Daubechies, I., 1992. Ten Lectures On Wavelets. Society for Industrial and Applied Mathematics.

Frank M., L., 1932. Vibration during acceleration through a critical speed. Applied Mechanics, Transaction of The American Society of Mechanical Engineers, 253–261.

Hammond, J., White, P., 1996. The analysis of non-stationary signals using time-frequency methods. Journal of Sound and Vibration 190 (3), 419–447.

Hassenpflug, H. L., Flack, R. D., Gunter, E. J., 1981. Influence of acceleration on the critical speed of a jeffcott rotor. Journal of Engineering for Power, Transactions of the ASME 103, 108–113.

Hu, H., 2006. Solution of a quadratic nonlinear oscillator by the method of harmonic balance. Journal of Sound and Vibration 293, 462–468.

Hu, H., 2007. Solution of a mixed parity nonlinear oscillator: Harmonic balance. Journal of Sound and Vibration 299, 331–338.

Hubbard, B. B., 1996. The world according to wavelets. A K Peters, Ltd.

Kerschen, G., Worden, K., Vakakis, A. F., Golinval, J.-C., 2006. Past, present and future of nonlinear system identification in structural dynamics. Mechanical Systems and Signal Processing 20, 505–592.

Khan, A. A., 1999. Ph.D. thesis on Parameter Estimation in Nonlinear Rotor-Bearing Systems through Volterra and Wiener Theories. I.I.T., Kanpur.

Kijewski, T., Kareem, A., 2002. On the presence of end effects and their melioration in wavelet based analysis. Journal of Sound and Vibration 256 (5), 980–988.

Lardies, J., Gouttebroze, S., 2002. Identification of modal parameters using the wavelet transform. International Journal of Mechanical Sciences 44, 2263–2283.

Lardies, J., Ta, M.-N., 2005. A wavelet based approach for the identification of damping in non-linear oscillator. International Journal of Mechanical Sciences 47, 1262–1281.

Le, T.-P., Argoul, P., 2004. Continuous wavelet transform for modal identification using free decay response. Journal of Sound and Vibration 277, 73–100.

Lin, J., Qu, L., 2000. Feature extraction based on morlet wavelet and its application for mechanical fault diagnosis. Journal of Sound and Vibration 234 (1), 135–148.

Mallat, S., 1998. A Wavelet Tour of Signal Processing. Academic Press.

Michaelis, M., Penz, S., Black, C., Sommer, G., Sep. 1993. Detection and classification of p waves using gabor wavelets. In: Computers in Cardiology 1993. Proceedings of IEEE. pp. 531–534.

Mickens, R. E., 1995. Oscillations in Planar Dynamic Systems. World Scientific Publishing Co. Pte. Ltd.

Nayfeh, A. H., 1973. perturbation Methods. John Wiley and sons.

Nayfeh, A. H., 1979. Nonlinear Oscillations. John Wiley and sons.

Nayfeh, A. H., 1981. Introduction to Perturbation Techniques. John Wiley and sons.

Newland, D., 1993. An introduction to Random vibrations, spectral and wavelet analysis. Longman Scientific and technical.

Newland, D., Oct. 1994a. Wavelet analysis of vibration, patr i : Theory. Journal of Vibration and Acoustics 116, 409–416.

Newland, D., Oct. 1994b. Wavelet analysis of vibration, patr ii : Wavelet maps. Journal of Vibration and Acoustics 11, 417–425.

Newland, D., Apr. 1999. Ridge and phase identification in the frequency analysis of transient signals by harmonic wavelets. Journal of Vibration and Acoustics 11.

O'Neil, P. V., 2003. Advanced Engineering Mathematics. Thomson Brooks / Cole.

Pachori, R. B., 2007. Ph.D. thesis on Methods Based on Fourier-Bessel Representation for Analysis of Nonstationary Signals. I.I.T., Kanpur.

Pachori, R. B., Sircar, P., 2006. Speech analysis using fourier-bessel expansion and discrete energy seperation algorithm. In: Proc. 12th Digital Signal Processing Workshop and 4th Signal Processing Education Workshop. Wyoming, USA.

Peng, Z., Chu, F., 2004. Application of the wavelet transform in machine condition monitoring and fault diagnostics : a review with bibliography. Mechanical Systems and Signal Processing 18, 199–221.

Potamianos, A., Maragos, P., May 1994. A comparison of the energy operator and hilbert transform approach for signal and speech demodulation. Signal Processing 37 (1), 95–120.

Ruzzene, M., Fasana, A., Garibaldi, L., Piombo, B., 1997. Natural frequencies and damping identification using wavelet transform : Application to real data. Mechanical Systems and Signal Processing 11 (2), 207–218.

Simonovski, I., Boltezar, M., 2003. The norms and variances of the gabor, morlet and general harmonic wavelet functions. Journal of Sound and Vibration 264, 545–557.

Slavic, J., Simonovski, I., Boltezar, M., 2003. Damping identification using a continuous wavelet transform: application to real data. Journal of Sound and Vibration 262, 291–307.

Staszewski, W., 1997. Identification of damping in mdof systems using time-scale decomposition. Journal of Sound and Vibration 203 (2), 283–305.

Staszewski, W., 1998. Identification of non-linear systems using multi-scale ridges and skeletons of the wavelet transform. Journal of Sound and Vibration 214 (4), 639–658.

Stoker, J., 1957. Nonlinear Vibrations in Mechanical and Electrical Systems. Interscience Publishers Ltd.

Ta, M.-N., Lardies, J., 2006. Identification of weak nonlinearities on damping and stiffness by the continuous wavelet transform. Journal of Sound and Vibration 293, 16–37.

Vyas, N. S., Gupta, K., Rao, J. S., 1987. Transient response of turbine blabe. 'The Theory of Machines and Mechanisms Proceedings of the 7th world congress 17-22 September 1987 Sevilla spain.

Worden, K., Tomlinson, G., 2001. Nonlinearity in Structural Dynamics: Detection, Identification and modelling. Institute of Physics Publishing, Bristol and Philadelphia.

List of publications from the present research work

1. R. Porwal, N.S. Vyas, "Damped quadratic and mixed-parity oscillator response using Krylov-Bogoliubov method and energy balance", Journal of Sound and Vibration, 309 (2007), 877-886.

2. R.Porwal, N.S. Vyas, "Errors in Nonlinear System Parameter Estimation Using Wavelet Transform" IMAC- XXVI, Orlando, Florida, USA, February 2008

3. R. Porwal , N.S. Vyas , "Nonlinear Damping Estimation of Self-Excited System Using Wavelet Transform" IMAC- XXVII, , Orlando, Florida, USA, February 2009.

4. R. Porwal , N.S. Vyas , "Stiffness nonlinearity classification using Morlet wavelet" The 2nd Conference on Dynamics, Vibration and Control; August 10-15, 2009, Chengdu, Sichuan, China
   The above paper is also published in the edited book "Dynamical Systems: Discontinuous, Stochasticity and time delay" A.C.J. Luo (ed.) from Springer Science, Chapter 23, Page 275-284.